UNIVERSITY OF TARTU

Faculty of Science and Technology

Institute of Technology

Stefan Heincz

carbon dioxide sensing in *Arabidopsis thaliana* mediated by liquid-to-liquid phase separation of Protein Phosphatase Type 2C homologs

Master's Thesis (30 ECTS)

Curriculum Bioengineering

Supervisors:

Associate Professor, PhD. Yuh-Shuh Wang

Associate Professor, PhD. Ivar Ilves

Professor, PhD. Hannes Kollist

Tartu 2024

Thank you, Yuh-Shuh and Ivar, for the hours of explaining and supervising,

and Hannes for the support.

Thank you Mikk, for caring and the right wrong buffers.

This thesis is dedicated to my parents who always support me.

Without you, this would have not been possible!

Tartu, 22.05.2024

Title

carbon dioxide sensing in *Arabidopsis thaliana* mediated by liquid-to-liquid phase separation of Protein Phosphatase Type 2C homologs

Abstract

Carbon dioxide sensing is crucial for plants to maintain a balance between exchange of gas and water vapor which directly affects tolerance of environmental stresses and ensures plant survival. Understanding CO_2 sensing in plants will therefore help to be more prepared for future challenges in food crop production caused by increased environmental stresses due to climate change. An up to this point nearly unstudied process in plants, the phase separation (PS) of proteins, has recently been shown *in vitro* to be the main mechanism of CO_2 sensing of a protein phosphatase type 2C (AP2C3) from *Arabidopsis thaliana*. PS describes the process of protein condensate droplet formation due to local enrichment of protein caused by interactive motifs usually located in an intrinsically disordered region (IDR) within the polypeptide backbone. In this study, we attempted to reproduce published results and screen for further IDR/PS mediated CO_2 sensitivity of PP2Cs by cloning, expression, and purification of AP2C1, AP2C4 and PP2C74, along with AP2C3, for *in vitro* imaging experiments. We successfully established a reliable laser scanning confocal microscopy imaging setup for monitoring the phase separation of purified proteins fused to fluorescent tags. However, CO_2-condensation of PP2C proteins could not be detected. Furthermore, we aimed to study PS and verify intracellular localisation of selected PP2C homologs *in planta* via a transient overexpression assay in *Nicotiana benthamiana*. Additionally, a connection of AP2C3 with the guard cell CO_2 signalling pathway by a bimolecular fluorescence complementation assay with Mitogen-activated Protein Kinase 12 (MPK12) was investigated. These experiments verified the intracellular localisation of selected homologs, the presence of biomolecular condensates for AP2C3/4 *in planta* and indicated interaction between AP2C3 and MPK12.

Keywords

Liquid-to-liquid Phase Separation, Protein Condensation, Protein Phosphatase 2C, CO2 Sensing in guard cells, Mitogen-Activated Kinase 12

CERCS

B310 Physiology of vascular plants (25 %)

B191 Plant biochemistry (25 %)

B225 Plant genetics (50%)

Pealkiri

Arabidopsis thaliana Proteiinfosfataas tüüp 2C homoloogvalkude faasiseparatsiooni poolt vahendatud süsinikdioksiidi sensor

Lühikokkuvõte

Süsinikdioksiidi tundlikkus on ülioluline protsess, mis aitab säilitada tasakaalu gaasi- ja veeauru vahetuse vahel taimes, ning mõjutab otseselt taimede keskkonnastressi taluvust ja elulemust. Selle protsessi molekulaarsete alusmehhanismide mõistmine aitab seega valmistuda põllumajandussektori ees seisvateks väljakutseteks, mis tulenevad kliimamuutustest tingitud keskkonnastressi süvenemisest. Hiljutiste *in vitro* uuringute põhjal on müürlooga *Arabidopsis thaliana* süsinikdioksiidi sensorsüsteemis oluline roll Proteiinfosfataas tüüp 2C (AP2C3) valgu faasiseparatsiooniprotsessil. Faasiseparatsioonitilkade ehk valgukondensaatide moodustumine valgulahustes on kontrollitud spetsiaalsete interaktsioonimotiivide poolt, mis tüüpiliselt paiknevad valkude olemuslikult struktureerimata piirkondades. Antud magistritöö kirjeldab PP2C perekonna fosfataaside AP2C1, AP2C4 ja PP2C74/AP2C3 valkude ekspresseerimist ja puhastamist, jätkamaks eelnevalt publitseeritud PP2C perekonna valkude faasiseparatsioonil põhineva süsinikdioksiidisensori toimimiseks oluliste valgupiirkondade kirjeldamist. Selleks seadistasime oma laboris laserskaneerival konfokaalmikroskoopial põhineva metoodika, mis võimaldab jälgida fluorestseeruva märgisega valkude faasikondensaatide moodustumist. Nende katsete käigus ei suudetud tuvastada uuritud PP2C valkude kondenseerumist. Lisaks uurisime PP2C homoloogvalkude faasiseparatsiooni ja lokalisatsiooni *Nicotiana benthamiana* lehtedes transientse üleekspressiooni abil. Analüüsisime ka AP2C3 fosfataasi ja Mitogeen - Aktiveeritud Proteiinkinaasi 12 (MPK12) omavahelise interaktsiooni võimalikku seotust sulgrakkude süsinikdioksiidi sensorrajaga, viies selleks läbi bimolekulaarse fluorestsentskomplementatsiooni katsed. Nende uuringute käigus kinnitati üle PP2C homoloogvalkude rakusisene lokalisatsioon *in planta* ja kirjeldati AP2C3 - MPK12 valkude interaktsiooni sulgrakkudes.

Võtmesõnad

Valkude faasiseparatsioon, Valkude kondenseerumine, Proteiinfosfataas 2C 3, CO2 sensor sulgrakkudes, Mitogeen - Aktiveeritud Proteiinkinaas 12

CERCS

B310 Soontaimede füsioloogia (25 %)

B191 Taimebiokeemia (25 %)

B225 Taimegeneetika (50%)

TABLE OF CONTENTS

TERMS, ABBREVIATIONS AND NOTATIONS

Alphabetically ordered:

AP2C3/PP2C5	–	Arabidopsis Phosphatase Type 2C 3
ATPase	–	Adenosine 5'-TriPhosphatase
BiFC	–	Bimolecular Fluorescence Complementation
CO_2	–	Carbon Dioxide
DNA	–	Deoxyribonucleic Acid
HCO_3^-	–	Bicarbonate
HT1	–	High Leaf Temperature 1
IDR	–	Intrinsically Disordered Region
KIM	–	Kinase Interaction Motif
LIC	–	Ligation Independent Cloning
LLPS	–	Liquid to Liquid Phase Separation
MPK/MAPK	–	Mitogen-activated Protein Kinase
PBS	–	Phosphate Buffered Saline
PEG	–	Polyethylene Glycol
dpi	–	Post Infiltration
PP2C	–	Protein Phosphatase Type 2C
PS	–	Phase Separation
RE	–	Restriction Enzyme
RT	–	Room Temperature
Sf9	–	*Spodoptera frugiperda*
Tstrep	–	Twin-strep
YFP	–	Yellow Fluorescent Protein

INTRODUCTION

"Life is a self-contained, self-regulating, self-organizing, self-reproducing, interconnected, open thermodynamic network of component parts which performs work, existing in a complex regime which combines stability and adaptability in the phase transition between order and chaos, as a plant, animal, fungus, or microbe."

(Macklem & Seely, 2010, p.2)

Macklem and Seely (2010) stated in their article "Towards a Definition of Life" that, "*… a clear idea of what life means remains elusive, and there is no universally accepted definition.*" (page 1). However, their approach to a definition is general but exact. Especially the connection of thermodynamic processes with a phase transition between order and chaos offers a new, more simplistic but less prone to scepticism perspective on mechanisms vital for life (Macklem & Seely, 2010) and brings the issue of this thesis to the point. Life can be characterized as the absence of unorder. Biochemical activities and thermodynamic mechanisms require the order of molecules and therefore separation of them into different concentrations. The principle of concentration gradients allows cells, for example, via the hydrogen potassium adenosine 5'-triphosphatase (ATPase), a membrane bound enzyme, to utilize energy stored in the thermodynamical highly energetic triphosphate bond of ATP to build up a hydrogen ion cell membrane potential that is utilized for life essential processes (Lee et al., 1979).

The entropic segregation of molecules and their properties to allow life to form relies on one basic principle - compartmentation. Classically, this driving force of evolution is understood as being dependent on membrane bound organelles as described in the previously mentioned example of ATPase. The general understanding appears to be as follows: The more sophisticated the structure of organelles and their circumcising phospholipid bilayers, the more complicated the resulting biochemical reactions can be. This is well demonstrated by evolutionary development of bacteria, archaea and eukaryotes and is broadly believed to have allowed the shift of single celled life forms to multicellular organisms. However, the existence of protein-coat-enclosed viral life forms or prions is neglected in the definition from Macklem and Seely (2010). Nonetheless, they follow the similar basic principle of absence of chaos and also prokaryotes utilize compartmentation (Murat et al., 2010).

The rapidly evolving research field studying membrane-less organelles based on the phenomena of phase separation (PS) provides a whole new perspective to this classical school of thought. Here it is suggested that compartmentation is not essentially dependent on a strict 'third party'-barrier that regulates concentration gradients but can also be achieved through dense association of alike macromolecules and 'clients' (Staples et al., 2023). In literature this phenomenon is described in the simplest form as PS or liquid condensation. Besides, Macklem and Seely (2010) state life as a *"… phase transition between order and chaos…"* (page 2) without restriction to rigid limitation of phases by third party structures for organization into membrane-bound organelles or protein coats/capsids. This highlights the importance of PS as a driving molecular force in life forms since many cells organize their reactions not only in the form of organelles but also membrane-less reaction centres (Gomes & Shorter, 2019) and brings Alexander Oparin's (1938) formerly rejected theory *The Origin of Life* back into the spotlight – he suggested that life's origin lies in spontaneously coacervated drops of organic material, consisting of molecules that would otherwise increase dilution of the overall solution components. This was not supported due to lacking explanation of membrane-bound organelle compartmentalization of eukaryotic cells driven solely by molecular dynamics (Oparin, 1938).

Cells have been shown to arrange constituents into organelles lacking membranes, indicating a need for a reappraisal of Oparin's coacervate hypothesis (Aumiller & Keating, 2015; Brangwynne et al., 2011; Feric et al., 2016). Many cellular organelles are indeed condensations of protein, nucleic acid, or both. Only within the nucleus, already a wide variety of structures such as Cajal bodies, nuclear speckles, paraspeckles, histone-locus bodies, nuclear gems, and promyelocytic leukaemia (PML) are formed by phase separation (Handwerger & Gall, 2006; Mao et al., 2011; Mitrea & Kriwacki, 2016). The cytoplasm also hosts various membrane-less organelles, such as P-bodies, stress granules, and germ granules (Decker & Parker, 2012; Mitrea & Kriwacki, 2016). In the past years substantial advancements in the comprehension of the molecular dynamics of membrane-less organelles have been set, including their formation, functions, regulatory mechanisms, and implications for human diseases (Gomes & Shorter, 2019). While LLPS is majorly studied in eukaryotic cells such as in fungal (e.g. *Saccaromyces cerevisiae*), animal (e.g. *Caenorhabditis elegans*) and mammalian cell line systems (Alberti et al., 2018; Boeynaems et al., 2018; Shin & Brangwynne, 2017), its importance within the plant kingdom remains to be investigated (Emenecker et al., 2020).

However, awareness about the potential of LLPS in plant physiological processes is rising. Zhang et al. (2022) have found that, "*The intrinsically disordered region from PP2C phosphatases functions as a conserved CO_2 sensor*", not only in fungi (*Candida albicans*) but also in plants (*Aarbidopsis thaliana*). This suggests PS playing a vital role in carbon dioxide (CO_2) sensing of plants and therefore regulating photosynthesis and a plethora of plant development and stress responses (Brock et al., 2010; Emenecker et al., 2020; Zhang et al., 2022). Since Zhang et al. (2022) only show CO_2-induced liquid condensation for plants by an *in vitro* assay via purified proteins, we hypothesized that this effect could also be detectable *in planta*. Furthermore, we aimed to verify whether the CO_2 dependency is caused by a reported N-terminal intrinsically disordered region (IDR) unique to only a few of the widely conserved Protein Phosphatases Type 2C (PP2C) protein family variants in *A. thaliana* by comparing with close homologs that lack IDR classification. Finally, we examined a potential connection between the PP2C family and the newly reported guard cell CO_2 sensing mechanism via MPKs using bimolecular fluorescence complementation (BiFC) assays (Takahashi et al., 2022; Yeh et al., 2023).

1 LITERATURE REVIEW

1.1 Phase separation

1.1.1 General aspects

Phase separation (PS) refers to the spontaneous partitioning of a homogeneous mixture into two or more distinct phases, each with its own unique composition and properties, by decreasing dilution of participating molecules. An example for PS in daily life would be salad dressing: mixed oil and vinegar form an emulsion and do not form a homogenous solution. This allows droplets to be formed. Separation typically occurs when the system reaches a thermodynamic equilibrium under certain conditions, such as changes in temperature, pH, pressure, or ionic and overall composition (Figure 1). It can result in the formation of liquid-liquid, liquid-solid, or gas-liquid phases. This phenomenon is governed by the minimization of free energy and is driven by various intermolecular forces and interactions between components. PS plays a critical role in numerous chemical processes, including polymerization, crystallization, and the formation of emulsions and colloidal systems (Flory, 1942; Staples et al., 2023).

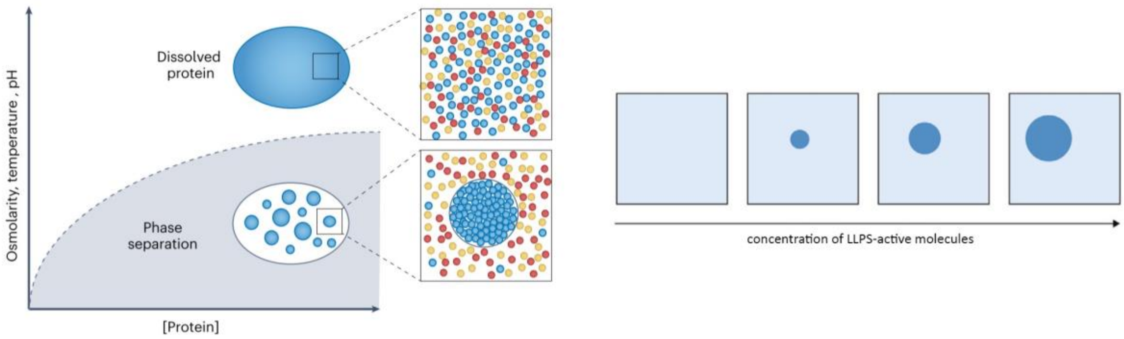

Figure 1: Key factors to drive phase separation of dissolved interactor into a dense state coexisting with a dilute phase. Adapted from Staples et al. (2022, left graph) and Emenecker & Holehouse (2020, right graph).

In biological systems, molecules, typically proteins and nucleic acids, separate from a homogeneous solution to form distinct liquid, gel-like or solid phases. This process is mediated by specialised domains within the polymer which are reserved for interaction with their environment. They direct the self-assembly of molecules driven by weak, non-covalent interactions such as hydrophobic interactions, electrostatic interactions, hydrogen bonding, cation-Pi interaction, Pi-Pi interaction and van der Waals forces (Staples et al., 2023). This thesis focuses on PS of proteins.

1.1.2 Molecular process

Nucleation: Initially, certain molecules within the solution aggregate to form small clusters or "seeds" known as nucleation sites. These nucleation sites serve as the starting point for PS (Flory, 1942).

Growth: Once nucleation occurs, additional molecules are recruited to the growing clusters, leading to their expansion. This process continues until distinct liquid, or gel-like phases are formed (Flory, 1942).

Coarsening: As the two-phase regimes grow, larger droplets or domains emerge and coalesce, driven by the minimization of free energy. This results in the formation of larger, more distinct phases, so-called droplets (Flory, 1942).

PS is often reversible, the separated phases can re-dissolve back into the original solution under certain conditions, such as changes in temperature, pH, or salt concentration. Additionally, the separated phases show dynamic behaviour, with molecules continuously exchanging between the phases. This allows rapid adaptation to changing cellular conditions. PS contributes to the selective partitioning of molecules into different phases based on their biochemical properties, such as size, charge, multivalency and specific molecular interactions (Figure 2). This selectivity plays a crucial role in organizing cellular components and regulating cellular processes (Boeynaems et al., 2018).

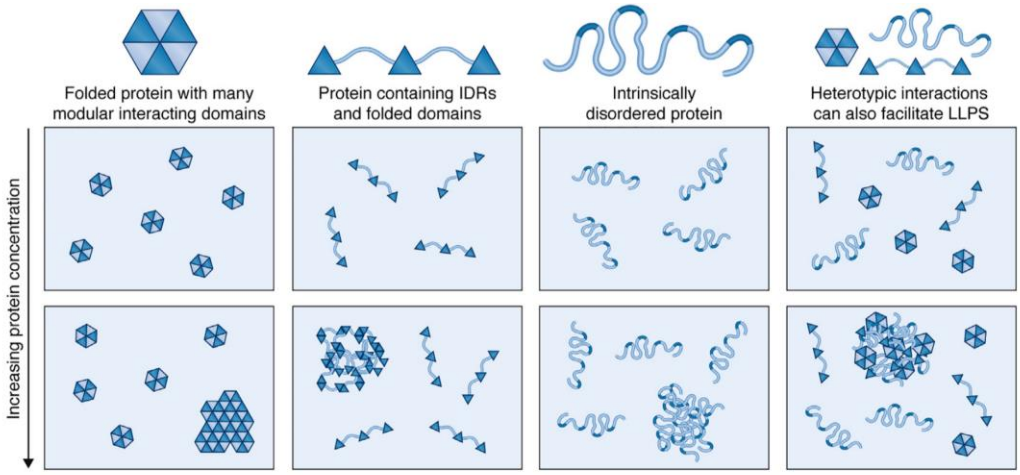

Figure 2: Multivalency is a pivotal mechanism for phase separation. Its properties are taking effect with raising protein concentration. Adapted from Emenecker & Holehouse (2020).

1.1.3 Membrane-less organelles

Overall, PS is a pivotal asymmetrical driving force in biology that contributes to the formation of membrane-less organelles and the further, higher order spatial organization of cellular components/compartments (Figure 3, page 6). The diversification of membrane-bound organelles with membrane-less structures is increasingly recognized as a key mechanism. Biomolecular condensates were shown to even provide an electrochemical potential in the same magnitude as conventional phospholipid bilayer enclosed structures (Posey et al., 2024). That underlies diverse intracellular processes and functions, such as stress granules, P-bodies, chromatin architecture, and nucleoli (Gomes & Shorter, 2019). These structures play essential roles in various cellular processes, including RNA metabolism, signalling, stress response, and degenerative disease. (Boeynaems et al., 2018; Gomes & Shorter, 2019; Mitrea & Kriwacki, 2016). Regime transition of macromolecules from a one-phase to a two-phase state provides infinite cooperative possibilities. Surrounding interactors can easily access these hypersensitive molecular triggers, resulting in efficient behaviour as an environmentally responsive switch (Emenecker & Holehouse, 2022; Yoo et al., 2019).

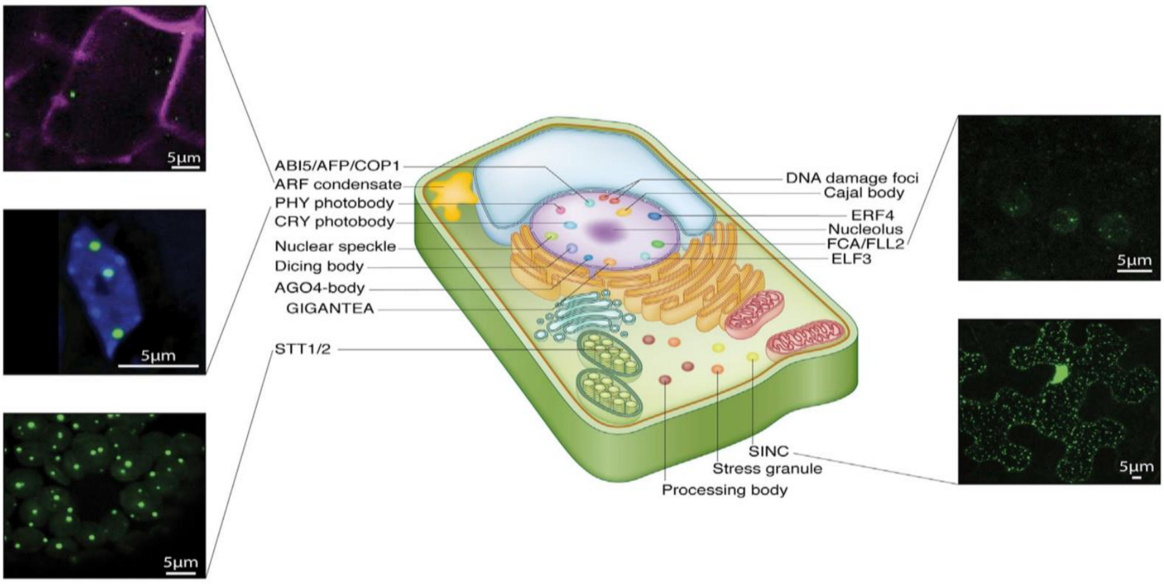

Figure 3: Representative overview of fluorescent labelled phase separated structures in plant cells. From Emenecker & Holehouse (2020).

1.1.4 Liquid condensation of proteins

Due to the reported characteristics of the protein homologs used for experiments in this study, the overall mechanistic focus lies on liquid-to-liquid phase separation (LLPS). Usually, LLPS is a demising of a protein distinct from the solution into dense, protein-rich spherical droplets caused by enrichment of aromatic amino acids and tracks of linear enriched amino acids (Das & Pappu, 2013; Dignon et al., 2020). This process depends on the overall concentration of proteins, pressure, temperature, ions in solution, pH, and detergent (Boeynaems et al., 2018; Emenecker et al., 2020). Importantly, this shift in concentration alters the total volume of the two-component system, simultaneously increasing the volume of the dense phase and decreasing the volume of the usually greater, surrounding diluted phase (Holehouse, 2019). In biological systems such as cells, a pure two-part system can never be assumed, thus complicating the assessment of processes substantially. This suggests that effects reported *in vitro* with single participants under generic buffer systems may not be fully applicable *in vivo* (Choi et al., 2019; Riback et al., 2020).

1.1.5 Intrinsically disordered regions

Protein condensate formation through LLPS is reportedly mediated by macromolecules capable of interacting extensively with their surroundings. This capacity is referred to as multivalence (Banani et al., 2017). In proteins, intrinsically disordered regions (IDRs), provide interactive properties by being not folded into a rigid entity. They exist in a various ensemble of dynamically changing conformations, being volatile in their degrees of freedom and therefore providing increased accessibility (Choi et al., 2019; Emenecker et al., 2020).

Banani et al. (2016) propose a '*scaffold and client*' model, which interprets protein condensates as multimeric complexes dependent on the cross-interaction of the participants. '*clients*', however, localize to the condensate even though they are neither necessary nor sufficient for LLPS assembly (Banani et al., 2016, 2017). Choi et al. (2019) go one step further and assume singular induction of the protein scaffold by a small '*sticker*' (Figure 4), which stands in contrast to the passive 'scaffold and client' model (Choi et al., 2019). For this thesis, interpreting PP2Cs and CO_2 as '*spacer and sticker*' respectively, as suggested by Choi et al. (2019) is appealing, since Zhang et al. (2022) state CO_2 acting as a '*molecular glue*', driving the association of PP2C polypeptides, and sticking together their IDRs. Staples at al. (2023) report CO_2 being a '*client*', participating and favouring the scaffolding of PP2C condensates mediated by CO_2-sensitive IDRs.

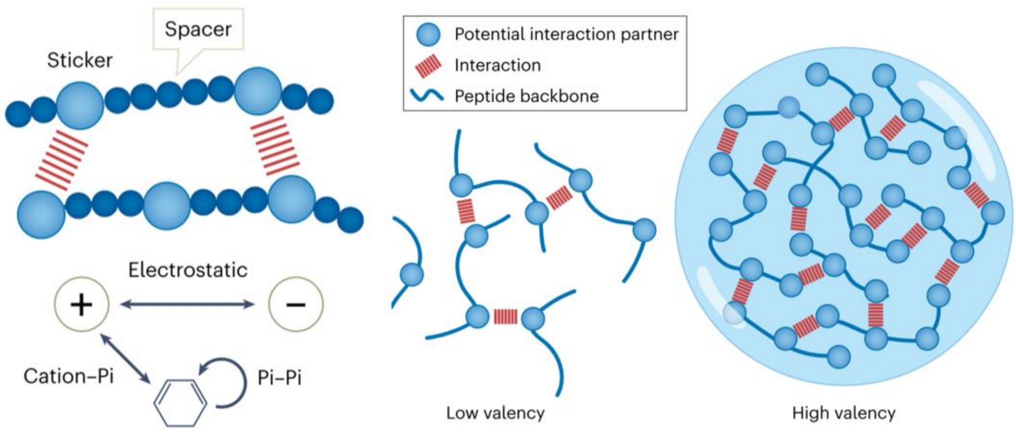

Figure 4: Sticker and Spacer model based on the interactivity of charged (stickers), aromatic (stickers) and hydrophilic (spacers) amino acid residues driving phase separation through multivalent properties in the polypeptide backbone. From Staples at al. (2020).

1.2 Condensation in the PP2C family

1.2.1 CO_2 – a '*molecular glue*'?

It is hypothesized that a set of polar amino acid sequence motifs enriched in serine and threonine residues within terminal IDRs in the PP2C protein family, provide CO_2-responsiveness (Emenecker & Holehouse, 2022; Klepikova et al., 2016; Staples et al., 2023; Zhang et al., 2022). However, the localisation of mentioned IDRs and motifs varies in respect to the phosphatase-active domain in different organisms. A direct interaction of the polar hydroxyl residues in serine and threonine is theorised to interact with the $C^{\delta+}{=}O^{\delta-}$ bond polarity of CO_2 molecules, despite CO_2 being hydrophobic (Kevin Leung et al., 2007; Zhang et al., 2022). This is speculated to increase local protein concentration by sticking sensitive IDRs together (Figure 5) (Zhang et al., 2022). However, this feature is not characteristic to all PP2Cs but presents in a smaller set of functionally conserved orthologs which have been identified by high-throughput screening and IUPred/UniProt based genome analysis using PLAAC, IUPred and local CIDER (Fuchs et al., 2013; Staples et al., 2023; Zhang et al., 2022). However, as Emenecker & Holehouse (2022) point out, the theory for the process for CO_2-induced LLPS on a molecular level has not been empirically proven yet and remains elusive.

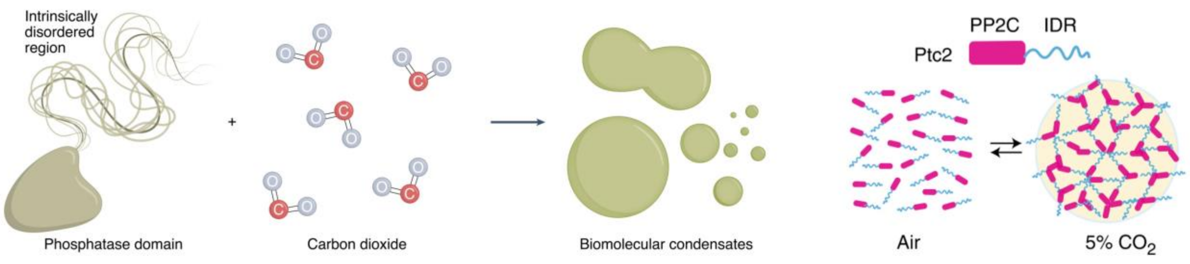

Figure 5: Scheme of the suggested hypothetical mechanism of CO_2 triggered phase separation by Protein Phosphatases Type 2C. Modified from Emenecker & Holehouse (2022, left) and Zhang et al. (2023, right).

1.2.2 PP2C condensation in fungi

In *Candida albicans*, an opportunistic human fungal pathogen that is a well-suited study organism for CO_2-sensing due to its pathogenic ability to grow in a wide range of CO_2 levels from 0.04 %/400 ppm (atmospheric concentration) up to 5 %/50,000 ppm (in host), dynamic formation of liquid condensates approximately 2 µm in diameter has been observed (Zhang et al., 2022). CO_2-driven, prion like domain dependent condensation of Ptc2 *in vivo* and phenotypic switching from white to opaque tuned by CO_2 levels *in vitro* was shown (Figure 6) (Zhang et al., 2022). Zhang e al. (2022) also showed that a deletion of the IDR in the Pt2c PP2C family member rendered *C. albicans* CO_2-insensitive, which was correlated to the lack of Pt2c condensates under high CO_2 conditions and a lower phosphatase activity. This study uncovered PP2C condensation being involved in environmental sensing and gene regulation up to translational control (Zhang et al., 2022). The ability to sense, modulate, and respond to CO_2 changes is crucial for the ecological fitness of an organism. Furthermore, as a previously underestimated process, PS plays various roles in fungal physiology, including regulation of autophagy, cell signalling pathways, transcriptional circuits, and establishment of asymmetry (Staples et al., 2023).

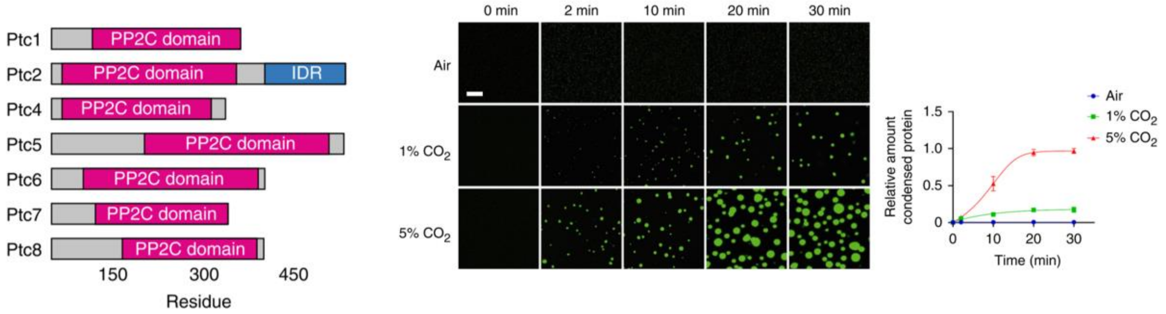

Figure 6: CO_2 and IDR dependent phase separation of the PP2C Ptc2. From Zhang et al. (2022).

1.2.3 PP2C condensation in plant

Surprisingly so, PS and connected CO_2 sensing has not been studied in plant systems. However, sensing and reacting to changing conditions is even more crucial for plants since they are unable to move and change their surrounding's conditions by relocation (Emenecker et al., 2020). So far, PS of plant PP2C homologs has solely been detected *in vitro* (Zhang et al., 2022). Zhang et al. (2022) purified two GFP-fused PP2C protein variants of *A. thaliana*; Arabidopsis Phosphatase Type 2C 3 (AP2C3, also named PP2C5 in literature) and 1 (AP2C1) from *E. coli*. Among 80 PP2Cs analysed, only AP2C3 and PP2C74, another more distant related homolog, was predicted to carry IDRs with polar P-regions but not prion like domains enriched in threonine and serine. However, only AP2C3 was shown to form condensates in an optical *in vitro* essay under higher CO_2 concentrations (1 %/10,000 ppm), unlike AP2C1 which lacks the functional IDR and was unable to respond to elevated CO_2 (Figure7) (Zhang et al., 2022). The other IDR-containing PP2C, PP2C74, was not investigated in respect to condensate formation in the same study.

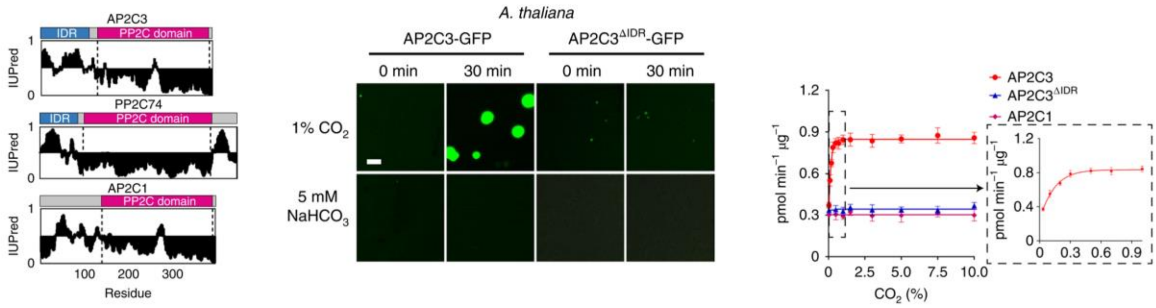

Figure 7: CO2 and IDR dependent phase separation of the PP2C AP2C3. From Zhang et al. (2022).

1.2.4 Background of AP2C3

AP2C3 is as a Mn^{2+}/Mg^{2+} dependent mitogen-activated protein kinase (MPK) phosphatase involved in stress-signalling, reportedly colocalised and interacting with stress-induced MPK3, MPK4 and MPK6, mostly in the nucleus (Brock et al., 2010; Cundari et al., 2009). Furthermore, it has been found by overexpression studies that AP2C3 induces ectopic proliferation of epidermal cells, which promotes stomata development in *A. thaliana*, and positively regulates seed germination, stomatal aperture, and abscisic acid-induced gene expression (Brock et al., 2010; Umbrasaite et al., 2010). This tight connection with developmental and environmental tuning suggests wide involvement of LLPS in plant signalling and its importance in CO_2 sensing (Emenecker et al., 2020).

1.2.5 Biological relevance of CO_2

Besides serving as the primary substrate for photosynthesis and biomass production, CO_2 functions as an important signalling molecule across various domains of life (Ainsworth & Long, 2005; Foyer & Noctor, 2020; Hall et al., 2010; Phelan et al., 2021; Wu et al., 2019). In plants it affects dynamics of guard cells and therefore opening and closing of stomatal pores which further modulates the ability to detect environmental and internal signals. It is crucial for plants to efficiently manage CO_2 uptake and the simultaneous loss of water caused by elevated opening of stomata. Therefore, to ensure optimal growth and survival, plants must maintain a balance of gas and water vapor exchange. This sensitive equilibrium is maintained by a complex signalling network mostly mediated by mitogen-activated protein kinases (MPKs) within guard cells that form stomata, largely influenced by the interplay between CO_2 levels and other crucial factors such as water availability, light intensity, and pathogen presence. In a recent study by Takahashi et al. (2022) the formation of a protein complex of MPK4/12 with the high leaf temperature 1 (HT1) protein kinase has been revealed to be triggered by elevated CO_2 and bicarbonate (HCO_3^-). HCO_3^- is an important intracellular signal molecule related to the CO_2 sensing pathway where CO_2 is imported by aquaporins and further converted into HCO_3^- by carbonic anhydrases, forming a reversible equilibrium (Grondin et al., 2015; Hu et al., 2009a). Dimerization of HT1 and MPK4/12 results in the inhibition of HT1, which is surprisingly not dependent on MPK's kinase activity (Takahashi et al., 2022; Yeh et al., 2023). Umarasite et al. (2010) and Brock et al. (2010) showed that PP2C clade B members such as AP2C2, AP2C3 and AP2C4 dephosphorylates MPK3, MPK4 and MPK6. Since both AP2C3 and MPK4/12 have been shown to be the CO2 sensor or as a constituent of the sensor, we hypothesise that an AP2C3:MPK4/12 module may also involve in CO_2/HCO_3^--sensing in plants. Figure 8 shows a summary of the enzymes active in the guard cell CO_2 signalling pathway.

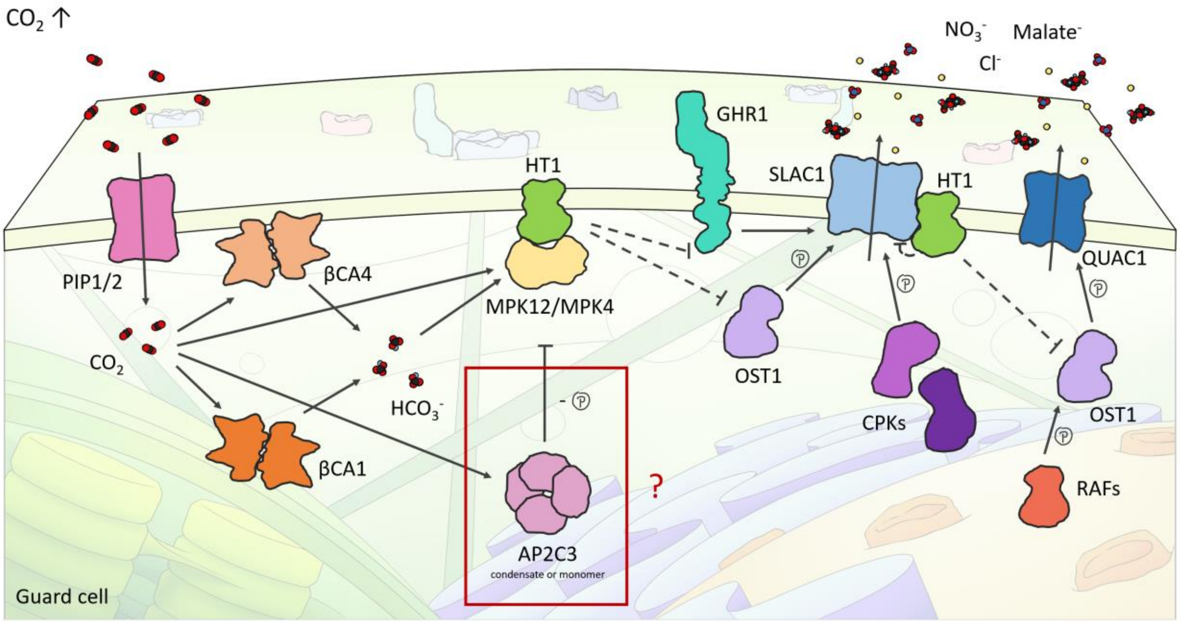

Figure 8: CO_2 signaling pathway in guard cells. Graphical summary of the suspected role of the Arabidosis Phosphatase Type 2C 3 in the on the current state of knowledge based suggested molecular CO_2 sensing pathway in guard cells. All interactions are supported by experimental findings although relations highlighted in the red rectangle are hypothetical (Hõrak et al., 2016; Hsu et al., 2018; Hu et al., 2009; Jakobson et al., 2016; Jalakas et al., 2021; Merilo et al., 2013; Nuhkat et al., 2021; Tõldsepp et al., 2018; Vahisalu et al., 2008; Zhang et al., 2020; Zhang et al., 2022). *Umarasite et al. (2010) and Brock et al. (2010) show that AP2C3 desphosphorylates MPK4 among others, suggesting direct interagction with very closely realted MPK12. It is unclear whether AP2C3 monomers or condensates would play a role in this pathway. Condensate formation is driven by molecular CO_2 (Zhang et al. 2023). Bicarbonate may inhibit PS of AP2C3 due to it's negative charge. Graphic designed by Triinu Arjus, modified.*

1.3 *A. thaliana's* PP2C gene family

1.3.1 PP2C phylogenetics and general characteristics

The PP2C gene family contains 78 coding genes and 109 non-redundant protein splice forms (Xue et al., 2008). It is separated into 13 major phylogenetic subfamilies, numbered A to L and all of them carry the catalytic phosphatase domain at the C-terminus (Schweighofer et al., 2004a; Xue et al., 2008). Most PP2Cs play a functional role in multiple tissues and their primary role lies in stress tolerance response (Xue et al., 2008). AP2C3 and AP2C1 are both clade B members, together with AP2C2, AP2C4, AP2C5, and AP2C6, whereas the PP2C74 homolog mentioned by Zhang et al. (2022) is a clade E member and therefore not as closely related to AP2C3 (Schweighofer et al., 2004a; Xue et al., 2008; Zhang et al., 2022). AP2C1/2/3/4 carry a kinase interaction motif (KIM) docking site on their N-terminus and AP2C2 is characterized by a serine enriched region proceeding the docking site (Schweighofer et al., 2004).

1.3.2 Expression levels, function & localization

Data from a high-resolution map of the *A. thaliana* developmental transcriptome based on RNA-seq profiling by Klepikova et al. (2016) reports that the expression levels of AP2C1 and PP2C74 are high at all developmental stages (Table 1). Total reads of RNA for others are low, whereby expression varies highly between developmental stages and tissue types, thus making it difficult to compare (Klepikova et al., 2016). Overall, however, a common characteristic is the major native expression of selected PP2C homologs in guard and mesophyll cells of leaves, cell types of high interest in respect to CO_2 signalling. This has been determined with the TraVa Gene expression profile database (http://travadb.org/) and BAR webservice (http://bar.utoronto.ca/). The intracellular localization of PP2C homologs is not determined with 100 percent accuracy, but clear focal regions of enriched concentrations have been reported by bimolecular fluorescence complementation (BIFC) interaction assays with MPKs (Brock et al., 2010; Fuchs et al., 2013; Tsugama et al., 2012; Umbrasaite et al., 2010).

Table 1: Overall specifications of used homologs. Overall homolog specifications collected from primary literature verified empirically, expression data summarized from a high-resolution map of the Arabidopsis thaliana developmental transcriptome based on RNA-seq profiling (Brock et al., 2010; Fuchs et al., 2013; Klepikova et al., 2016; Schweighofer et al., 2004b, 2007; Tsugama et al., 2012; Umbrasaite et al., 2010, 2011; Xue et al., 2008)*. Values for expression level in vivo are representing raw absolute RNA read counts for the whole, fully developed third leaf to maintain comparability. IDR: threonine and serine enriched and classified as being CO2 responding by Zhang et al. (2022).*

Homolog	Locus / Gene	Cellular Localization	Clade	cDNA [bp]	Polypeptide Length [aa]	MW [kDa]	Isoelectric Point	IDR	Expression level in vivo
AP2C1	AT2G30020	Chloroplast/Plastid	B	1185	396	42.4	7.92	No	13457
AP2C2	AT1G07160	Chloroplast	B	1167	380	40.7	7.38	No	1
AP2C3	AT2G40180	Nucleus, Mitochondrion	B	1332	390	42.6	6.53	Yes	2
AP2C4	AT1G67820	Chloroplast, Nucleus	B	1332	445	49.4	8.32	No	41
PP2C74	AT5G36250	Nucleus, Plasma Membrane	E (a)	1383	448	49.3	7.89	Yes	1193

2 AIM OF THE THESIS

Based on the recent findings of AP2C3 being able to sense CO2 via liquid-to-liquid phase separation (LLPS) *in vitro* and MPK4/12 being part of the CO_2/bicarbonate sensor *in planta*, we hypothesise that AP2C3 may regulate MPK4/12-mediated CO_2 sensing via LLPS *in planta*.

Therefore, following aims for this thesis can be stated:

1. **Reproduction** of published results from Zhang et al. (2022) by *in silico* characterisation and expression of selected PP2C homologs to further develop a reproducible CO_2 controlled imaging system for reliable detection of condensation of PP2Cs *in vitro*.
2. **Determination** of CO_2 driven LLPS of further selected closely related PP2C homologs *in vitro*.
3. **Extension** of PP2C related condensation studies to *in planta* systems, further demonstration and examination of CO_2 dependent condensate dynamics *in planta*.
4. **Connecting** the PP2C family to the guard cell CO_2 signalling pathway via MPKs by a BiFC assay.

3 EXPERIMENTAL PART

3.1 MATERIALS AND METHODS

3.1.1 Materials

Sequential List of materials and their origin provided in the appendix (page 59).

3.1.2 Methods

3.1.2.1 In silico polypeptide analysis

3.1.2.1.1 Sequence alignment

A multiple sequence alignment of AP2C1, AP2C2, AP2C3, AP2C4 and PP2C74 was performed using the web based Clustal Omega (1.2.4) (https://www.ebi.ac.uk/jdispatcher/msa/clustalo) service for phylogenetical analysis (Madeira et al., 2022). Native polypeptide sequences were obtained for each gene using the mentioned locus in Table 1 (page 11) from the UniProt (https://www.uniprot.org/) databank in FASTA file format. Due to the big difference of PP2C74 to all other homologs two alignments were generated. Their serine/threonine enriched regions, overall similarity, and conserved regions were analysed manually. All sequences are reported as reviewed on UniProt (SwissProt). Used sequences are provided in the appendix (page 53).

3.1.2.1.2 Structural analysis

Predicted folding of selected polypeptides was obtained from AlphaFold2 Protein Structure Data Base (https://alphafold.ebi.ac.uk/) and screenshots providing the best viewing angle on unstructured domains were saved from entries on 22.04.2024 (16:30). Based on that, an overall assessment and comparison of homologs was performed to further categorize expected properties. For used entries' UniProt codes see Table 2. The open-source online lab book service Benchling® 2024 (https://www.benchling.com/) was used for further analysis and visualization of recombinant DNA, plasmids, constructs, and fusion protein sequences.

Table 2: UniProt codes for used homolog sequences and structural studies. Used names for similar homologs vary in literature.

Homolog	Gene	UniProt code	Other names
AP2C1	AT2G30020	O80871	PP2C25
AP2C2	AT1G07160	Q8RX37	PP2C2
AP2C3	AT2G40180	Q9XEE8	PP2C30, PP2C5
AP2C4	AT1G67820	Q9FXE4	PP2C14
PP2C74	AT5G36250	Q9FG61	PP2C74

3.1.2.2 In vitro condensate studies

3.1.2.2.1 *E. coli* system

3.1.2.2.1.1 Cloning

Coding sequences of AP2C1 (AT2G30020), AP2C3 (AT2G40180), AP2C4 (AT1G67820) and PP2C74 (AT5G36250) with a yellow fluorescent protein (YFP) cDNA and a coding sequence for a 6x histidine-tag located on the 5'-end were PCR amplified from 35S:(gene)-YFP/pCAMBIA1390 template plasmids (provided by Yuh-Shuh Wang and Oleksii Yadlos). All primers used are listed in Table 3 (page 15), and were synthesised by the Integrated DNA Technologies, Inc.. For AP2C1-YFP/AP2C4-YFP the forward primer introduced a *Bam*HI recognition site and the reverse primer an *Eco*RI site for cloning. For AP2C3-YFP/PP2C74-YFP the forward primer introduced a *Sal*I site and the reverse primer a *Not*I site. PCR mixtures contained 0.5 µL of each primer (10 µM), 0.4 µL of 10 mM dNTPs (Thermo Scientific™), 0.2 µL of Phusion DNA Polymerase (Thermo Scientific™), 4 µL of 5× HF Phusion Buffer (Thermo Scientific™) and varying amounts of template DNA with a total volume of 20 µL. PCR program settings of the thermos cycler (Aeris™ TAS™ Thermo Cycler, Peltier Technology) were as follows: a first denaturation step at 98°C for 30 seconds, followed by 3 cycles of denaturation at 98°C for 10 seconds, primer annealing at 53°C for 15 seconds and extension at 72°C for 30 seconds. Additional 27 cycles were carried out with a higher annealing temperature at 58°C. A final extension step at 72°C for one minute was also added. Depending on their purity, PCR products were either PCR purified, or gel purified using the FavorPrep™ PCR Purification Mini Kit (FAVORGEN® Biotech Corporation), following the manufacturer's manual. DNA was eluted with 36.5 µL of elution buffer. Purified PCR products (~35.5 µL) were digested with appropriate restriction enzymes by adding 4 µL of 10X FastDigest buffer (Thermo Scientific™) and 0.25 µL of each restriction enzyme (FD *Bam*HI, FD *Eco*RI, FD *Sal*I, FD NotI, Thermo Scientific™) and incubated at 37 °C for at least 1 h. The pET28a plasmid was digested with 0.5 µL of appropriate REs in a final volume of 20 µL. The digests were purified using the FavorPrep™ PCR Purification Mini Kit and ligation was set up for 20 minutes at room temperature (RT) with 0.2 µL of digested pET28a vector, 1 µL of digested insert, 1 µL of 10X ligase buffer (Thermo Scientific™), 0.2 µL of T4 DNA ligase (Thermo Scientific™) and 7.6 µL ddH$_2$O in a final volume of 10 µL. Subsequently, *E. coli* (DH10β) transformation was performed by adding 100 µL of competent cells to 10 µL ligation mixture. After incubation on ice for 15 minutes and heat-shock treatment in a 42 °C water bath for 90 seconds the samples were cooled down immediately on ice for 2 minutes. Subsequently, 300 µL of liquid LB medium was added and the mixture was incubated at 37 °C for 30 min before plating on solid LB medium containing kanamycin antibiotic (50 µg/mL). Plates were incubated at 37 °C overnight. A positive colony verified by colony PCR for each construct was selected and cultured in 4 mL of liquid LB and 50 µg/mL kanamycin antibiotic in an incubator at 37 °C and 220 rpm overnight. Plasmid was extracted following the FavorPrep™ Plasmid Extraction Mini Kit procedure (FAVORGEN® Biotech

Corporation) and quantified with a NanoDrop 2000 spectrophotometer (Thermo Scientific™) by loading 1.6 µL and sent for verification by Sanger sequencing. Sequence analyses and alignments were conducted in Benchling.

Table 3: Detailed cloning specifications of E. coli expression templates.

cDNA	Template	Primer	Primer sequence	Primer info	Final product
AP2C1-YFP	35S:AP2C1-YFP/pCAMBIA1390	XIX-09 f	aaggatccTCTTGCTCCGTCGC	AP2C1_BamHI	AP2C1-YFP/pET-28a
		XIX-13 r	ctgaattctaagcgtaatctggaacatc	HAstop_EcoRI	
AP2C3-YFP	35S:AP2C3-YFP/pCAMBIA1390	XIX-07 f	aagtcgaCAACTCTCAAAGAATCCGAT	AP2C3_SalI	AP2C3-YFP/pET-28a
		XIX-21 r	ctgcggccgctaagcgtaatctggaacatc	HAstop_NotI	
AP2C4-YFP	35S:AP2C4-YFP/pCAMBIA1390	XIX-10 f	aaggatccACTAATAAACTTCGCTCAGAA	AP2C4_BamHI	AP2C4-YFP/pET-28a
		XIX-13 r	ctgaattctaagcgtaatctggaacatc	HAstop_EcoRI	
PP2C74-YFP	35S:PP2C74-YFP/pCAMBIA1390	XIX-06 f	aagtcgactcGGGTCCTGCTTATCATCA	PP2C74_SalI	PP2C74-YFP/pET-28a
		XIX-21 r	ctgcggccgctaagcgtaatctggaacatc	HAstop_NotI	

3.1.2.2.1.2 Expression & extraction

For expression of recombinant PP2C-YFP variants in bacteria, BL21 (DE3) pLysS competent *E. coli* cells (kindly provided by Ivar Ilves) were transformed (PP2C gene)-YFP/pET-28a plasmids following the general protocol as described in chapter 3.1.2.2.1.1. (page 14). The cell suspension was spread on LB plates containing 50 µg/mL kanamycin and incubated over night at 37 °C. Cells were scraped off the plate the next morning and inoculated in 50 mL Difco™ LB Broth (LB) (Lennox) containing 50 µg/mL kanamycin at 180 rpm at 37 °C (Multitron shaker, Infors HT) as a starter culture. Before reaching the log phase, the culture was added to 1 L of LB containing 50 µg/mL kanamycin and directly divided evenly into two 2 L flasks and shaked at 180 rpm at 37 °C. Incubation lasted until an OD_{600} of 0.4 and the shaker was then switched to 18 °C for another hour of incubation. OD_{600} was checked again to not exceed 1. Isopropyl β-d-1-thiogalactopyranoside (IPTG) were added for a final concentration of 500 µM to induce protein expression which is controlled by the lac operon. Cultures were left shaking over night at 18 °C and harvested the next day after 20 hours post induction by centrifugation in centrifuge bottles (Nalegene®, 500 mL) at 5000 rpm/4,248 g for 10 min in a Sorvall Lynx 6000 centrifuge (Thermo Scientific™) with a F12-6x500 LEX rotor (Thermo Scientific™). From here on, all steps were performed at 4 °C or on ice. Cell pellets were further resuspended in phosphate buffered saline (PBS), transferred to 50 mL tubes (Thermo Scientific™) and spun down using a 5810R table-top centrifuge (Eppendorf®, A-41-8 rotor) with 4000 rpm until the supernatant was clear. The washed pellet was resuspended in 12.5 mL lysis buffer (25 mM HEPES pH 7.6, 500 mM NaCl, one tablet Roche Protease Inhibitor Cocktail 2 (SIGMA®)) per 50 mL and flash frozen in liquid nitrogen for storage at -80 °C.

Cell lysate was thawed by putting falcons into beakers filled with tap water until only a small amount of ice remained. 1 mg/mL lysozyme (SIGMA Life Science) was added and incubated while slowly spinning for 30 min. *E. coli* cells were disrupted by sonication using a Sonoplus Sonicator (Bandelin Electronics) for three times with 40-50 % power, 40 seconds each. In between repetitions, samples were cooled and mixed for two minutes on ice. For clearing the lysate, the cell suspension was transferred to SS34 centrifuge tubes (Nalgene®) and centrifuged at 20,444 rpm/50,000 g in a Sorvall Lynx 6000 centrifuge (Thermo Scientific™) with a A27-8x50 (Thermo Scientific™) rotor for 30 minutes. Supernatant was flash frozen in liquid nitrogen for storage at -80 °C.

3.1.2.2.1.3 Purification

0.5 mL PureCube 100 Ni-NTA-Agarose (Cube Biotech) were loaded into 10 mL Poly-Prep® chromatography columns (Bio-Rad) and pre-equilibrated by washing it 3 times with 1 mL of N500 wash buffer (25 mM Hepes pH 7.6, 500 mM NaCl, 0.2 mM PMSF, 20 mM imidazole). High grade Milli-Q® (IQ 7000, LC-Pak, Millipore) was used for all buffers and washing steps. Resin was again resuspended in 0.5 mL N500 buffer and added to extracts for batch binding. Extract was slowly mixed with the resin for 1 h, resuspended and loaded into columns. Flow through was collected. Settled resin was washed for 3 times with N500 buffer with 10 column volumes and 2 times with N300 low imidazole (Fisher Scientific) wash buffer (25 mM Hepes pH 7.6, 300 mM NaCl, 20 mM imidazole). Protein was eluted with N300 elution buffer (25 mM Hepes, pH 7.6, 300 mM NaCl, 300 mM imidazole) in 8x 500 µL fractions. Fractions and resin were checked under UV light for fluorescence and successful elution. Fractions were flash frozen in liquid nitrogen for storage at -80 °C.

3.1.2.2.2 Bac-to-Bac® baculovirus expression system in insect cells

The overall procedure was performed following the Bac-to-Bac® Baculovirus Expression System User Guide from Invitrogen™ (life technologies™) (Technologies, 2015).

3.1.2.2.2.1 Cloning

pFastBac™ recombinant constructs with a Twin strep (Tstrep)-mVen-TEV-(*PP2C-gene*)/pFastBac1 general architecture were prepared for expression of PP2C coding genes in *Spodoptera frugiperda* (Sf9) insect cells. The overall procedure was conducted similarly as explicitly described in chapter 3.1.2.2.1.1. (page 14). Following Protocol changes were applied: Primers were designed to amplify the coding sequence of the PP2C gene with a stop codon and are listed in Table 4 (page 17). The forward primer introduced a *Bst*XI recognition site and the reverse primer a *Bcu*I site. For digestion, 0.25 µL FD *Bcu*I and FD *Sal*I (Thermo Scientific™) were added to each PP2C PCR product in a 20 µL reaction. As accepting vector, a Tstrep-mVen-TEV-MPK12/pFastBac1 plasmid, provided by Yuh-Shuh Wang, was digested with FD *Bst*XI and FD *Bcu*I to replace the MPK12 with the PP2C gene. The digested vector and PP2C insert were purified, ligated with T4 DNA ligase, and used to transform *E. coli* as described in chapter 3.1.2.2.1.1. (page 14). Transformed *E. coli* was plated on LB agar plates with ticarcillin (80 µg/mL) as a more stable substitute of ampicillin.

Table 4: Detailed cloning specifications of insect cell expression templates.

cDNA	Template	Primer	Primer sequence	Primer info	Final product
AP2C1	35S:AP2C1-YFP/pCAMBIA1390	XIX-26 f	cttccaaATGTCTGGTTCTTGCTCCGTCGCC	AP2C1_BstXI	Tstrep-mVen-TEV-AP2C1/pFastBac1
		XIX-27 r	cgactagtcaTATGAACTGGCGTAAAGGG	AP2C1_BcuI	
AP2C3	35S:AP2C3-YFP/pCAMBIA1390	XIX-28 f	cttccaaATGTCTGGTCAACTCTCAAAGAATCCGATC	AP2C3_BstXI	Tstrep-mVen-TEV-AP2C3/pFastBac1
		XIX-29 r	cgactagtcaTGGAAGAAAGTTTTGTAGCTG	AP2C3_BcuI	
AP2C4	35S:AP2C4-YFP/pCAMBIA1390	XIX-30 f	cttccaaATGTCTGGTACTAATAAACTTCGCTCAGAAG	AP2C4_BstXI	Tstrep-mVen-TEV-AP2C4/pFastBac1
		XIX-31 r	cgactagtcaGCCTTTGTAATGGTTGAGAT	AP2C4_BcuI	
PP2C74	35S:PP2C74-YFP/pCAMBIA1390	XIX-32 f	cttccaaATGTCTGGTGGGTCCTGCTTATCATCAT	PP2C74_BstXI	Tstrep-mVen-TEV-PP2C74/pFastBac1
		XIX-33 r	cgactagtcactctttggttgggacatatac	PP2C74_BcuI	

3.1.2.2.2.2 Bac-to-Bac™ transformation / Bacmid assembly

For bacmid assembly, 1 µL of purified pFastBac-vector (about 300 ng) each was used to transform DH10Bac™ competent *E. coli.* The general protocol described in 3.1.2.2.1.1 (page 14) was used. Competent cells were kindly provided by Ivar Ilves. Transformed cell cultures were plated on LB agar plates containing 50 µg/mL kanamycin, 7 µg/mL gentamicin, 10 µg/mL tetracycline, 100 µg/mL X-gal (*Phyto*Technology Laboratories®) and 40 µg/mL IPTG. Naked baculovirus DNA was then purified from positive (white) bacterial colonies cultured over night with all appropriate antibiotics using an Invitrogen™ Purelink™ purification kit (life technologies™).

3.1.2.2.2.3 Transfection & viral amplification

Frozen Sf9 cell aliquots were kindly provided by Ivar Ilves. Cells were thawed and multiplied for further steps and grown at 27 °C without a raised CO_2 atmosphere and were dislodged from the surface by simple washing with a stream of media. EX-CELL® 420 (Merck®) serum free media warmed up to 27 °C was used for all steps. Cells were multiplied on a 10 cm cell culture petri dish (Greiner Bio-One GmbH) and checked for acceptable condition and division activity. $8x10^5$ Sf9 cells were transfected with the naked, dried bacmid DNA pellet dissolved in 100 µL media and 5 µL thoroughly mixed transfection 007 Reagent (Icosagen®). Transfection was carried out on a 6-well tissue cell culture dish (Corning), by adding the mix in drops after plated cells have settled (30 min). Each well incubated with approximately 2 mL of media. After 4 h, the media was replaced. For each PP2C variant one well was infected, together with a negative control. Virus containing media was collected after 4 days, spun down at 1500 rpm in a 5810R table-top centrifuge (Eppendorf®, A-41-8 rotor) for 7 min, transferred to a new tube and stored at 4 °C and protected from light as P1 stock. Two more rounds of amplification were required to reach sufficient viral titre. P2 stock was prepared by infection of $8x10^6$ Sf9 cells with 0.5 mL of P1 on a 10 cm cell culture dish. The stock was directly added to the 10 mL media after cells settled. P2 stock was harvested after 3 days. Harvested media was treated as described above and stored as seed stock at 4 °C in the dark. For P3 stock amplification, 100 µL of P2 were added to a 30 mL media on a 15 cm cell culture petri dish (Sarsted). $20x10^6$ cells were plated on the petri dish and let settle down for 30 min before use.

3.1.2.2.2.4 Expression & extraction

55.5 mL of Sf9 culture in logarithmic phase with a concentration of 10.8×10^6 cells/mL were mixed with 30 mL of fresh P3 stock each and the final volume was adjusted to 300 mL with fresh media in separate 1 L cell culture flasks. The with 2×10^6 cells/mL started cultures were grown for 48 h at 27 °C with 135 rpm shaking. To harvest cells, cultures were gradually cooled down to 4 °C while centrifuging in a Sorvall Lynx 6000 centrifuge (Thermo Scientific™) equipped with a F12-6x500 LEX rotor (Thermo Scientific™) at 2000 rpm/680 g for 10 min twice in 500 mL centrifuge bottles (Nalgene®). All following steps were performed on ice or at 4 °C. Pellets were washed with ice-cold PBS and spun down in a 5810R table-top centrifuge (Eppendorf®, A-41-8 rotor) twice at 2000 rpm for 7 min. Pellets were resuspended in 15 mL lysis buffer (25 mM Hepes NaOH pH 7.6, 500 mM NaCl, 0.1% Tween 20 (Fisher BioReagents™), 1 mM DTT (Serva), 1x Roche Protease Inhibitor Cocktail 2 (SIGMA®)). High grade Milli-Q® (IQ 7000, LC-Pak, Millipore) water was used for all buffers and washings. Samples were checked under UV light for fluorescence and flash frozen in liquid nitrogen for storage at -80 °C.

Cell lysate was thawed and subsequently homogenised with a 40 mL Dounce grinder and B pestle (Kontes Glass CO.) by applying 15 strokes. The grinder was kept on ice and precooled. For clearing the lysate, the cell suspension was transferred to SS34 centrifuge tubes (Nalgene®) and centrifuged at 20,444 rpm/50,000 g in a Sorvall Lynx 6000 centrifuge (Thermo Scientific™) with a A27-8x50 rotor (Thermo Scientific™) for 20 minutes. The supernatant was transferred to fresh 50 ml centrifuge (Thermo Scientific™).

3.1.2.2.2.5 Purification

To prepare Strep-Tactin® XT 4Flow® high-capacity resin (IBA Lifesciences Gmbh) with a capacity of 14 mg/mL for batch binding, 4x 0.5 mL resin were preequilibrated with N500 wash buffer (25 mM Hepes NaOH pH 7.6, 500 mM NaCl, 0.1% Tween 20 (Fisher BioReagents™), 1 mM DTT (Serva), 0.2 mM PMSF (Thermo Scientific™)). Protein extract was added, and tubes were incubated on a rotator, mixing it slowly for 1 h. The resin beads were spun down in a table-top centrifuge at 3000 rpm for 5 min and the supernatant was removed. The beads were suspended in a small amount of N500 wash buffer and transferred to a 10 mL Poly-Prep® chromatography column (Bio-Rad) and washed 4 times with 10 column volumes of N500 wash buffer. Protein was eluted with N500 elution buffer (25 mM Hepes NaOH pH 7.6, 500 mM NaCl, 0.1% Tween 20 (Fisher BioReagents™), 50 mM biotin (VWR Life Science)) in 8x 500 or 600 µL fractions into 1.5 mL Protein LoBind Eppendorf Tubes®. Fractions and resin were checked under UV light for fluorescence and flash frozen in liquid nitrogen for storage at -80 °C.

3.1.2.2.3 Protein Quantification

For overall analysis of proteins in 10 % SDS polyacrylamide gels, all protein samples from various stages of purifications were mixed with 2x SDS-PAGE sample buffer, boiled at 100 °C for 10 min and stored at

-20 °C. 3-5 µL of samples were run together with a 10-180 kDa prestained protein molecular weight standard ladder (Thermo Scientific™) in self-cast gels using gel equipment from Bio-Rad. A current of 150 V was applied until the dye in the sample passed the barrier from the stacking to the resolution gel. For separation of proteins, a current of 180 V was applied for approximately 1 h. Gels were stained with Page Blue Protein Staining Solution (Thermo Scientific™) and scanned in an Epson Perfection V800 Photo scanner.

For protein quantification on a SDS-PAGE gel, at least 4 different concentrations of BSA standard (provided by Ivar Ilves) were loaded alongside the samples on the same gel. Scanned pictures were used to quantify the intensity of protein bands based on a formerly established BSA standard curve using Fiji software (ImageJ). Specifically, the signal intensity of the selected peak at the expected molecular weight was measured. A regression function was established using BSA standard measurements from the same gel and the equation was used for approximation of expressed protein amounts. Values were corrected for BSA overestimation with a value of 0.6 and for the real loaded protein volume. Calculations and regressions were performed in Excel | Microsoft 356®. Molarity of protein solution was quantified after dialysis into physiological buffer.

Following equation was used for further approximate fraction's molarity:

$$\mu M = \frac{c\ [\mu g * mL^{-1}]}{MW\ [kDa]}$$

Table 5: Molecular weights of used fusion proteins for determination of fraction molarity.

Expressed protein	Molecular weight [kDa]
AP2C1-YFP	74.3
AP2C3-YFP	75.3
AP2C4-YFP	81.2
PP2C74-YFP	83.7
Tstrep-mVen-TEV-AP2C1	74.7
Tstrep-mVen-TEV-AP2C3	74.9
Tstrep-mVen-TEV-AP2C4	81.6
Tstrep-mVen-TEV-PP2C74	83.2
AP2C3-YFPn	54.0
AP2C4-YFPn	60.8
MPK11-YFPc	62.6
MPK12-YFPc	62.6

3.1.2.2.4 Buffer exchange & storage

Expressed protein was aliquoted into 50 µL aliquots before storing at -80 °C in a high salt elution buffer for long term storage. All dilutions and aliquots were prepared in 0.5 mL Protein LoBind Eppendorf Tubes®. Prior to imaging experiments, a buffer exchange was carried out by using Slide-A-Lyzer® Dialysis Casettes with molecular weight cut-off of 10 kDa and capacity of 0.5 - 3 mL (Thermo Scientific™). The low salt plant physiological buffer contained 20 mM Tris–HCl pH 7.5, 15 mM NaCl, 135 mM KCl, 1.5 mM MgCl2. Cassettes were kept in 2 L physiological buffer at 4 °C while being gently stirred, buffer was exchanged after 5 h and samples extracted on the following day. Only one fraction for each construct was dialysed at a time. For short term storage, dialysed solutions were stored at 4 °C for up to 5 days. Samples stored at - 80 °C were used with only 1 freeze-thaw cycle.

3.1.2.2.5 Imaging

500 µL (5 µM) protein solutions were prepared freshly for each studied homolog from thawed, previously dialysed samples using ice cold 10x physiological buffer. It is crucial, not to stress the protein with salt/buffer concentrations that divert from the original concentrations too much in one step. For example, if one protein sample is very concentrated and only 1-10 µL was to be added to a final volume of 500 µL, the dilution should be executed in two steps (e.g. a 1:10 dilution followed by a 1:50 dilution if 1 µL of native protein solution is added). Samples were centrifuged at 4 °C at max speed in an Eppendorf table-top centrifuge prior to imaging to remove any potential aggregates from the solution. If no additional CO_2 was applied, imaging was performed at room temperature (RT) and ~300-400 ppm CO_2. Utilized glass slides and sample vessels varied throughout the process (see result).

3.1.2.2.5.1 Fluorescent microscope

A custom-built Zeiss Fluorescent Microscope System was used for imaging experiments with low range elevated CO_2 concentrations. The system consisted of a CoolLED pE-4000 fluorescent light source, set to emit 490 nm light. Excitation light was directed through a polychroic mirror (69002bs, Chroma) transparent in the following regions: 420-470 nm, 509-550 nm, and 595-750 nm (more than 90%). An emission filter with the bandwidth of 525/36 was used for imaging YFP (Ex/Em λ: 513/530) and mVenus (Ex/Em λ: 515/527) fluorescent tags. Image sequences were captured using a Zeiss EC Plan-NEOFLUAR 40x/0.75 objective and excitation duration was chosen by the program automatically. Emission filters were controlled by a LUDL MAC6000 Filter Wheel System. The microscope was controlled by VisiView software (Visitron Systems). Fiji (ImageJ) was used to analyse images and time lapse videos.

CO_2 conditions were controlled by a custom build CO_2 pump (constructed by Andres Punn). Samples were incubated in a small chamber with an atmospheric pressure of ~100 ppm for low CO_2 conditions and a humidity of 100 %. High humidity was provided by applying wet soaked filter papers onto the wall of the imaging chamber. For high CO_2 conditions, ~3000 ppm CO_2 were applied. CO2 concentrations and humidity were measured with a Li-850 CO_2/H_2O Gas Analyzer from LI-COR® through a tube directly accessing the imaging chamber. Samples were loaded on custom built imaging chambers which consisted of a conventional coverslip and microscopy glass slides with a spacer of two layers of double-sided tape on two opposing sides in between as depicted in. Images were acquired right on the edge of the coverslip/glass at the phase barrier from liquid phase to the surrounding air.

3.1.2.2.5.2 Laser scanning confocal microscope

To gain higher resolution and gas accessibility, protein solutions were examined using a Zeiss LSM 900 laser scanning confocal microscope operated by ZEN blue version 3.7 (Zeiss). Both mVenus and YFP tagged recombinant proteins were excited with a single 488 nm laser set to a power of 0.2-1.5 %, depending on overall fluorescence intensities. The detection spectrum was set for 410-650 nm. A Zeiss Plan-Apochromat 20x/0.8 M27 objective was used. Signal was acquired by a GaAsP-PMT1 photomultiplier. The pinhole was set to 1 AU with a varying gain from 500-700. Scanning speed was set as fast as possible while maintaining an acceptable resolution. Very high solution is not overly crucial, but being able to follow and identify single particles is. To apply high CO_2 conditions a Pecon® Integrated XLmulti S2 Incubator system was used. Additionally, high CO_2 concentrations of ~10,000 ppm (1%) and ~50,000 ppm (5%) were applied using a Lab-Tek™ S compact heating insert (Pecon®) and PM 2000 RBT© incubator lid (Pecon®). Although samples were not heated, the heating insert was used for thorough fixation of microscopy slides, vessels, and petri dishes to the LSM 900's ASI PZ-2000 XYZ Series Automated Stage with a Piezo Z-Axis Top Plate. The incubator pump, which is linked to a Zeiss CO_2-module, was set to a low level (1-2) in ZEN. A certain set of microscopy slides and multi well plates described in 3.2.3.2 (page 34) was covered with gas permeable foil (Sigma-Aldrich, Diversified Biotech). For analysation of condensation and aggregation dynamics, Z-stacks were recorded. However, for final qualitative assessment, only single slice snap shots without maximum projection or further enhancements were considered. Settings for recorded images varied, but 2146x1246 pixels with a 16-bit depth were commonly used.

3.1.2.3 In planta localization & condensation studies

3.1.2.3.1 Plant maintenance

Nicotiana benthamiana (tobacco) plants were seeded in plastic pots filled with a mixture of peat and perlite mixed in a 2:1 ratio and were kept in a short-day growth room with a photoperiod of 10 hours, temperature of 23 °C at daytime and 21 °C at night. LED Tube lamps (Phillips) emitted a photosynthetic photon flux density of 120 µmol photons $m^{-2}s^{-1}$. Air humidity was controlled to a level of 55 %. Approximately 4-week-old tobacco plants were used for infiltration.

3.1.2.3.2 *Agrobacterium tumefaciens* transformation

For transformation of *N. benthamiana* plants, the *Agrobacterium tumefaciens* strain GV3101 was transformed with selected plasmids (Holsters et al., 1980; Koncz & Schell, 1986). p35S:AP2C1-YFP/pCAMBIA1390, p35S:AP2C3-YFP/pCAMBIA1390, p35S:AP2C4-YFP/pCAMBIA1390, p35S:PP2C74-YFP/pCAMBIA1390 plasmids were formerly cloned by Oleksii Yadlos and introduced by a heat-shock treatment into *A. tumefaciens*. Approximately 500 ng of plasmid was added to an aliquot of 100 µL competent cells, followed by 15 min incubation at 36 °C. 300 µL of LB medium was added before mixtures were incubated at 28 °C for 1 h. After plating of cell transformation reactions on agar LB plates containing gentamicin (50 µg/mL) and kanamycin (µg/mL) and incubation in plastic bags for two days at 28 °C. Additionally, a glycerol stock of *A. tumefaciens* carrying a P19/pCAMBIA1390 gene silencing suppressor plasmid (provided by Yuh-Shuh Wang) was streaked on an agar LB plate containing kanamycin (µg/mL) and gentamicin (50 µg/mL) and incubated for two days in plastic bags at 28 °C. Plates were stored at 4 °C in plastic bags.

Table 6: Combinations of constructs/plasmids for intracellular localisation experiments.

Combination	PP2C gene	Supressor
1	p35S:AP2C1-YFP/pCAMBIA1390	P19/pCAMBIA1390
2	p35S:AP2C3-YFP/pCAMBIA1390	P19/pCAMBIA1390
3	p35S:AP2C4-YFP/pCAMBIA1390	P19/pCAMBIA1390
4	p35S:PP2C74-YFP/pCAMBIA1390	P19/pCAMBIA1390

3.1.2.3.3 Tobacco infiltration

When plants were ready for infiltration, positive colonies were cultured in 1 mL liquid LB medium (kanamycin 50 µg/mL, gentamycin 50 µg/mL) in a shaker (28 °C, 220 rpm) overnight. Fresh infiltration buffer containing 10 mM $MgCl_2$, 10 mM MES pH 5.6 and 200 µM acetosyringone was prepared on the following day. For preparation of the infiltration mixture, an *Agrobacterium* strain carrying a PP2C gene variant was added to 1 mL of infiltration buffer together with the strain containing the P19 gene. An appropriate amount of each bacterial culture was added to the buffer directly for a final OD_{600} of 0.05 or 0.1 of each strain. After 2 h incubation in darkness, agrobacterial mix was applied to leaves using 1 mL syringes (NORM-JECT®-F Luer Solo, B. Braun) without a needle-tip. Infiltrated regions were marked, and plants were put back into the short-day growth room for 2 or 3 days, respectively before imaging.

3.1.2.3.4 Imaging

Prior to confocal examination, leaves were checked for even transformation with a Zeiss SteREO fluorescent stereomicroscope equipped with a HXP 120 lighting unit and PlanApoS 1.5x FWD 30mm objective. On the LSM 900 confocal microscope, EC Plan-Neofluar 10x/0.30 M27, Plan-Apochromat 20x/0.8 M27, and Plan-Apochromat 63x/1.40 Oil DIC M27 objectives from Zeiss were used. For imaging with the 63x oil immersion objective, Immersol™ 518 F immersion oil from Zeiss was used. Samples were excited with a 488 nm laser set to 0.5-2 % intensity. Three acquisition channels for image acquisition were set up, resulting in a merged image showing YFP emission, autofluorescence of chlorophyll and cell structures in conventional phase contrast. Recombinant YFP linked to PP2C variants was excited with a wavelength of 508 nm and the detection spectrum was set for 410-599 nm. Autofluorescence (chlorophyll A) was excited with a wavelength of 655 nm and the detection spectrum was set for 599-700 nm. The gain for the detecting GaAsP-PMT1 photomultiplier was set to 625 V and the pinhole was set to 1 AU. An ESID detector, collecting 400 nm wavelength light, was set up additionally with a digital signal gain of 10.1 for conventional phase contrast images. Samples were prepared on conventional microscopy glass slides. Small, rectangular pieces of leaf tissue were cut out of the infiltrated regions using a scalpel and put onto the glass slide together with water. A quadratic coverslip was settled onto the leaf piece, while making sure to trap as little air bubbles as possible. The prepared glass slide was then turned upside down for imaging. The top cell layer of leaf was imaged. In case of presence of condensates, it was necessary to lower the gain and laser power substantially. Overexposure was prevented by lowering the laser power ½ or ¼ of the initial value and applying 100-150 V gain less.

To study CO_2 dependent condensate dynamics, plants were incubated with low (100 ppm) and high CO_2 (800 ppm) prior to imaging using a custom-built device. Another custom-built device was used for transporting cut leaves in a low CO_2 environment (100 ppm) and storing them until they were imaged. Cut leaf samples were prepared as fast as possible and imaged right away. Furthermore, leaves were incubated in the microscopes CO_2 incubator at 1 % and 5 % CO_2 with and without being covered with a coverslip. This was managed by taping the cut leaf's section to the class slides with double sided tape.

3.1.2.4 Bimolecular fluorescence complementation study (BiFC)

3.1.2.4.1 Plant maintenance

See chapter 3.1.2.3.1 (page 21).

3.1.2.4.2 Cloning

For this experiment, selected PP2C homolog constructs fused to a split YFP-c part have been formerly prepared by Oleksii Yadlos. MPK11/12 fusions with split YFP-n for interaction dependent complementation of the fluorescent domain remained to be cloned. For preparation of these constructs, 35S:MPK12-YFPn/pCAMBIA1390 and 35S:MPK11-YFPn/pCAMBIA1390 were prepared by ligation independent cloning (LIC). Insert amplification was performed as described in chapter 3.1.2.2.1.1 (page 14). MPK11/pPR3-N and MPK12/pPR3-N templates, provided by Yuh-Shuh Wang, were used. Two rounds of PCR were performed to add a 15 bp adaptor sequence for LIC. The first primers were designed to anneal only to the gene of interest with partial LIC adaptor sequence, while a pair of universal primers with a full LIC adaptor sequence was used for the 2nd round of PCR. Primers were synthesised by Microsynth AG. 31.8 µL purified PCR products were incubated for five minutes at RT with 0.2 µL T4 DNA Polymerase (Thermo Scientific™), 4 µL 10X FD buffer (Thermo Scientific™), and 4 µL 10mM dCTP (Fermentas) followed by purification. For 35S:YFPn/pCAMBIA1390 vector preparation, 35S:YFPn/pCAMBIA1390 was linearized with FD *Eco*72I (Thermo Scientific™) followed by PCR purification. Next, 20 µL vector were treated for five minutes at RT with 0.2 µL T4 DNA Polymerase, 4 µL 10X FD buffer, 4 µL 10mM dGTP (Fermentas), and 13.8 µL ddH_2O followed by PCR purification (FAVORGEN® Biotech Corporation). The prepared insert was mixed with vector and incubated for 10 min. Plasmid amplification, purification and quantification was performed following the general protocol described in chapter 3.1.2.2.1.1 (page 14).

Table 7: Detailed cloning specifications of BiFC templates.

(c)DNA	Template	Primer	Primer sequence	Primer info	Final product
MPK11	MPK11/pPR3-N	IV-77 f	aactcacgATGTCAATAGAGAAACCATTC	MPK11 BiFC	
		IV-78 r	acacacgcacAGGGTTAAACTTGACTG	MPK11 BiFC	
MPK12	MPK12/pPR3-N	IV-08 f	aactcacgATGTCTGGAGAATC	MPK12 BiFC	
		IV-09 r	acacacgcacGTGGTCAGGA	MPK12 BiFC	
MPK11-LIC	MPK11	III-37 f	AATTCTCTAACTCACGATG	LIC-BiFC	35S:MPK11-YFPn/pCAMBIA1390
		III-38 r	CTCACCATTAACACACGCAC	LIC-BiFC	
MPK12-LIC	MPK12	III-37 f	AATTCTCTAACTCACGATG	LIC-BiFC	35S:MPK12-YFPn/pCAMBIA1390
		III-38 r	CTCACCATTAACACACGCAC	LIC-BiFC	

3.1.2.4.3 *Agrobacterium tumefaciens* transformation

Transformation of *Agrobacterium* was performed following the protocol as in 3.1.2.3.2. (page 21). 35S:AP2C1-YFPc/pCAMBIA1390, 35S:AP2C3-YFPc/pCAMBIA1390, 35S:AP2C4-YFPc/pCAMBIA1390, 35S:PP2C74-YFPc/pCAMBIA1390, 35S:MPK11-YFPn/pCAMBIA1390, 35S:MPK12-YFPn/pCAMBIA1390, and P19_35S:Nuc-mCherry-HA/pCAMBIA1390 plasmids were added to GV3101 aliquots.

3.1.2.4.4 Tobacco infiltration and experiment repetition

Infiltration of tobacco leaves was performed following the in chapter 3.1.2.3.3. (page 22) described protocol. In general, one *Agrobacterium* strain carrying a PP2C gene fused to the C-terminal split part of YFP was combined with a strain carrying a MPK variant fused to the N-terminal split part of YFP. To every mixture a third strain carrying the cDNA for the P19 gene silencing suppressor and a nuclear localized Nuc-mCherry fluorescent tag was added. The final OD_{600} for each strain in mixtures was 0.025. Interaction of different combinations were tested in independent experiments. Samples were examined 2- and 3-days post-infiltration to take variation in expression levels into account.

Table 8: Combinations of constructs/plasmids used for BiFC experiments.

Combination	PP2C gene	MPK gene	Suppressor/nuclear control
1	35S:AP2C3-YFPc/pCAMBIA1390	35S:MPK11-YFPn/pCAMBIA1390	P19_35S:Nuc-mCherry-HA/pCAMBIA1390
2	35S:AP2C3-YFPc/pCAMBIA1390	35S:MPK12-YFPn/pCAMBIA1390	P19_35S:Nuc-mCherry-HA/pCAMBIA1390
3	35S:AP2C4-YFPc/pCAMBIA1390	35S:MPK11-YFPn/pCAMBIA1390	P19_35S:Nuc-mCherry-HA/pCAMBIA1390
4	35S:AP2C4-YFPc/pCAMBIA1390	35S:MPK12-YFPn/pCAMBIA1390	P19_35S:Nuc-mCherry-HA/pCAMBIA1390
5	35S:AP2C1-YFPc/pCAMBIA1390	35S:MPK11-YFPn/pCAMBIA1390	P19_35S:Nuc-mCherry-HA/pCAMBIA1390
6	35S:AP2C1-YFPc/pCAMBIA1390	35S:MPK12-YFPn/pCAMBIA1390	P19_35S:Nuc-mCherry-HA/pCAMBIA1390
7	35S:PP2C74-YFPc/pCAMBIA1390	35S:MPK11-YFPn/pCAMBIA1390	P19_35S:Nuc-mCherry-HA/pCAMBIA1390
8	35S:PP2C74-YFPc/pCAMBIA1390	35S:MPK12-YFPn/pCAMBIA1390	P19_35S:Nuc-mCherry-HA/pCAMBIA1390

3.1.2.4.5 Imaging

The LSM 900 laser scanning confocal microscope equipped with a Plan-Apochromat 20x/0.8 M27 objective from Zeiss was used for image acquisition. Samples were excited with a 488 nm laser for detection of complemented YFPn/c (Ex/Em λ: 508/524) and a 561 nm laser for detection of the mCherry (Ex/Em λ: 587/610) nuclear control. Detection spectra were set up in two channels for sequential scanning to prevent bleed through. YFPn/c pairs were detected with a bandwidth of 400-

578 nm and mCherry with a bandwidth of 578-649 nm. Used intensities were not fixed and needed to be adjusted for each experiment to ensure optimal signal and prevent overexposure. At least five non-overlapping, randomly selected regions of three leaves were examined for each combination. All parameters were kept identical for all samples examined on the same day.

3.1.2.4.6 Quantification and statistical analysis

Nuclear globular structures were identified by creating a mask based on the nuclear mCherry control using the “analyze particles” function in Fiji (ImageJ). By this, all cell structures and scattered light that do not match a certain size and circular structure in the detected spectrum were excluded from the following intensity measurement. The mask was applied subsequently to the YFP channel which allowed direct comparison of intensity (total number of pixels) measurements. Lower and upper thresholds were adjusted depending on protein expression and scattered light which caused fluctuation of signal strength. Thresholds were kept constant for each independent experiment. The code for the used Macro is provided in the appendix (page 56). Measured intensity values were further analysed in Excel | Microsoft 356® and R Studio (4.4). Data was normalized for variability in transformation and expression by calculating a YFP/mCherry signal ratio for each measured nucleus to provide comparability within the experiment. For experimentally paired measurements, a t-test has been performed to test for statistically significant difference of averages of YFP/mCherry signal ratios with a significance level of $p < 0.05$.

3.1.2.4.7 Western Blot

Around 30 mg of infiltrated leaf samples were collected and ground under repeated liquid nitrogen flash freezing and beating with glass beads. Leaf powder was solubilized and boiled at 100 °C in 60 µL of freshly prepared extraction buffer (24 mM EDTA pH 8.0, 100 mM Tris–HCl pH 6.8, 4% w/v SDS, 864 mM β-mercaptoethanol, 20% v/v glycerol, and 0.005% w/v bromophenol blue) for 10 min (Tsugama et al., 2011). After centrifugation at max speed for 10 min, 8 µL of each sample were loaded on a 10% SDS polyacrylamide gel together with a 10-180 kDa prestained protein ladder (Termo Scientific™). Proteins were transferred onto a PVDF membrane (Immobilon-P). Immunodetection of HA-tagged proteins was carried out with 1:10000 diluted monoclonal mouse Anti-HA.11 Epitope Clone:16B12 antibody from BioLegend in 1 % fat free skimmed milk (Valio) followed by incubation with 1:5000 goat-anti mouse IgG (H+L) horseradish peroxidase conjugated (Invitrogen™) secondary antibody prepared in 1 % BSA (Fisher Scientific). Protein bands were developed with a chemiluminescent detection kit (Amersham ECL Western Blotting Analysis System) on AGFA CP-BU NEW Medical X-Ray film (blue). All reagents were kindly provided by Ivar Ilves.

3.2 RESULTS & DISCUSSION

Besides Arabidopsis Phosphatase Type 2C (AP2C) 3, which has been reported by Zhang et al. (2022) to form CO_2 induced condensates *in vitro*, also Protein Phosphatase Type 2C (PP2C) 74 was examined this study as a second potential PP2C homolog forming biomolecular condensates. PP2C74 was predicted *in silico* to carry motifs supporting LLPS by Zhang et al. (2022) but not tested experimentally. AP2C1, AP2C2 and AP2C4, the closest related clade B homologs of AP2C3, were selected as negative controls for phase condensation studies.

3.2.1 *In silico* polypeptide analysis

3.2.1.1 Sequence alignments

To investigate potential sequence differences between AP2C1, AP2C2, AP2C3 and AP2C4 homologs that could cause the unique CO_2-sensitivity of AP2C3 and resulting phase condensation, a BLAST sequence alignment was performed. Overall, sequences are quite different, but the enzymatically active phosphatase domain and 11 amino acids spanning motif within the N-terminal IDRs are conserved in length and functionally similar amino acids. Substrate specificity of PP2Cs could be an explanation for the sequence variation. AP2C3 contains a unique, 18-amino acid long extension of the N-terminus. This domain could be of further interest since it carries 3 lysine residues. Lysine is reportedly important for CO2 sensing of proteins via carbamylation (Meigh, 2015). However, further functional classification requires more elaborate sequence analysis tools. The overall distribution of serine/threonine residues at the N-terminus was also assessed since Zhang et al. (2022) stated a local enrichment of these residues could drive phase separation. A certain level of serine residue conservation and enrichment within the N-terminal IDR regions is visible. At this stage however, it is not possible to classify them further as the distribution appears to be random in a simple sequence alignment. Length variations of the polypeptide backbone are deposited on the N-termini, which are less conserved than C-termini. The small highly conserved region is located approximately in the middle of IDRs of AP2C1/2/3/4 (for AP2C1 from residue 96 to 105). The consensus sequence KRKXXXXLXI for the four homologs matches the consensus sequence architecture [(K/R)$_{3–4}$,X$_{1-6}$,(L/I),X,(L/I)] for a kinase interaction motif (KIM) published by Ho et al. (2003). This feature is consistent with the finding by Schweighofer et al. (2004) that PP2C clade B members possess unique MPK binding sites and provides the basis for interaction of these phosphatases with MPKs (Ho et al., 2003). The presence of KIMs in clade B PP2Cs also lend support to our hypothesis that selected PP2C homologs may interact with MPK4 and MPK12, which constitute the CO2/bicarbonate sensor together with the HT1 kinase to regulate stomatal responses (Takahashi et al., 2022; Yeh et al., 2023).

A second sequence alignment was performed to include PP2C74, which was reported to contain a N-terminal IDR like AP2C3, and thus may also undergo LLPS (Zhang et al., 2022). We were interested in structural similarities of AP2C3 and PP2C74 that could justify similar behaviour. PP2C74 proved to be most distantly related to all other homologs and is therefore perturbing the alignment quality, but a part of the conserved KIM-sequence is also visible in PP2C74. It lacks however the second part of the recognition site, and one lysine is substituted with arginine. This suggests that the motif is rendered nonfunctional. Protein sequence alignments are provided in the appendix (page 54 & 55).

3.2.1.2 3D structure

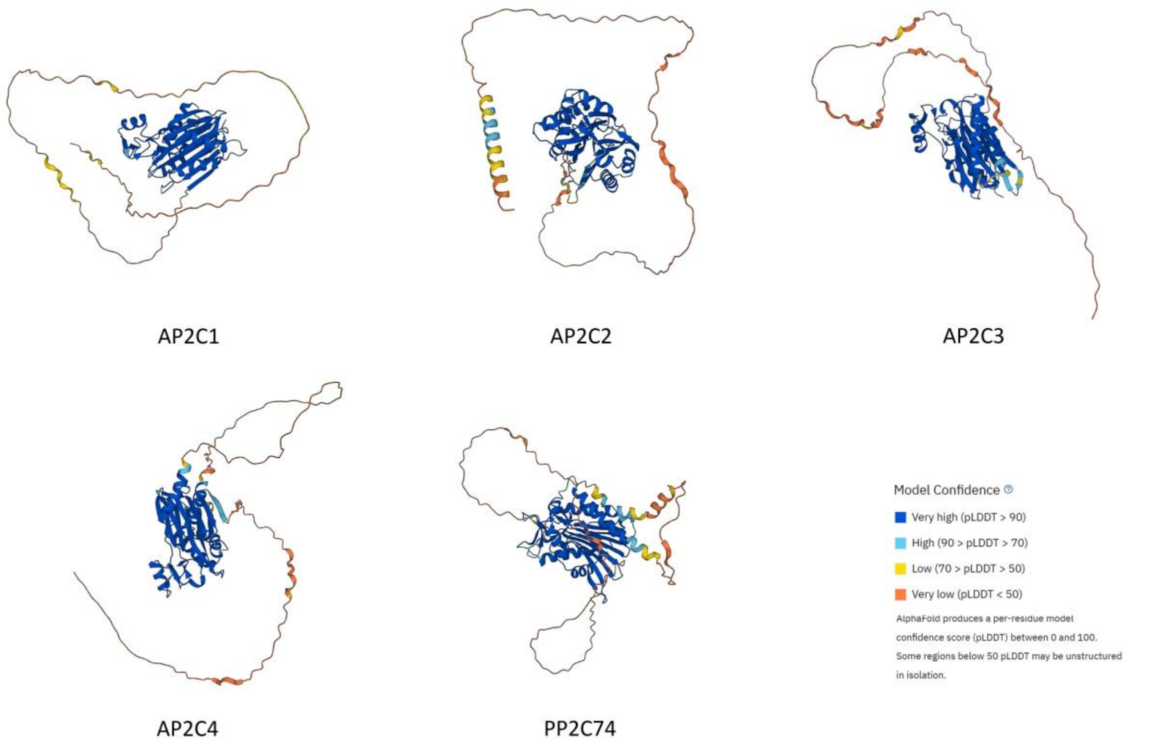

Figure 9: Reviewed Alpha Fold 3D model predictions of selected PP2C homologs. From Alpha Fold Protein Structure Databank (https://alphafold.ebi.ac.uk, 22.04.2024, 12:35)

AlphaFold generates predictions based on a per-residue model confidence score (pLDDT) between 0 and 100. Predicted regions below 50 pLDDT may be unstructured in isolation and are characterised by existing in an ensemble of structural conformations. Therefore, the N-termini of AP2C1-4 and PP2C74 appeared to be unstructured. This stands in contrast to classifications by Zhang et al. (2022) (Figure 7, page 9). The authors state that CO_2 responsiveness depends on IDRs which are unique to AP2C3 and PP2C74 (Zhang et al., 2022). The N-terminal IDRs based on AlphaFold structural prediction are overall similar in length, except that PP2C74 contains a N-terminal IDR that is approximately half the size of others and only PP2C74 carries an IDR on the C-terminus.

Table 9: Exact locations of mentioned characteristic domains within the polypeptide backbone. Reported numbers based on structural model predicted by AlphaFold.

Homolog	Length [aa]	N-terminal IDR	Additional IDR	Enzym. domain	MPK binding site
AP2C1	396	M1-E128		G139-L392	Yes
AP2C2	380	M1-G112		G122-L376	Yes
AP2C3	390	M1-K116		Y128-L385	Yes
AP2C4	445	M1-A109	R343 - P404	G120-L440	Yes
PP2C74	448	M1-T47	N144 – N167, P388-E448	T67-L384	No

AP2C4 and PP2C74 are predicted to carry another probable IDR as insertions within the phosphatase domain, which are highlighted in the sequence alignment in the appendix (page 54). Sequence alignments show a resemblance of insertion sequences of AP2C4 and PP2C74. A graphical display of the serine/threonine residue distribution within the IDR predicted by UniProt shows clear clustering as reported for AP2C3 by Zhang et al. (2022) and compares the size and architecture of IDRs of selected homologs overall. However, it is not possible to verify functionality of these motifs at this stage. IDRs within the phosphatase domains of AP2C4 and PP2C74 were excluded from Figure 10 due to Zhang et al. focusing on the N-terminal IDRs. The globular and rigidly structured phosphatase domain shows a high confidence score of over 90 in all structural models which coincides with its high conservation. It is mostly organized by alpha-helices and beta-sheets. For exact locations of mentioned characteristic domains within the polypeptide backbone see Table 9.

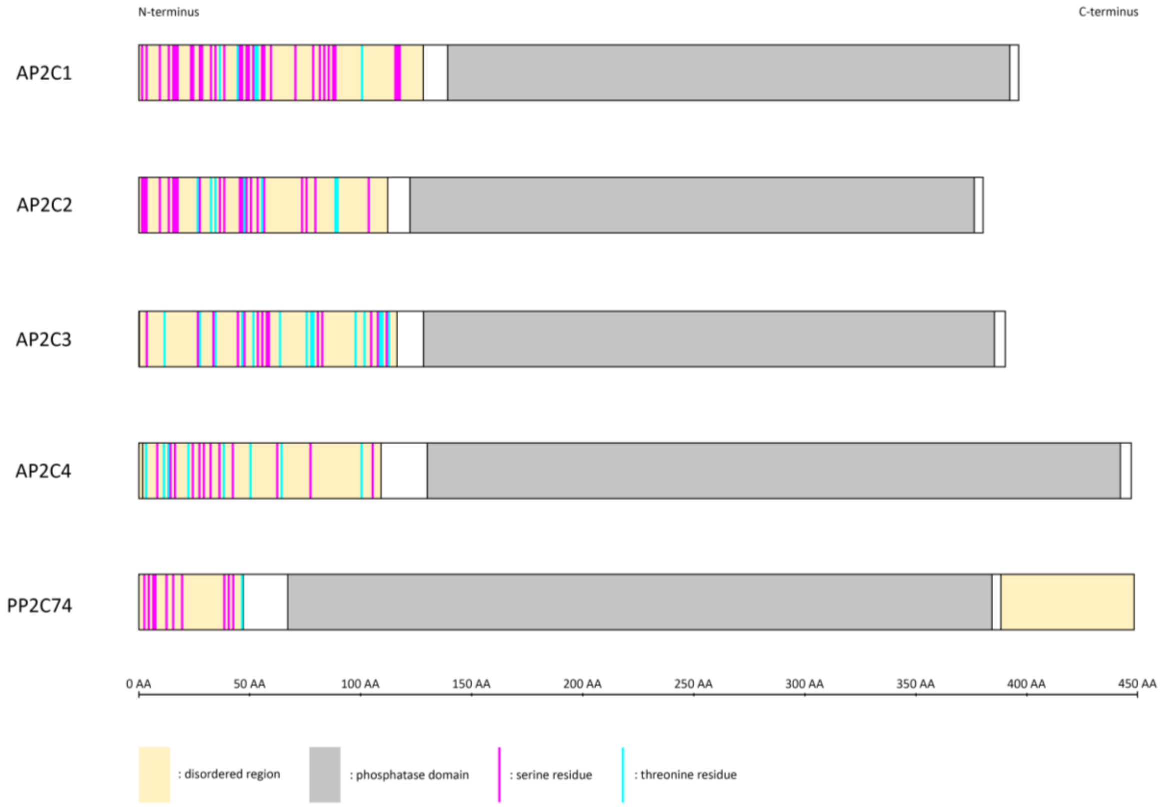

Figure 10: Native protein homolog structure scheme of selected PP2Cs with hihglighted serine and threonineresidues in the N-terminal IDRs to demonstrate enriched clusters. Structural features were categorized based on the probable structure models in the AlphaFold Protein Structure Databank and residues were identified manually

3.2.2 Cloning

AP2C2 cDNA was not available at the beginning of this study and therefore is excluded from the following experiments.

3.2.2.1 pET-28 constructs

We first attempted to express all PP2Cs in *E. coli* since AP2C1-GFP and AP2C3-GFP were successfully purified from *E. coli* by Zhang et al. (2022). We fused PP2Cs with a C-terminal YFP and a N-terminal 6xHis-tag in the pET-28a vector. Cloning of all AP2Cs was successful, but not for PP2C74 despite repeated tries and changing of cloning strategy. A possible explanation could be a leaky promoter activity and toxicity of the PP2C74 protein in *E. coli*. However, this remains to be verified. Notably, Zhang et al. (2023) identified PP2C74 as one of the only two IDR-containing PP2Cs from *Arabidopsis thaliana* but did not examine CO_2-induced LLPS of PP2C74 *in vitro*.

3.2.2.2 pFastBac constructs

Due to unsuccessful cloning of PP2C74 in pET-28a and problems of AP2C3 purification from *E. coli* (discussed below), we switched to the baculovirus/insect cell expression system. All four PP2Cs were successfully cloned into the pFastBac1 vector with a N-terminal twin strep tag-mVenus fusion followed by a TEV protease site (Tstrep-mVen-TEV) to allow cleavage of tags when necessary.

3.2.2.3 pCAMBIA1390 constructs

For *in planta* analyses of sub-cellular localization of PP2Cs and potential interaction with MPKs using bimolecular fluorescence complementation (BiFC) assays, PP2Cs were cloned into a pCAMBIA1390 vector, a T-DNA binary vector that allows agrobacterium-mediated gene expression in plant cells. PP2Cs were fused to a C-terminal YFP for localization studies, whereas PP2Cs and MPKs were fused to split YFPs (YFPc for PP2Cs and YFPn for MPKs) for BiFC assays.

3.2.3 *In vitro* condensate studies

3.2.3.1 Expression & purification

Recombinant protein variants of PP2C homologs were expressed in two different systems fused with fluorescent tags to be studied in *in vitro* imaging experiments. Detailed assessment of protein behaviour at different stages of purification provided first indication of condensation of PP2C homologs.

3.2.3.1.1 Bacterial system

Purification of AP2C1 and AP2C4 fused to a His affinity tagged yellow and fluorescent protein (YFP) was successful with high yield, but some of the protein remained bound to the nickel affinity column even after the elution steps with higher concentrations (500 mM) of imidazole according to the fluorescence.

The yield was significantly lower in case of AP2C3-YFP and it eluted from the column with avery low efficiency, since the column glowed under blue light, but eluted fractions did not (Figure 11). The weak fluorescence of AP2C3-YFP extract during purification already hinted at problems in obtaining intact fusion protein of AP2C3, but not in case for AP2C1 and AP2C4.

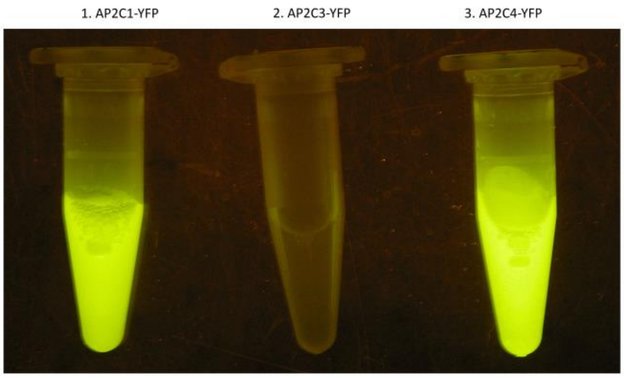

Figure 11: Comparison of eluted fraction #2 of purified homologs under UV light. AP2C3 (# 2) does not show fluorescence.

The molarity of eluted fractions ranged approximately from 12 to 40 µM, while AP2C1-YFP was the most concentrated and AP2C4-YFP the lowest (appendix, page 58). The purity of protein samples was not high (Figure 16, left gel), and the enriched protein was present as more than one species, indicated by three protein bands on the SDS-PAGE around the expected molecular weight of approximately 70 kDa (Figure 12, rectangle #1-3, page 31). Possible explanations for these impurities can be proteolysis or co-purification of chaperons bound to the purified protein. Interestingly, AP2C3 was purified and eluted with decent yield, but only two enriched bands around 70 kDa were visible on the gel (Figure 12, rectangle #4 & #5, page 31). This suggests that only the bound contaminants and proteolytic products of the purified protein were eluted and that full length AP2C3-YFP aggregated and crashed out of solution, rendering it tightly bound to the resin. This is a characteristic problem described in literature for purification of proteins capable of phase separation (Alberti et al., 2019). These proteins are tricky to purify due to their high sensitivity to surroundings and being prone to aggregation at high protein concentrations (Alberti et al., 2019).

Due to the inefficient purification of the most interesting variant - AP2C3-YFP, unsuccessful cloning of PP2C74-YFP, and the overall low purity of the resulting proteins, we switched to an insect cell expression system.

Table 10: Molecular weight of purified recombinant proteins.

Expressed protein	Molecular weight [kDa]
AP2C1-YFP	74.3
AP2C3-YFP	75.3
AP2C4-YFP	81.2
PP2C74-YFP	83.7
Tstrep-mVen-TEV-AP2C1	74.7
Tstrep-mVen-TEV-AP2C3	74.9
Tstrep-mVen-TEV-AP2C4	81.6
Tstrep-mVen-TEV-PP2C74	83.2
AP2C3-YFPn	54.0
AP2C4-YFPn	60.8
MPK11-YFPc	62.6
MPK12-YFPc	62.6

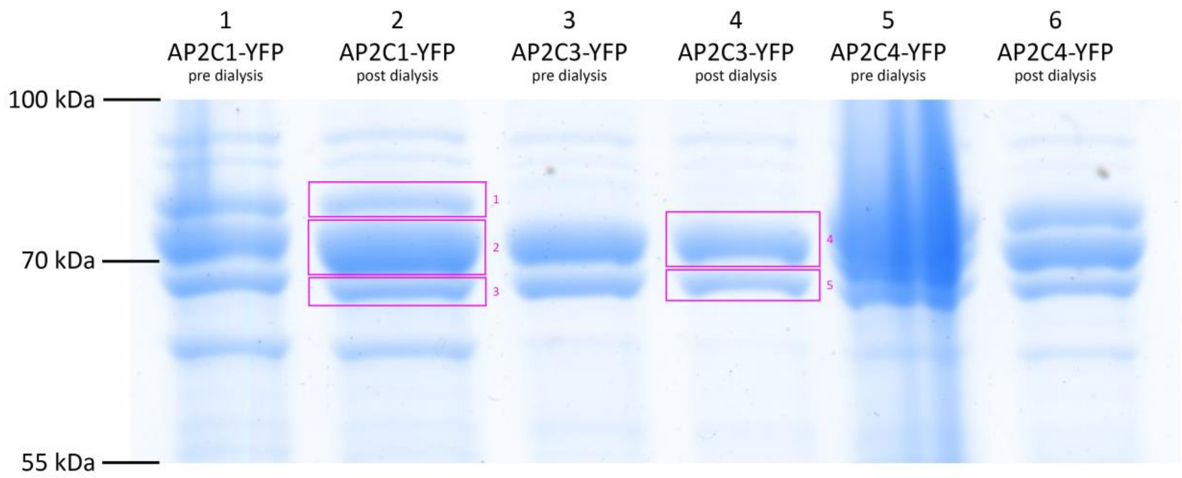

Figure 12: Comparison of purified homologs in E. coli suggesting that full length AP2C3-YFP was not successfully eluted. For exact size of expected purified proteins see table 10. AP2C3 (column 3 & 4) is missing the heaviest species present in case of other homologs. This correlates with absent fluorescent signal under UV-light. For an initial establishment of conditions for a reliable in vitro imaging system, protein fractions were dialysed into physiological buffer. No loss of protein after dialysis (Figure 11, column 2, 4 and 6) in comparison to solutions before dialysis occurred (Figure 11, column 1, 3 and 5). 2 µL of sample loaded.

3.2.3.1.2 Insect cell system

For protein expressed in insect cell, only the PP2C names without the twin-strep(Tstrep)-mVenus-TEV-tag will be mentioned in the following for simplification.

Eluted protein fractions were analysed in SDS-PAGE and yielded acceptable amounts of sufficiently concentrated protein the mobility of which was around the expected molecular weight between 100 kDa and 70 kDa (Figure 13, page 32). AP2C3, however, showed very low signal (#3), suggesting that purification of this protein was unsuccessful or the viral titre in the infection stocks was too low. Colony-PCR was performed with samples from the insect cell expression culture for troubleshooting. Amplified DNA of the coding sequence for the AP2C3 gene is absent (Figure 14, page 32), which indicates that the expression culture was not infected with the virus and therefore expression of protein did not occur.

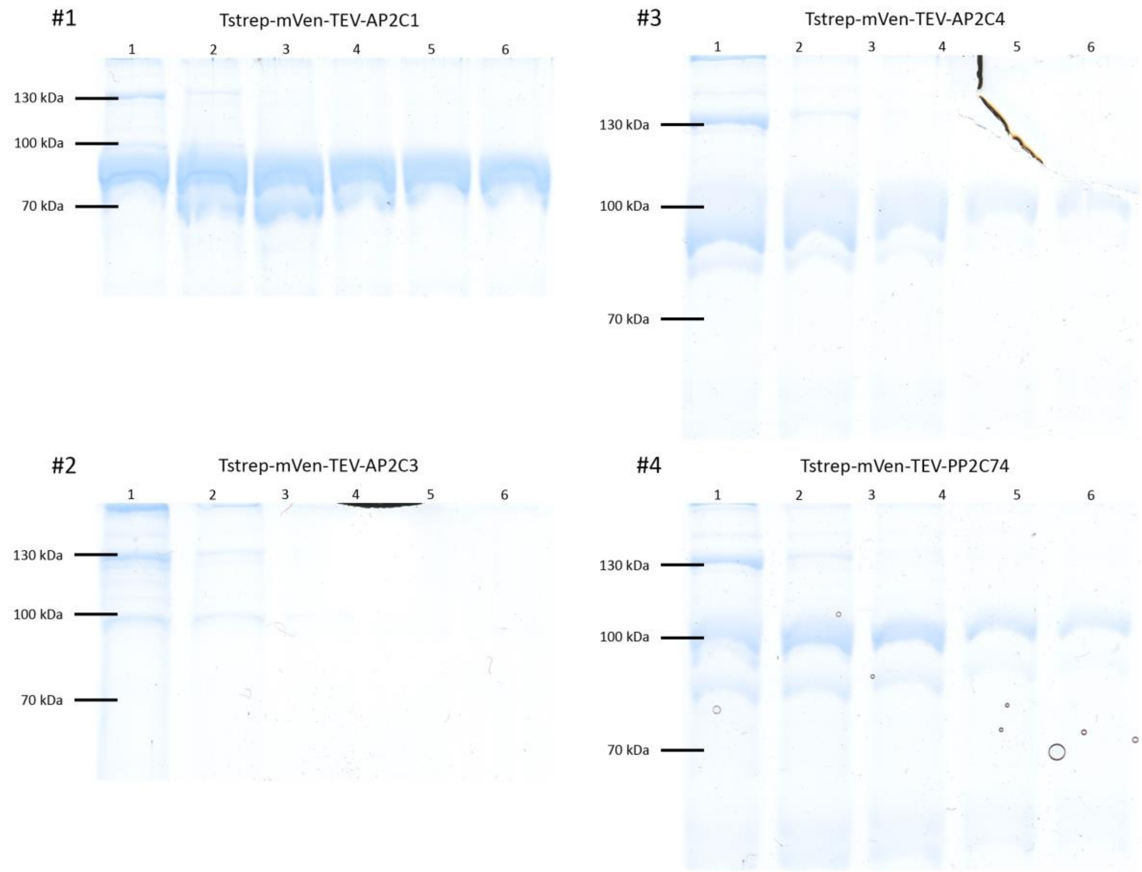

Figure 13: Comparison of 4 variant purification gels loaded with elution fractions #2-7 of purified PP2Cs. Gel samples were collected directly after elution in high salt concentrated buffer. AP2C3 does not show desired bands (#2). Other purifications were successful. Lower visible molecular weight species may be proteolytic products. 2 µL of sample loaded.

Expression and purification of AP2C3 was performed again along with several changes to optimize conditions by Ivar Ilves. For this attempt, the respective baculovirus was constructed again and 0.6 mL pre-equilibrated resin was used dilute the protein more on the resin and lower the risk of aggregation on the column. It was possible to acquire high quality, pure AP2C3 in the 2nd attempt (Figure 15, page 33).

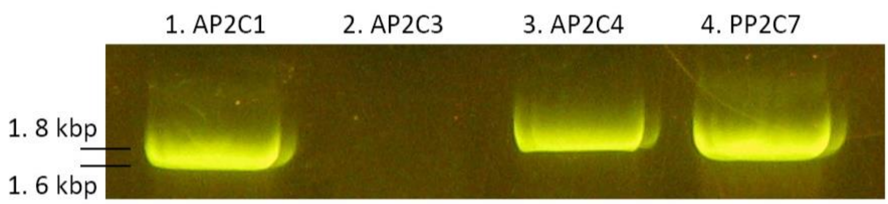

Figure 14: Trouble shooting for unsuccessful purification of AP2C3 in insect cell. Colony PCR products loaded onto 1 % agarose gel picture to test for transcription of PP2C-variant cDNA. Primers annealing to the bacmid backbone and mVenus tag were used. AP2C3 does not show amplification, hence culture was not infected, and construct was not expressed.

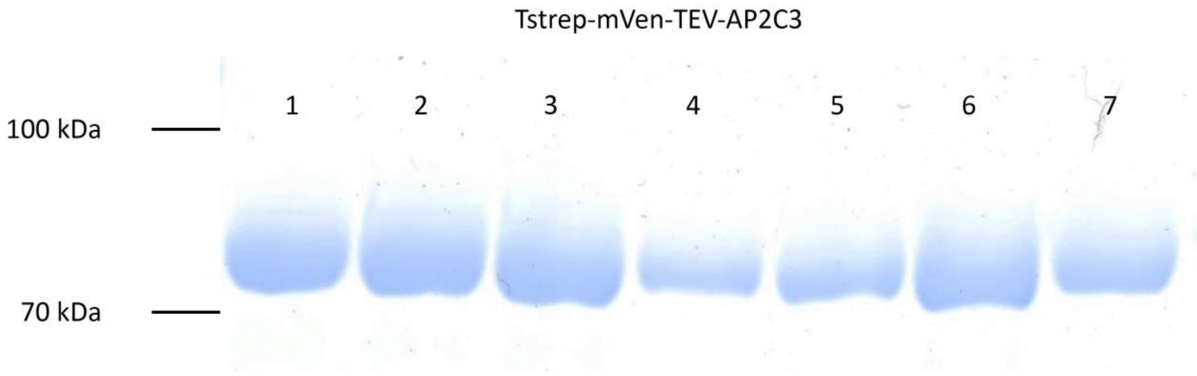

Figure 15: Second attempt of expression and purification in insect cell system of twin-strep-mVen-TEV-AP2C3 by Ivar Ilves. Fractions show perfect purity and no contaminants and the protein came off the column very slowly. 3 µL of sample loaded.

Overall protein yield from the baculoviral/insect cell system was high (appendix, page 58) and the quality of eluted fractions in case of all homologs was consistent. However, proteins were sticking strongly to the column and eluted slower than expected (Figure 13, 15, 16 (right), page 32, 33) in comparison to purification from E. coli (Figure 16, left gel). Usually most of the soluble protein is washed off within three elution fractions (Figure 16, left gel). From insect cells however, protein was still eluted in high concentration up to the 8th fraction (Figure 16), suggesting stong interactions with the resin. This is supported by the harsh conditions needed for the resin regeneration after the protein purification (1 M NaOH) and suggests aggregation or even condensation of protein on the resin.

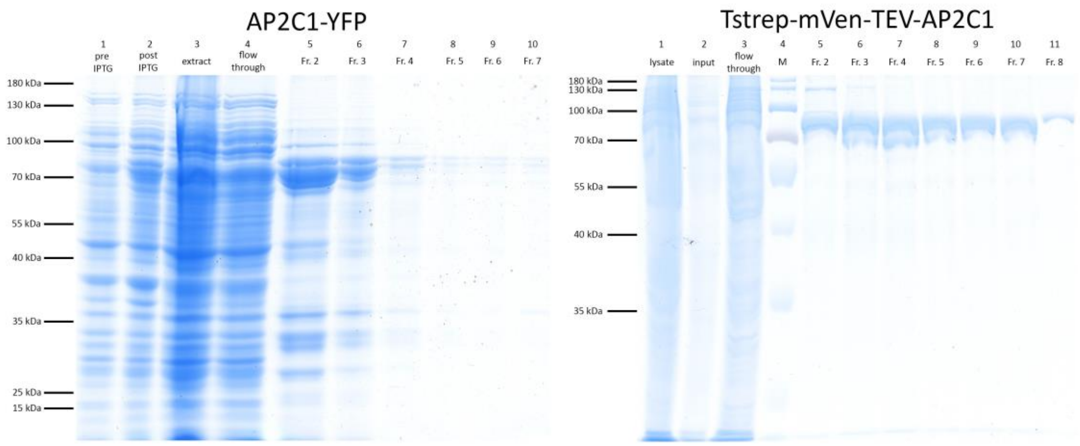

Figure 16: Comparison of bacterial (left) and insect cell (right) system expression and purification samples. Gels are representative for all successful performed experiments. 2 µL of sample loaded.

Overall quality and purity of the protein differs strongly depending on the used expression and purification methods (Figure 16). According to fluorescence and elextrophoresis analysis, the overall expression level of the protein is better in the bacterial system, but the final purity and yield proved to be, as expected, higher in the insect cell system.

3.2.3.2 Imaging

In vitro imaging of 5 µM purified protein was performed to investigate CO_2 dependent aggregation and condensation of AP2C3 and PP2C74. AP2C1 and AP2C4 were used as negative controls to study differences in dynamics since AP2C1 has been experimentally shown by Zhang et. al (2022) to not form aggregates under high CO_2. AP2C4 is a close homolog of AP2C1, and both were reported to lack the IDR (Zhang et al., 2022).

The biggest challenge in imaging protein phase separation *in vitro* triggered by low molecular interactors such as CO_2 is maintaining gas accessibility and preventing evaporation at the same time. CO_2 needs to be applied to the system over the gaseous phase surrounding the sample since adding bicarbonate compounds would immediately produce charged ionic species and therefore change the ionic strength of the buffer. Phase separation and condensates are highly sensitive to charged molecules since the studied proteins are originally embedded in a highly complex, well buffered cellular environment/compartment, regulated by multiple interactors. Every added chemical would therefore result in changed dynamics of the studied system. For example, it is still in question whether CO_2 alone or bicarbonate as well regulates the CO_2 sensing pathway, and if bicarbonate can even inhibit phase condensation. Notably, Zhang et al. (2022) reported that bicarbonate could not induce condensate formation of AP2C3, even when supplied at concentrations which could produce dissolved CO2 equivalent to 1 % CO2 or higher.

Furthermore, classical phase separating systems consist out of macromolecular scaffolding molecules, but this case, the so called ‘sticker’ is a low molecular compound, which stands in direct competition with chemical properties of molecules similar in size. It is crucial to avoid evaporation of buffer due to the change in volume and therefore concentration of all participating agents. Protein concentration also affects phase separation strongly. Higher protein concentrations enhance condensation in general. In addition, drying of sample during imaging leads to crystallization of buffer salts, resulting in elevated nucleation points for condensation and changed buffer component concentrations. This will enhance aggregation. All parameters need to remain constant for data collection.

3.2.3.2.1 Fluorescent microscope

Due to the available microscope setup being an upright light microscope, the imaged sample needed to be covered with a coverslip. Without applying a coverslip on top, the objective got into contact with the imaged droplet since the droplets vertical diameter is bigger than the working distance of the objective. An attempt to increase gas accessibility was made by creating a small imaging chamber between the glass slide and coverslip as described in the methods section. This chamber was filled with 50 µL protein solution and was imaged right on the border of gaseous and liquid phase. AP2C1 and PP2C74 showed different behaviour in this setup (Figure 17, page 35), CO_2 dependent aggregation within 30 min of PP2C74 was suspected while AP2C1 consistently showed no aggregation. However, it was not possible to reproduce this result for PP2C74 and we suspect drying of the sample to be the reason for aggregation. PP2C74 remained to show aggregation in repeated experiments, but enrichment could not be assumed since already a lot of aggregates were present from the beginning. As AP2C3 was not ready at this stage and gas accessibility was still an unsure factor, we decided to proceed with experiments under the inverted confocal microscope.

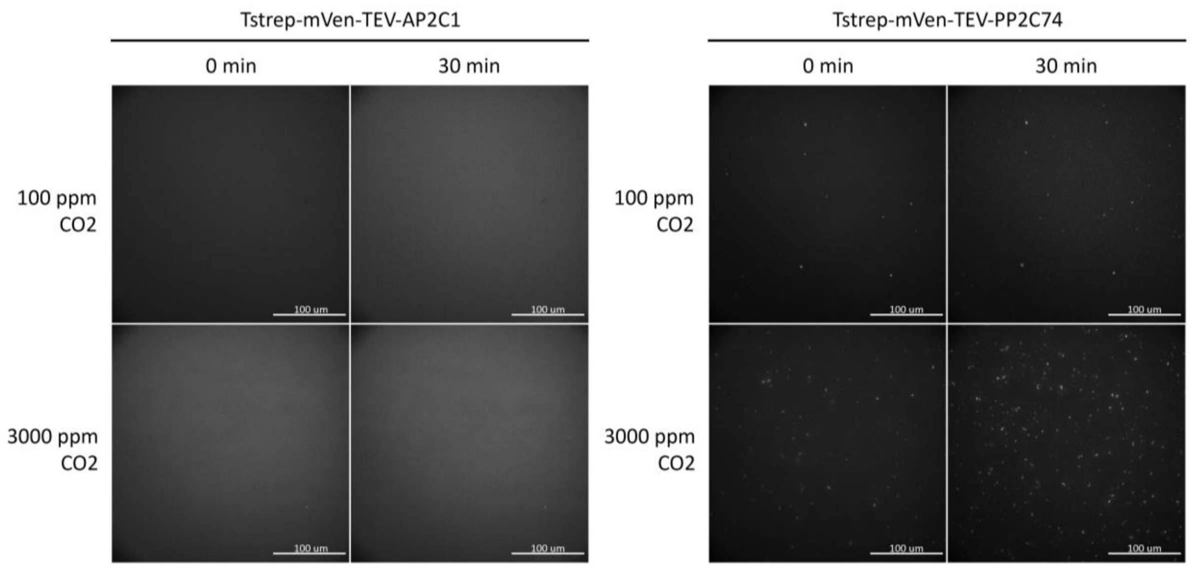

Figure 17: Aggregation of PP2C74 (right) under the fluorescent microscope after 30 min. AP2C1's appearance (left) remains unchanged. We suspect that protein aggregates are already formed prior to the experiment and sink down onto the imaged surface during the time lapse, further enriched by drying of the sample. This implies wrongly crowding of protein. This experiment was not reproducible.

3.2.3.2.2 Confocal microscope

The inverted confocal microscope allowed a very different approach to image protein samples. Imaging from below allowed pipetting a droplet of protein solution onto the microscopy vessel without covering it and therefore ensuring gas accessibility. After testing conventional cell culture imaging vessels (Lab-Tek®) made from plastic with 200 µL chambers, it became clear that the low working distance of the used objective and high noise due to the plastic's light diffraction required high end confocal microscopy slides. For this, we chose commercially available 35 mm petri dishes with a 20 mm wide and 0.16 – 0.19 mm thin No. 1.5 cover glass bottom (MATTEK®). This allowed focusing onto the top glass surface. Ambient room CO_2 concentration and humidity was measured using the LI-COR® gas analyser to ensure preparation and application of protein samples at non-inducing conditions. While values did not deviate from natural conditions in the room, the Pecon® incubator seemed to be leaking, elevating the CO_2 concentration in the direct vicinity to at least 5000 ppm (0.5 %) without switching on the pump. No solution for this problem was found. For ambient CO_2 experiments, the incubator was switched off and the lid with the CO_2 inlets was placed as far away as possible from the specimen while keeping agitation in the big incubator high by leaving slits open and having air conditioning switched on. While gas accessibility was improved, evaporation of buffer became a bigger problem. Humidity could not be controlled, and quite dry air was blown onto the sample by the standard Pecon® cell incubator system. To prevent drying, an imaging chamber was set up by cutting a square into a gas permeable observation gel (CAROLINA®) pressed on a 20 mm cover glass. 100 µL of protein solution was pipetted into the cut space, covered with a cover slip and imaged for indicated periods. In first trials, PP2C74 showed already an increase in aggregates after 10 min when being incubated with 5 % CO_2 (Figure 18) while AP2C1 remained unaffected.

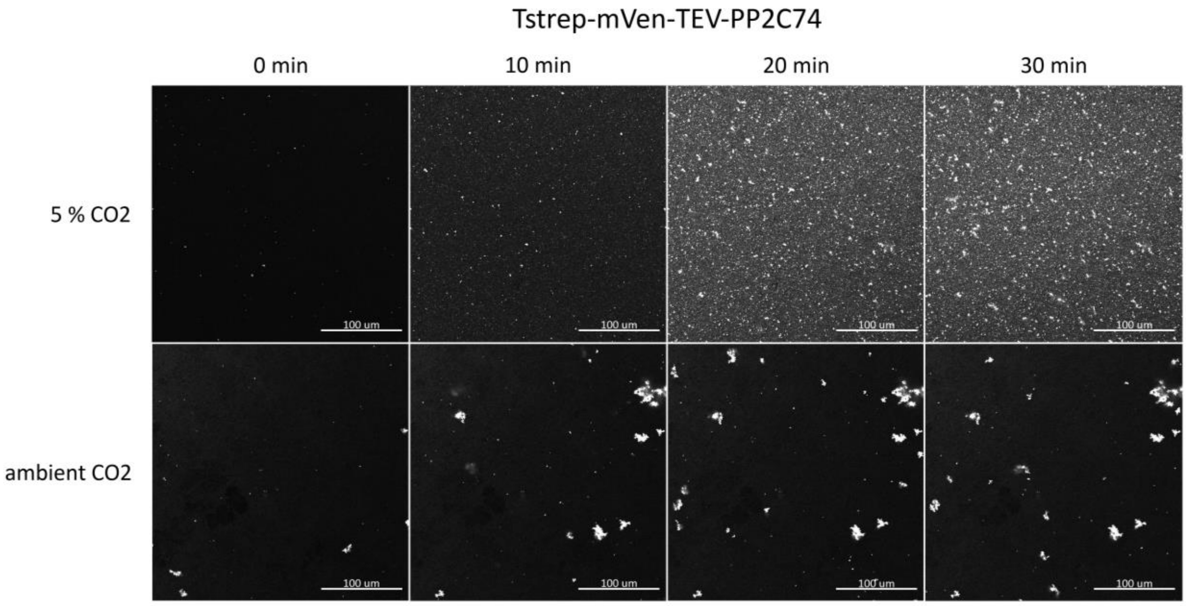

Figure 18: Time lapse showing protein crowding dependent on elevated CO2 for PP2C74. No fissure/budding was detected, visible aggregates did not move after attachment to the surface.

After further trials, however, it appeared that aggregates would just sink down during incubation since floating aggregates in higher planes of the examined droplet became less. The observed CO_2-dependent aggregate formation of PP2C74 was not reproducible in later assays.

In literature, LLPS is described as a highly dynamic process. We expected to see liquid like vesicles moving around on the examined surface, but the observed aggregates seemed to be very rigid. Aggregates appeared to sink down and stick to the glass surface and the overall background signal on the surface increased a lot over time, suggesting that protein in solution sediments. Since the used microscopy vessels are designed to provide conditions for growing cell cultures by allowing adhere to the surface, we concluded that the surface is too sticky and promoting protein aggregation. Therefore, coating of the imaging surface is required to ensure dynamic behaviour of protein droplets. First, we tested coating the glass slide with a solution containing 1 mg/ml BSA for 1 hour, but this did not change the appearance of samples at all. Zhang et al. (2022) reported in their methodical part that a polyethylene-glycol-silane (PEG-silane) pacified microscopy slide was used. PEG is a hydrophilic polymer and crowding agent. However, it was not possible to find commercially available PEG-coated microscopy slides. Using a custom-made chambered microscopy slide coated with 98 % PEG and 2 % PEG-Biotin with a cover glass bottom, kindly provided by Sergei Kopantšuk, we were able to perform another set of experiment with a more ideal surface (Figure 19). To ensure that only newly formed aggregates are imaged, samples were spun down at max. speed for 10 min at 4 ° C before imaging.

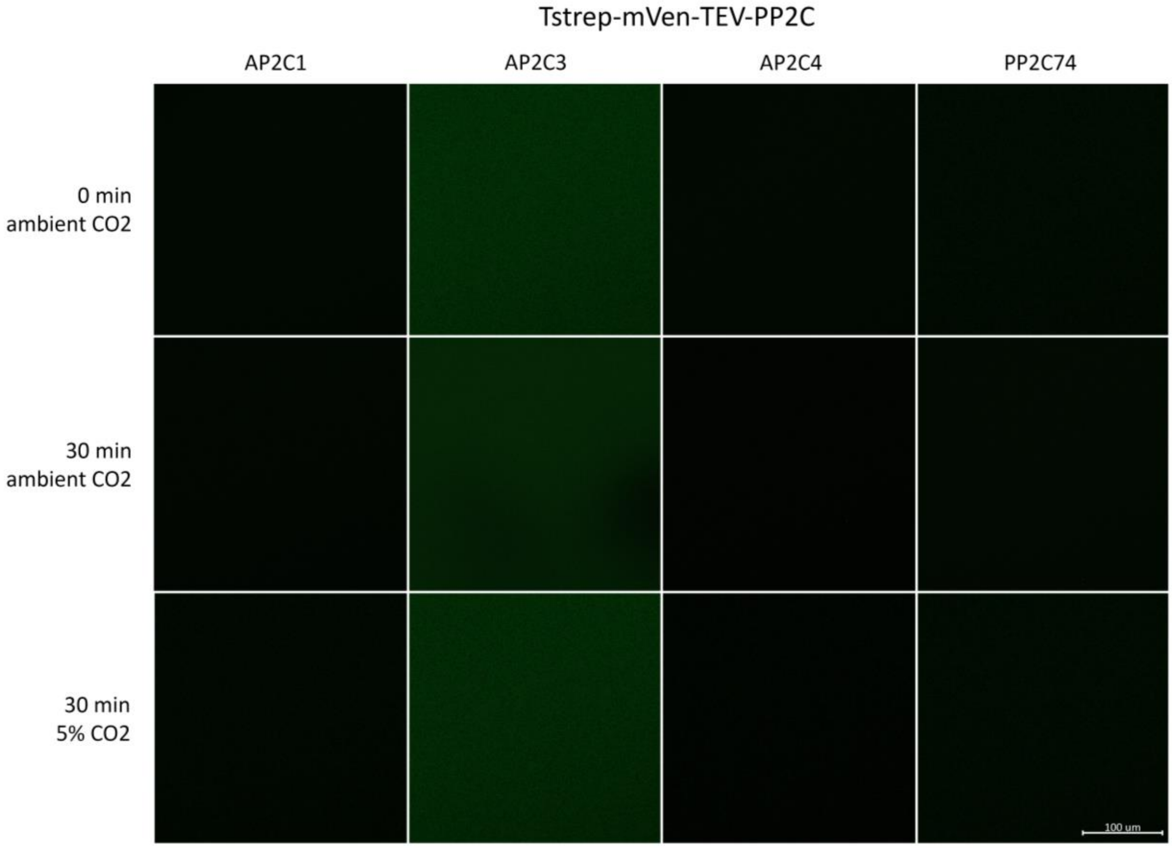

Figure 19: Confocal imaging using a PEG pacified microscopy slide. No effect and no aggregates visible for all PP2C homologs, fluorescent signal remains evenly distributed. 25 µL of protein solution was loaded and imaging chambers were uncovered.

The coated slide was tested by applying the maximal possible volume of 25 µL protein solution and subsequent scanning in varying conditions with and without covering the chambers with gas permeable foil. Signal noise, sedimentation and aggregation of proteins was reduced dramatically, resulting in absolutely no change in appearance after up to one hour. This supported our conclusion that formerly detected aggregates were artefacts stuck to the glass surface.

3.2.4 *In planta* localization & condensate studies

An *in planta* transient overexpression assay was performed to verify the localisation of PP2C homologs in a more natural condition. Furthermore, this experiment should give insight into the ability of homologs to condensate in its biological surroundings. This is crucial to exclude the possibility that *in* *vitro* detected aggregates and condensates are artefacts caused by the conditions applied in the experiment.

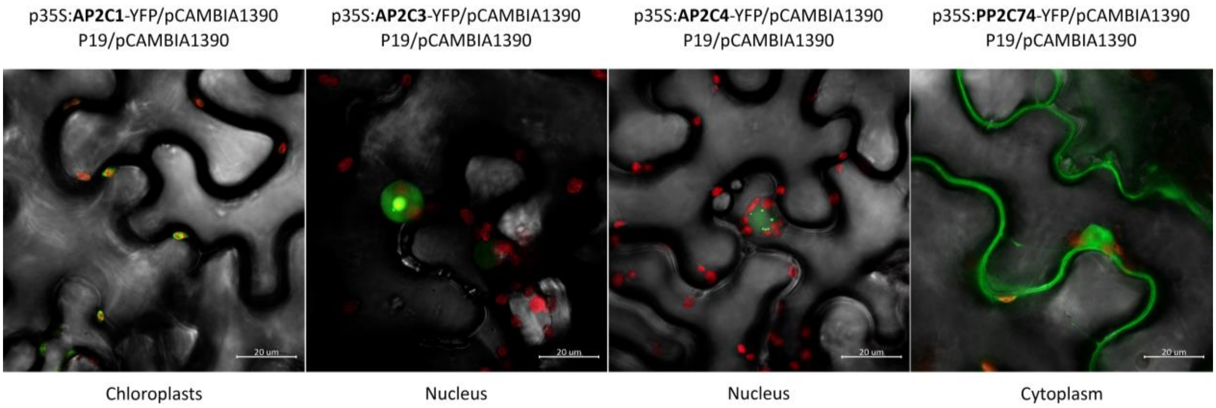

Figure 20: Localization and condensation of PP2C homologs in an in planta transient overexpression essay. AP2C3 consistently shows very big aggregations/condensates in the nucleus, sometimes the whole nucleus is glowing brightly. It was not possible to test whether these condensates preferably locate in the nucleolus. AP2C4 shows very fine, dynamically moving foci, fission and budding of such was observed. Pictures reliably represent overall localization. All images acquired 2 dpi. Pictures showing 3 merged channels: YFP fluorescence depicted in green, autofluorescence of chloroplasts depicted in red, dark lines show the plant cell wall in phase contrast (ESID).

The optimal OD_{600} for infiltration mixtures was determined to be 0.05 for this experiment to allow detection of aggregates/condensates but not resulting in heavy overexpression and aggregation of protein. The observed intracellular localisations were similar to reported localisations in literature for all four PP2C homologs: AP2C3 and AP2C4 mainly in the nucleus, AP2C1 is associated with chloroplasts and PP2C74 is localised in the cytosol and nucleus (Figure 20). We found that condensate detection and formation is time dependent, which may be related to the accumulated protein levels. AP2C3 and AP2C4, in particular, showed very clear and large aggregates/condensates for samples imaged after 3 days post infiltration (dpi). At this point, it is not possible to distinguish between aggregation and condensation of PP2C homologs since overexpression profoundly changes protein dynamics. Consequently, we suspect aggregation/condensation for all four homologs, but magnification and resolution were not high enough to classify it sufficiently in smaller cellular compartments like chloroplasts. However, it was clearly visible that AP2C3 is a lot more prone to aggregation than others (Figure 20).

3.2.5 Interaction between PP2Cs and MPKs

To test whether selected PP2C homologs interact with mitogen-activated protein kinases (MPKs) and thereby connecting PP2Cs to the MPK4/12-mediated guard cell CO_2 signalling pathway, a bimolecular fluorescence complementation assay (BiFC) was performed. In this experiment, MPK variants are fused to a N-terminal half of YFP (MPK-YFPn) and PP2C homologs are fused to a C-terminal half of YFP (PP2C-YFPc). The split fluorescent tags do not emit light when illuminated with a wavelength suitable for YFP excitation. Only when a MPK and PP2C variant colocalize in a cellular compartment, the split YFP tags can be reconstituted and thus emit signal. If such colocalization takes place, interaction of the proteins carrying the fluorescent tag snippets can be inferred and can be measured based on the fluorescence intensity after being normalised by another fluorescent protein serving as the control of expression level. However this experiment does not allows detection of dynamic interaction since the reconstitution of split YFP is irreversible.

We focused on the interaction of AP2C3 and MPK12 since they have been shown to be involved in CO2 sensing. AP2C4 and MPK11 were selected as negative controls for their high sequence homology, but distinct functionality to AP2C3 and MPK12, respectively, in respect to CO2 responsiveness. Our initial BiFC experiments revealed interaction within the nucleus for AP2C3 and MPK12; therefore, a nuclear localised mCherry construct was co-infiltrated to serve as an internal control for the expression levels. Based on prior observations that condensate formation *in planta* is time- or expression-level dependent, it was necessary to test whether interaction is dependent on similar factors as well. Small aggregates/condensates were present in experiments imaged at 3 dpi for interaction of AP2C3 and MPK12. More importantly, clear YFP signals were often observed in the combination of AP2C3-MPK12 pair, less in the AP2C3-MPK11 pair, and none in the pairs with AP2C4.

3.2.5.1 Quantification of interaction

The reconstituted YFP fluorescence signal was normalized by a ratio calculation with measured mCherry fluorescence within the nucleus. First, nuclei were marked based on mCherry fluorescence, and the YFP channel was measured at the same area. Confocal settings for each experiment were adjusted based on the signal intensity of both YFP and mCherry channels but were kept constant across different samples within each experiment. Therefore, it is not possible to pull all experiments for statistical analyses together. For 6 out of 8 experimental pairs, the combination of MPK12 and AP2C3 shows a higher YFP/mCherry signal ratio average and a clearly segregated distribution of measurement values (Figure 21 and 22, page 40). Averages of single experiments were statistically tested for significance of difference of averages by applying a t-test with a significance threshold of $p < 0.05$. All 6 experiments show a statistically significant difference of averages. There is no difference in interaction visible for samples imaged at 2 dpi (Figure 21, page 40) or 3 dpi (Figure 22, page 40).

For experiment 3 (Figure 21, page 40) and 4 (Figure 22, page 40) not showing a significant difference we suspect a methodical error. This is supported by the fact that these experiments were performed with the same agrobacterium cultures and were infiltrated at the same day. Since the overall YFP/mCherry signal ratio is also very low for both data, it is very likely, that construct was not expressed sufficiently in this experiment. For a more detailed presentation of data distribution, averages and statistical significance of independent experiments, see graphs in the appendix (page 57).

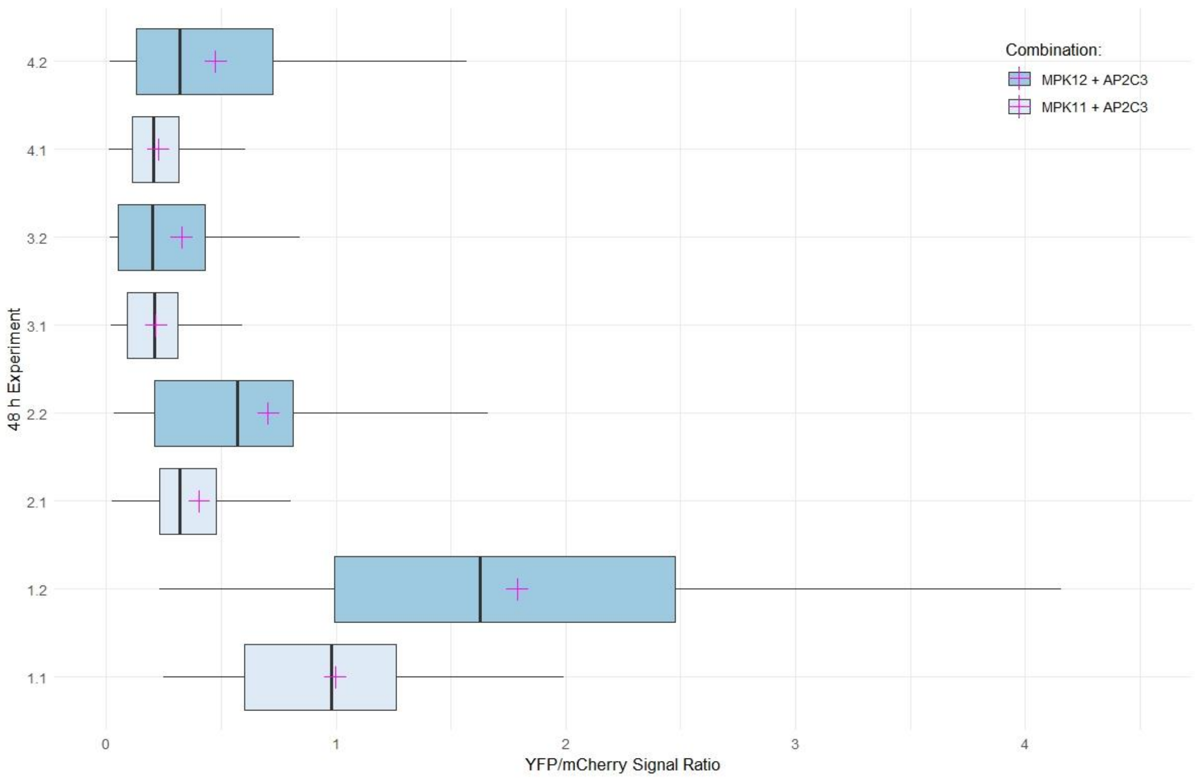

Figure 21: Comparison of YFP/mCherry fluorescent signal ratios of BiFC experiments imaged 48 h after infiltration for experimental pairs containing MPK11-YFPc+AP2C3 and MPK12-YFPc+AP2C3. Experiments with a similar first number have been performed in the same batch and imaged on the same day and are therefore directly comparable. Averages depicted as a magenta cross for each single experiment.

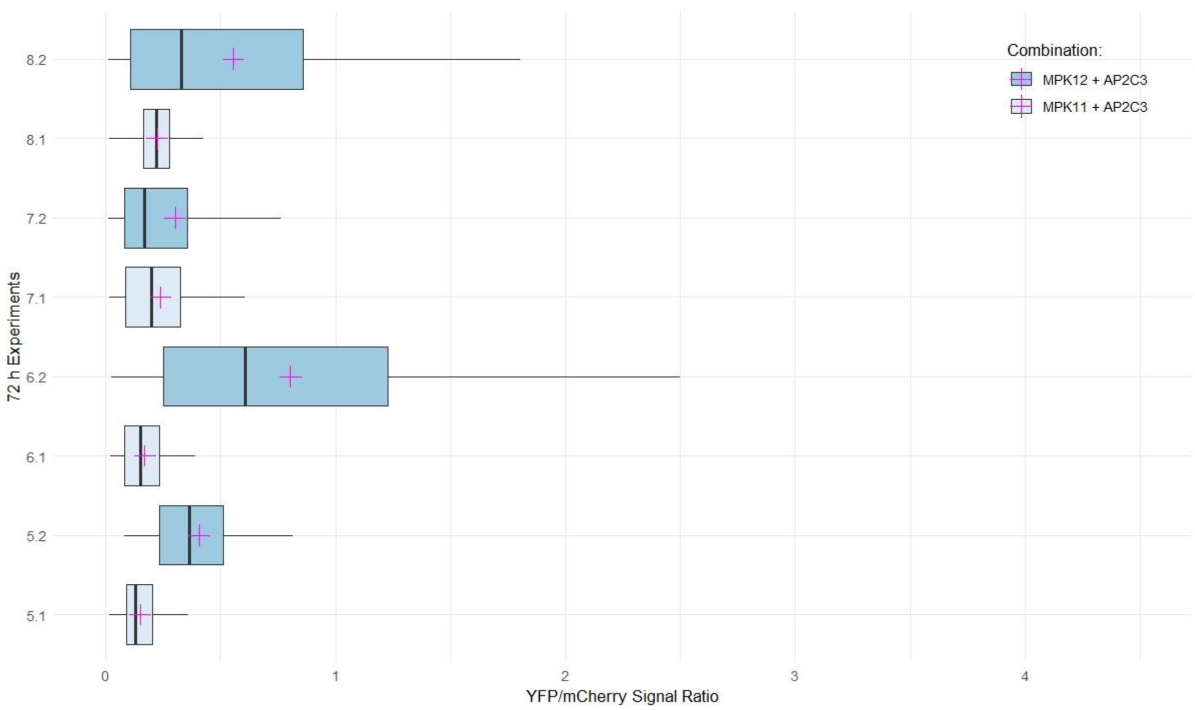

Figure 22: Comparison of YFP/mCherry fluorescent signal ratios of BiFC experiments imaged 72 h after infiltration for experimental pairs containing MPK11-YFPc+AP2C3 and MPK12-YFPc+AP2C3. Experiments with a similar first number have been performed in the same batch and imaged on the same day and are therefore directly comparable. Averages depicted as a magenta cross for each single experiment.

3.2.5.2 *Western Blot*

We performed western blot to prove that proteins of interest were successfully expressed in imaged plant tissue (Figure 23). Interestingly, for leaves co-infiltrated with MPK12 and AP2C3 (Figure 23, lane 5), only one band was visible despite that MPK12 or AP2C3 alone was clearly expressed and appeared as discernible bands on the gel for controls (Figure 23, lanes 1 & 3). This stands in contrast to AP2C3 and MPK11 (lane 6), where two distinct bands are visible. The absence of separated bands for the MPK12 and AP2C3 combination may indicate tight association of these two proteins even in the highly denaturing condition of SDS-PAGE. For the AP2C4 + MPK11/12 combination however, visibility of only one band is not caused by potential interaction but is more likely due to the similar molecular weight of recombinant proteins (Table 10, page 31). MPK11/12 weights 62.6 kDa and AP2C4 60.8 kDa. The 10% SDS-PAGE cannot resolve such small differences in molecular weight.

	1	2	3	4	5	6	7	8	
MPK12-YFPn	+				+		+		MPK12-YFPn
MPK11-YFPn		+				+		+	MPK11-YFPn
AP2C3-YFPc			+		+	+			AP2C3-YFPc
AP2C4-YFPc				+			+	+	AP2C4-YFPc

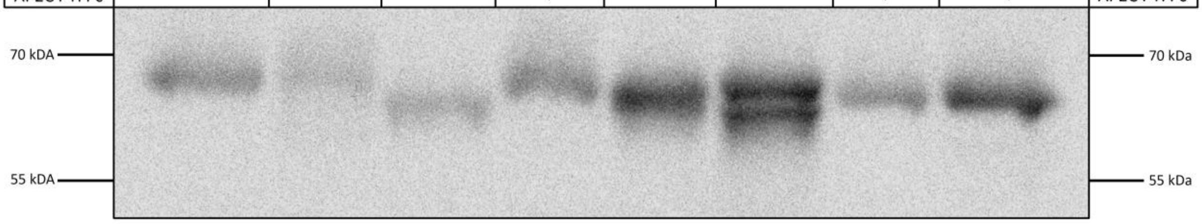

Figure 23: BiFC western blot to verify expression of protein of interest. For molecular weight of fusion proteins, see Table 5 (PAGE).

We attempted to resolve MPK11/12 interaction with AP2C3 better by running the SDS-PAGE for 1 hour longer. A weak second band appeared for the MPK12+AP2C3 combination (Figure 24). This is likely to be unbound AP2C3, since it weighs 8 kDa less than MPK12 with a weight of 54.0 kDa.

MPK12-YFPn	+		MPK12-YFPn
MPK11-YFPn		+	MPK11-YFPn
AP2C3-YFPc	+	+	AP2C3-YFPc
AP2C4-YFPc			AP2C4-YFPc

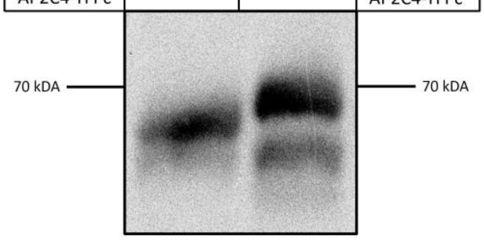

Figure 24: BiFC western blot of MPK11/12+AP2C3 with higher resolution.

3.3 Conclusion

Based on the conducted experiments we conclude that AP2C3 is a very sensitive, tricky protein to work with and this supports the suggestion of it being capable of liquid-to-liquid phase separation (LLPS). Purification steps and buffer exchanges must be performed with caution and protein concentration in solution and especially on the column should not be too high while freeze-thaw cycles should be kept to a minimum. We accomplished to establish a practical *in vitro* phase separation imaging system based on confocal microscopy with coated microscopic. Gas accessibility of specimens while preventing evaporation of buffer is crucial to provide constant conditions. Reproducible condensate formation remains to be detected successfully in imaging experiments and a positive control for phase separating protein remains to be prepared to proof the functionality of the developed system. A very plausible explanation for the absence of condensates for *in vitro* experiments so far is a flawed design of the large N-terminal fusion of twin strep and mVenus tag in the baculoviral/insect cell system, potentially sterically hindering the accessibility for phase separation essential N-terminal IDR to CO_2. This very likely blockage of the IDR essential for the CO_2 sensing and crowding mechanism would prevent phase separation. This is supported by the suspected condensation of AP2C3-YFP due to unsuccessful elution from the purification column. For bacterial expression, the fluorescent tag was fused to the C-terminus ofPP2Cs, while only a short His tag for purification was attached to the N-terminus, thus maintaining accessibility of the IDR.

To test this, a TEV-protease digest for cleavage of the fused tags should be performed. Hypothetically, this should restore the accessibility of the IDR and allow condensates to form. For LLPS detection, phase contrast light microscopy on PEG-pacified microscopy slides should be performed. Further, a low stochiometric mixture of cleaved and tagged protein can be prepared or protein can be labelled with fluorophores using commercially available kits to attempt detection of condensate formation in a fluorescent imaging experiment if phase contrast imaging turns out to be insufficient.

Usage of coated imaging surfaces is important to maintain mobility of small condensates and to detect droplet dynamics due to fission and fusion. Furthermore, since the largest aggregates/condensates detected in *in planta* essays were approximately 1-2 µm in size, the used magnification for *in vitro* assays should be increased to at least 63x. PEG-coated microscopy slides provide very low noise for aggregation and allow the usage of inversion objectives while being able to keep the sample uncovered since they are best used in an inverted microscope. This will increase imaging quality and make it easier to identify biomolecular condensates. At the same time, volumes of imaged droplets should be decreased to a minimum to allow CO_2 to enter the solution.

Furthermore, we conclude that an interaction between AP2C3 and MPK12 is highly probable, thus supporting our hypothesis of connection between LLPS-based CO_2 sensing by AP2C3 and the recently identified MPK12/HT1 CO_2/bicarbonate sensor in the guard cell signalling pathway. However, further repetitions of experiments combined with phosphatase and kinase assays are required to gain more insights on the CO_2-sensing mechanism.

To acquire more information about the nature of functional motifs active in CO2 sensing and further identification of molecular processes involved in CO_2 sensing, more elaborate in silico analyses based on our performed sequence alignment need to be performed using PLAAC, IUPred and local CIDER sequence analysis tools.

SUMMARY

In this study, phase separation and probable partitioning in biomolecular condensates, a phenomenon which is recently gaining extensive awareness in research due to its non-membrane bound compartmentalization properties within cells, of a selection of plant protein phosphatase type 2C homologs triggered by carbon dioxide has been studied *in vitro* and *in planta*. Phase condensation of proteins, in this case liquid-to-liquid phase condensation, describes the coexistence of two- or multi-phase protein systems in dense and dilute phase. The ability to form biomolecular condensates via phase separation and reversible association of multivalent macromolecules is embedded in the polypeptide sequence via interactive motifs located in intrinsically disordered domains. These domains mediate interaction with the surrounding dilute phase through by not forming higher level structural organisation and therefore existing in an ensemble of 'fuzzy' confirmations.

For this project, recombinant AP2C1, AP2C3, AP2C4 and PP2C74 proteins fused to a twin-strep affinity and mVenus fluorescent tag were successfully cloned, expressed and purified in an baculovirus expression system and purified via Tstrep®/Streptactin® mediated affinity chromatography. The purified protein was then used to set up a reliable, reproducible imaging assay using a confocal microscope to detect condensation formation of protein under elevated CO_2 concentrations. We found that coating of imaging surfaces, maintaining gas accessibility and prevention of evaporation are critical factors for studying condensate formation of proteins triggered by low molecular, gaseous 'stickers' like CO_2. However, we could not detect whether the condensation of purified PP2C homologs takes place due to a suspected flaw in the design of the fusion proteins supposedly blocking the IDR which is essential for condensate formation. Therefore, we were unable to compare *in vitro* the previously described CO_2 sensitivity of AP2C3 to another suggested CO_2 sensor, PP2C74, or investigate CO2 insensitivity of closely related homologous phosphatases from the same clade as AP2C3.

We verified the previously reported intracellular localisation pattern and detected variable aggregate/condensate formation *in planta* of selected PP2C homologs in a transient overexpression experiment. Furthermore, using a bimolecular fluorescent complementation assay, we collected data that strongly indicates interaction of AP2C3 with mitogen-activated protein kinase (MPK) 12, an enzyme that has been shown to be directly involved in the CO_2 signalling pathway in guard cells, but not MPK11. All other studied PP2C homologs did not interact with MPK12 or MPK11.

However, further experiments processing the purified fusion protein to ensure accessibility of the phase separation driving IDR, studying condensation *in planta* in a more natural setting and verifying interaction of AP2C3 and MPK12 must be conducted to further understand CO2 sensing in plants. This will help to be prepared for increasing environmental stresses caused by the emerging threat of climate change and therefore cope with more challenges in food crop production.

REFERENCES

Ainsworth, E. A., & Long, S. P. (2005). What have we learned from 15 years of free-air CO2 enrichment (FACE)? A meta-analytic review of the responses of photosynthesis, canopy properties and plant production to rising CO2. *New Phytologist*, *165*(2), 351–372. https://doi.org/10.1111/J.1469-8137.2004.01224.X

Alberti, S., Gladfelter, A., & Mittag, T. (2019). Leading Edge Primer Considerations and Challenges in Studying Liquid-Liquid Phase Separation and Biomolecular Condensates. *Cell*, *176*, 419–434. https://doi.org/10.1016/j.cell.2018.12.035

Alberti, S., Saha, S., Woodruff, J. B., Franzmann, T. M., Wang, J., & Hyman, A. A. (2018). A User's Guide for Phase Separation Assays with Purified Proteins. *Journal of Molecular Biology*, *430*(23), 4806. https://doi.org/10.1016/J.JMB.2018.06.038

Aumiller, W. M., & Keating, C. D. (2015). Phosphorylation-mediated RNA/peptide complex coacervation as a model for intracellular liquid organelles. *Nature Chemistry 2015 8:2*, *8*(2), 129–137. https://doi.org/10.1038/nchem.2414

Banani, S. F., Lee, H. O., Hyman, A. A., & Rosen, M. K. (2017). Biomolecular condensates: organizers of cellular biochemistry. *Nature Reviews Molecular Cell Biology 2017 18:5*, *18*(5), 285–298. https://doi.org/10.1038/nrm.2017.7

Banani, S. F., Rice, A. M., Peeples, W. B., Lin, Y., Jain, S., Parker, R., & Rosen, M. K. (2016). Compositional Control of Phase-Separated Cellular Bodies. *Cell*, *166*(3), 651–663. https://doi.org/10.1016/J.CELL.2016.06.010

Boeynaems, S., Alberti, S., Fawzi, N. L., Mittag, T., Polymenidou, M., Rousseau, F., Schymkowitz, J., Shorter, J., Wolozin, B., Van Den Bosch, L., Tompa, P., & Fuxreiter, M. (2018). Protein Phase Separation: A New Phase in Cell Biology. In *Trends in Cell Biology* (Vol. 28, Issue 6, pp. 420–435). Elsevier Ltd. https://doi.org/10.1016/j.tcb.2018.02.004

Brangwynne, C. P., Mitchison, T. J., & Hyman, A. A. (2011). Active liquid-like behavior of nucleoli determines their size and shape in Xenopus laevis oocytes. *Proceedings of the National Academy of Sciences of the United States of America*, *108*(11), 4334–4339. https://doi.org/10.1073/PNAS.1017150108/ASSET/9530B829-7948-4296-BE4C-95F7DA1ED7C4/ASSETS/GRAPHIC/PNAS.1017150108EQ3.GIF

Brock, A. K., Willmann, R., Kolb, D., Grefen, L., Lajunen, H. M., Bethke, G., Lee, J., Nürnberger, T., & Gust, A. A. (2010). The Arabidopsis Mitogen-Activated Protein Kinase Phosphatase PP2C5 Affects Seed Germination, Stomatal Aperture, and Abscisic Acid-Inducible Gene Expression. *Plant Physiology*, *153*(3), 1098–1111. https://doi.org/10.1104/PP.110.156109

Choi, J. M., Dar, F., & Pappu, R. V. (2019). LASSI: A lattice model for simulating phase transitions of multivalent proteins. *PLOS Computational Biology*, *15*(10), e1007028. https://doi.org/10.1371/JOURNAL.PCBI.1007028

Cundari, T. R., Wilson, A. K., Drummond, M. L., Gonzalez, H. E., Jorgensen, K. R., Payne, S., Braunfeld, J., De Jesus, M., & Johnson, V. M. (2009). *CO 2-Formatics: How Do Proteins Bind Carbon Dioxide?* https://doi.org/10.1021/ci9002377

Das, R. K., & Pappu, R. V. (2013). Conformations of intrinsically disordered proteins are influenced by linear sequence distributions of oppositely charged residues. *Proceedings of the National Academy of Sciences of the United States of America*, *110*(33), 13392–13397. https://doi.org/10.1073/PNAS.1304749110/SUPPL_FILE/SAPP.PDF

Decker, C. J., & Parker, R. (2012). P-Bodies and Stress Granules: Possible Roles in the Control of Translation and mRNA Degradation. *Cold Spring Harbor Perspectives in Biology*, *4*(9), a012286. https://doi.org/10.1101/CSHPERSPECT.A012286

Dignon, G. L., Best, R. B., & Mittal, J. (2020). Biomolecular phase separation: From molecular driving forces to macroscopic properties. *Annual Review of Physical Chemistry*, *71*(Volume 71, 2020), 53–75. https://doi.org/10.1146/ANNUREV-PHYSCHEM-071819-113553/CITE/REFWORKS

Emenecker, R. J., & Holehouse, A. S. (2022). Intrinsically disordered CO2 sensors. *Nature Cell Biology*, *24*(7), 1013–1014. https://doi.org/10.1038/s41556-022-00957-1

Emenecker, R. J., Holehouse, A. S., & Strader, L. C. (2020). *Emerging Roles for Phase Separation in Plants*. https://doi.org/10.1016/j.devcel.2020.09.010

Feric, M., Vaidya, N., Harmon, T. S., Kriwacki, R. W., Pappu, R. V, Correspondence, C. P. B., Mitrea, D. M., Zhu, L., Richardson, T. M., & Brangwynne, C. P. (2016). Coexisting Liquid Phases Underlie Nucleolar Subcompartments Article Coexisting Liquid Phases Underlie Nucleolar Subcompartments. *Cell*, *165*, 1686–1697. https://doi.org/10.1016/j.cell.2016.04.047

Flory, P. J. (1942). Thermodynamics of High Polymer Solutions. *The Journal of Chemical Physics*, *10*(1), 51–61. https://doi.org/10.1063/1.1723621

Foyer, C. H., & Noctor, G. (2020). Redox Homeostasis and Signaling in a Higher-CObinf2einf World. *Annual Review of Plant Biology*, *71*(Volume 71, 2020), 157–182. https://doi.org/10.1146/ANNUREV-ARPLANT-050718-095955/CITE/REFWORKS

Fuchs, S., Grill, E., Meskiene, I., & Schweighofer, A. (2013). *Type 2C protein phosphatases in plants*. https://doi.org/10.1111/j.1742-4658.2012.08670.x

Gomes, E., & Shorter, J. (2019). The molecular language of membraneless organelles. *Journal of Biological Chemistry*, *294*(18), 7115–7127. https://doi.org/10.1074/JBC.TM118.001192

Grondin, A., Rodrigues, O., Verdoucq, L., Merlot, S., Leonhardt, N., & Maurel, C. (2015). Aquaporins Contribute to ABA-Triggered Stomatal Closure through OST1-Mediated Phosphorylation. *The Plant Cell*, *27*(7), 1945–1954. https://doi.org/10.1105/TPC.15.00421

Hall, R. A., de Sordi, L., MacCallum, D. M., Topal, H., Eaton, R., Bloor, J. W., Robinson, G. K., Levin, L. R., Buck, J., Wang, Y., Gow, N. A. R., Steegborn, C., & Mühlschlegel, F. A. (2010). CO2 Acts as a Signalling Molecule in Populations of the Fungal Pathogen Candida albicans. *PLOS Pathogens*, *6*(11), e1001193. https://doi.org/10.1371/JOURNAL.PPAT.1001193

Handwerger, K. E., & Gall, J. G. (2006). Subnuclear organelles: new insights into form and function. *Trends in Cell Biology*, *16*(1), 19–26. https://doi.org/10.1016/J.TCB.2005.11.005

Ho, D. T., Bardwell, A. J., Abdollahi, M., & Bardwell, L. (2003). A docking site in MKK4 mediates high affinity binding to JNK MAPKs and competes with similar docking sites in JNK substrates. *Journal of Biological Chemistry*, *278*(35), 32662–32672. https://doi.org/10.1074/jbc.M304229200

Holehouse, A. S. (2019). IDPs and IDRs in biomolecular condensates. *Intrinsically Disordered Proteins: Dynamics, Binding, and Function*, 209–255. https://doi.org/10.1016/B978-0-12-816348-1.00007-7

Holsters, M., Silva, B., Van Vliet, F., Genetello, C., De Block, M., Dhaese, P., Depicker, A., Inzé, D., Engler, G., Villarroel, R., Van Montagu, M., & Schell, J. (1980). The functional organization of the nopaline A. tumefaciens plasmid pTiC58. *Plasmid*, *3*(2), 212–230. https://doi.org/10.1016/0147-619X(80)90110-9

Hõrak, H., Sierla, M., Tõldsepp, K., Wang, C., Wang, Y. S., Nuhkat, M., Valk, E., Pechter, P., Merilo, E., Salojärvi, J., Overmyer, K., Loog, M., Brosché, M., Schroeder, J. I., Kangasjärvi, J., & Kollist, H. (2016). A Dominant Mutation in the HT1 Kinase Uncovers Roles of MAP Kinases and GHR1 in CO2-Induced Stomatal Closure. *The Plant Cell*, *28*(10), 2493–2509. https://doi.org/10.1105/TPC.16.00131

Hsu, P. K., Takahashi, Y., Munemasa, S., Merilo, E., Laanemets, K., Waadt, R., Pater, D., Kollist, H., & Schroeder, J. I. (2018). Abscisic acid-independent stomatal CO2 signal transduction pathway and convergence of CO2 and ABA signaling downstream of OST1 kinase. *Proceedings of the National Academy of Sciences of the United States of America*, *115*(42), E9971–E9980. https://doi.org/10.1073/PNAS.1809204115/SUPPL_FILE/PNAS.1809204115.SAPP.PDF

Hu, H., Boisson-Dernier, A., Israelsson-Nordström, M., Böhmer, M., Xue, S., Ries, A., Godoski, J., Kuhn, J. M., & Schroeder, J. I. (2009a). Carbonic anhydrases are upstream regulators of CO2-controlled stomatal movements in guard cells. *Nature Cell Biology 2010 12:1*, *12*(1), 87–93. https://doi.org/10.1038/ncb2009

Hu, H., Boisson-Dernier, A., Israelsson-Nordström, M., Böhmer, M., Xue, S., Ries, A., Godoski, J., Kuhn, J. M., & Schroeder, J. I. (2009b). Carbonic anhydrases are upstream regulators of CO2-controlled stomatal movements in guard cells. *Nature Cell Biology 2010 12:1*, *12*(1), 87–93. https://doi.org/10.1038/ncb2009

Jakobson, L., Vaahtera, L., Tõldsepp, K., Nuhkat, M., Wang, C., Wang, Y. S., Hõrak, H., Valk, E., Pechter, P., Sindarovska, Y., Tang, J., Xiao, C., Xu, Y., Gerst Talas, U., García-Sosa, A. T., Kangasjärvi, S., Maran, U., Remm, M., Roelfsema, M. R. G., … Brosché, M. (2016). Natural Variation in Arabidopsis Cvi-0 Accession Reveals an Important Role of MPK12 in Guard Cell CO2 Signaling. *PLOS Biology*, *14*(12), e2000322. https://doi.org/10.1371/JOURNAL.PBIO.2000322

Jalakas, P., Nuhkat, M., Vahisalu, T., Merilo, E., Brosche, M., & Kollist, H. (2021). Combined action of guard cell plasma membrane rapid- and slow-type anion channels in stomatal regulation. *Plant Physiology*, *187*(4), 2126–2133. https://doi.org/10.1093/PLPHYS/KIAB202

Kevin Leung, *,†, Ida M. B. Nielsen, ‡ and, & Kurtz§, I. (2007). Ab Initio Molecular Dynamics Study of Carbon Dioxide and Bicarbonate Hydration and the Nucleophilic Attack of Hydroxide on CO2. *The Journal of Physical Chemistry B*, *111*(17), 4453–4459. https://doi.org/10.1021/JP068475L

Klepikova, A. V, Kasianov, A. S., Gerasimov, E. S., Logacheva, M. D., & Penin, A. A. (2016). *A high resolution map of the Arabidopsis thaliana developmental transcriptome based on RNA-seq profiling*. https://doi.org/10.1111/tpj.13312

Koncz, C., & Schell, J. (1986). The promoter of TL-DNA gene 5 controls the tissue-specific expression of chimaeric genes carried by a novel type of Agrobacterium binary vector. *MGG Molecular & General Genetics*, *204*(3), 383–396. https://doi.org/10.1007/BF00331014/METRICS

Lee, H.-C., Breitbart, H., Berman, M., & Forte, J. G. (1979). POTASSIUM-STIMULATED ATPase ACTIVITY AND HYDROGEN TRANSPORT IN GASTRIC MICROSOMAL VESICLES *. *Biochimica et Biophysica Acta*, *553*, 107–131.

Macklem, P. T., & Seely, A. (2010). Towards a Definition of Life. *Perspectives in Biology and Medicine*, *53*(3), 330–340. https://doi.org/10.1353/pbm.0.0167

Madeira, F., Pearce, M., Tivey, A. R. N., Basutkar, P., Lee, J., Edbali, O., Madhusoodanan, N., Kolesnikov, A., & Lopez, R. (2022). Search and sequence analysis tools services from EMBL-EBI in 2022. *Nucleic Acids Research*, *50*(W1), W276–W279. https://doi.org/10.1093/NAR/GKAC240

Mao, Y. S., Zhang, B., & Spector, D. L. (2011). Biogenesis and function of nuclear bodies. *Trends in Genetics*, *27*(8), 295–306. https://doi.org/10.1016/J.TIG.2011.05.006

Meigh, L. (2015). CO2 carbamylation of proteins as a mechanism in physiology. *Biochemical Society Transactions*, *43*(3), 460–464. https://doi.org/10.1042/BST20150026

Merilo, E., Laanemets, K., Hu, H., Xue, S., Jakobson, L., Tulva, I., Gonzalez-Guzman, M., Rodriguez, P. L., Schroeder, J. I., Broschè, M., & Kollist, H. (2013). PYR/RCAR Receptors Contribute to Ozone-, Reduced Air Humidity-, Darkness-, and CO2-Induced Stomatal Regulation. *Plant Physiology*, *162*(3), 1652–1668. https://doi.org/10.1104/PP.113.220608

Mitrea, D. M., & Kriwacki, R. W. (2016). Phase separation in biology; functional organization of a higher order. *Cell Communication and Signaling 2016 14:1*, *14*(1), 1–20. https://doi.org/10.1186/S12964-015-0125-7

Murat, D., Byrne, M., & Komeili, A. (2010). *Cell Biology of Prokaryotic Organelles*. https://doi.org/10.1101/cshperspect.a000422

Nuhkat, M., Brosché, M., Stoelzle-Feix, S., Dietrich, P., Hedrich, R., Roelfsema, M. R. G., & Kollist, H. (2021). Rapid depolarization and cytosolic calcium increase go hand-in-hand in mesophyll cells' ozone response. *New Phytologist*, *232*(4), 1692–1702. https://doi.org/10.1111/NPH.17711

Oparin, A. I. (1938). The Origin of Life. *McMillan, New York*.

Phelan, D. E., Mota, C., Lai, C., Kierans, S. J., & Cummins, E. P. (2021). Carbon dioxide-dependent signal transduction in mammalian systems. *Interface Focus*, *11*(2). https://doi.org/10.1098/RSFS.2020.0033

Posey, A. E., Bremer, A., Erkamp, N. A., Pant, A., Knowles, T., Dai, Y., Mittag, T., & Pappu, R. (2024, unpublished). *Biomolecular Condensates are Defined by Interphase Electric Potentials*. https://doi.org/10.2139/SSRN.4785780

Riback, J. A., Zhu, L., Ferrolino, M. C., Tolbert, M., Mitrea, D. M., Sanders, D. W., Wei, M. T., Kriwacki, R. W., & Brangwynne, C. P. (2020). Composition-dependent thermodynamics of intracellular phase separation. *Nature 2020 581:7807*, *581*(7807), 209–214. https://doi.org/10.1038/s41586-020-2256-2

Schweighofer, A., Hirt, H., & Meskiene, I. (2004a). Plant PP2C phosphatases: Emerging functions in stress signaling. In *Trends in Plant Science* (Vol. 9, Issue 5, pp. 236–243). https://doi.org/10.1016/j.tplants.2004.03.007

Schweighofer, A., Hirt, H., & Meskiene, I. (2004b). Plant PP2C phosphatases: Emerging functions in stress signaling. *Trends in Plant Science*, *9*(5), 236–243. https://doi.org/10.1016/j.tplants.2004.03.007

Schweighofer, A., Kazanaviciute, V., Scheikl, E., Teige, M., Doczi, R., Hirt, H., Schwanninger, M., Kant, M., Schuurink, R., Mauch, F., Buchala, A., Cardinale, F., & Meskiene, I. (2007). The PP2C-Type Phosphatase AP2C1, Which Negatively Regulates MPK4 and MPK6, Modulates Innate Immunity, Jasmonic Acid, and Ethylene Levels in Arabidopsis. *The Plant Cell*, *19*(7), 2213–2224. https://doi.org/10.1105/TPC.106.049585

Shin, Y., & Brangwynne, C. P. (2017). Liquid phase condensation in cell physiology and disease. *REVIEW SUMMARY ▼CELLULAR BIOPHYSICS*. https://doi.org/10.1126/science.aaf4382

Staples, M. I., Frazer, C., Fawzi, N. L., & Bennett, R. J. (2023). Phase separation in fungi. *Nature Microbiology 2023 8:3*, *8*(3), 375–386. https://doi.org/10.1038/s41564-022-01314-6

Takahashi, Y., Bosmans, K. C., Hsu, P. K., Paul, K., Seitz, C., Yeh, C. Y., Wang, Y. S., Yarmolinsky, D., Sierla, M., Vahisalu, T., McCammon, J. A., Kangasjärvi, J., Zhang, L., Kollist, H., Trac, T., & Schroeder, J. I. (2022). Stomatal CO2/bicarbonate sensor consists of two interacting protein kinases, Raf-like HT1 and nonkinase-activity activity requiring MPK12/MPK4. *Science Advances*, *8*(49). https://doi.org/10.1126/SCIADV.ABQ6161/SUPPL_FILE/SCIADV.ABQ6161_SM.PDF

Technologies, L. (2015). *Bac-to-Bac ® Baculovirus Expression System An efficient site-specific transposition system to generate baculovirus for high-level expression of recombinant proteins*.

Tõldsepp, K., Zhang, J., Takahashi, Y., Sindarovska, Y., Hõrak, H., Ceciliato, P. H. O., Koolmeister, K., Wang, Y. S., Vaahtera, L., Jakobson, L., Yeh, C. Y., Park, J., Brosche, M., Kollist, H., & Schroeder, J. I. (2018). Mitogen-activated protein kinases MPK4 and MPK12 are key components mediating CO2-induced stomatal movements. *Plant Journal*, *96*(5), 1018–1035. https://doi.org/10.1111/TPJ.14087

Tsugama, D., Liu, S., & Takano, T. (2011). *A rapid chemical method for lysing Arabidopsis cells for protein analysis*. https://doi.org/10.1186/1746-4811-7-22

Tsugama, D., Liu, S., & Takano, T. (2012). A putative myristoylated 2C-type protein phosphatase, PP2C74, interacts with SnRK1 in Arabidopsis. *FEBS Letters*, *586*(6), 693–698. https://doi.org/10.1016/J.FEBSLET.2012.02.019

Umbrasaite, J., Schweighofer, A., Kazanaviciute, V., Magyar, Z., & Ayatollahi, Z. (2010). MAPK Phosphatase AP2C3 Induces Ectopic Proliferation of Epidermal Cells Leading to Stomata Development in Arabidopsis. *PLoS ONE*, *5*(12), 15357. https://doi.org/10.1371/journal.pone.0015357

Umbrasaite, J., Schweighofer, A., & Meskiene, I. (2011). Substrate analysis of arabidopsis pp2c-type protein phosphatases. In *Methods in Molecular Biology* (Vol. 779, pp. 149–161). Humana Press Inc. https://doi.org/10.1007/978-1-61779-264-9_8

Vahisalu, T., Kollist, H., Wang, Y. F., Nishimura, N., Chan, W. Y., Valerio, G., Lamminmäki, A., Brosché, M., Moldau, H., Desikan, R., Schroeder, J. I., & Kangasjärvi, J. (2008). SLAC1 is required for plant guard cell S-type anion channel function in stomatal signalling. *Nature 2008 452:7186*, *452*(7186), 487–491. https://doi.org/10.1038/nature06608

Wu, A., Hammer, G. L., Doherty, A., von Caemmerer, S., & Farquhar, G. D. (2019). Quantifying impacts of enhancing photosynthesis on crop yield. *Nature Plants 2019 5:4*, *5*(4), 380–388. https://doi.org/10.1038/s41477-019-0398-8

Xue, T., Wang, D., Zhang, S., Ehlting, J., Ni, F., Jakab, S., Zheng, C., & Zhong, Y. (2008). Genome-wide and expression analysis of protein phosphatase 2C in rice and Arabidopsis. *BMC Genomics*, *9*. https://doi.org/10.1186/1471-2164-9-550

Yeh, C. Y., Wang, Y. S., Takahashi, Y., Kuusk, K., Paul, K., Arjus, T., Yadlos, O., Schroeder, J. I., Ilves, I., Garcia-Sosa, A. T., & Kollist, H. (2023). MPK12 in stomatal CO2 signaling: function beyond its kinase activity. *New Phytologist*, *239*(1), 146–158. https://doi.org/10.1111/nph.18913

Yoo, H., Triandafillou, C., & Drummond, D. A. (2019). Cellular sensing by phase separation: Using the process, not just the products. *Journal of Biological Chemistry*, *294*(18), 7151–7159. https://doi.org/10.1074/JBC.TM118.001191

Zhang, L., Takahashi, Y., Hsu, P. K., Kollist, H., Merilo, E., Krysan, P. J., & Schroeder, J. I. (2020). FRET kinase sensor development reveals SnRK2/OST1 activation by ABA but not by MeJA and high CO2 during stomatal closure. *ELife*, *9*, 1–74. https://doi.org/10.7554/ELIFE.56351

Zhang, M., Zhu, C., Duan, Y., Liu, T., Liu, H., Su, C., & Lu, Y. (2022). The intrinsically disordered region from PP2C phosphatases functions as a conserved CO2 sensor. *Nature Cell Biology*, *24*(7), 1029–1037. https://doi.org/10.1038/S41556-022-00936-6

APPENDIX – Supplementary Materials

Confocal microscopy images supporting observations, unverified: All AP2C3, high CO_2, unpacified silicate surface.

Drying of sample (lower buffer level, rim)

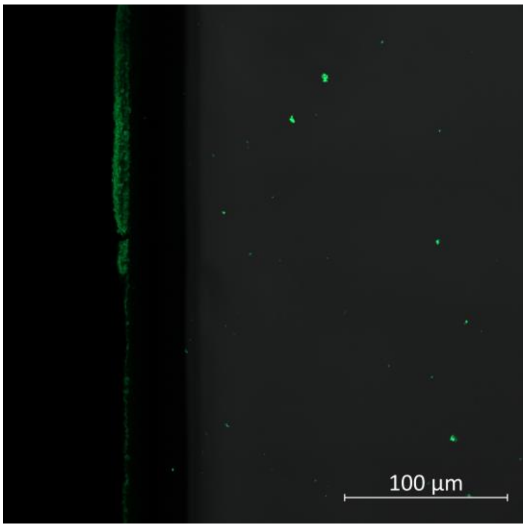

Sedimentation (bleached region after 30 min)

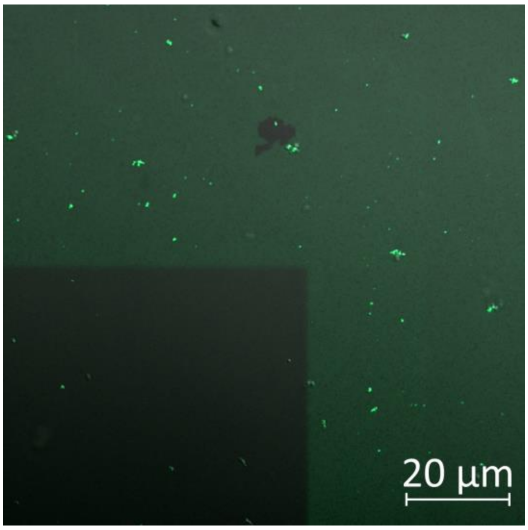

Suspected buffer salt crystallisation

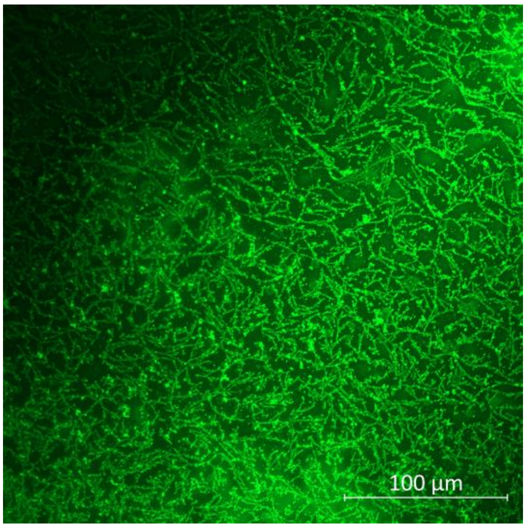

Aggregation

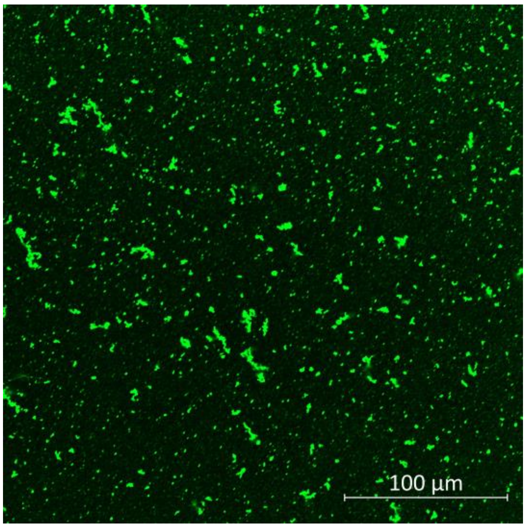

Suspected condensates (top of droplet, moving)

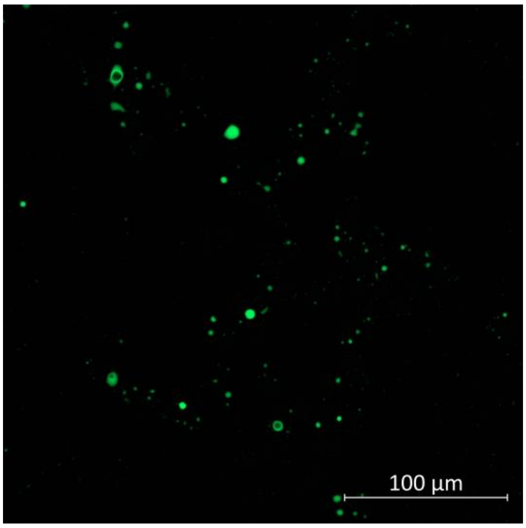

Suspected LLPS

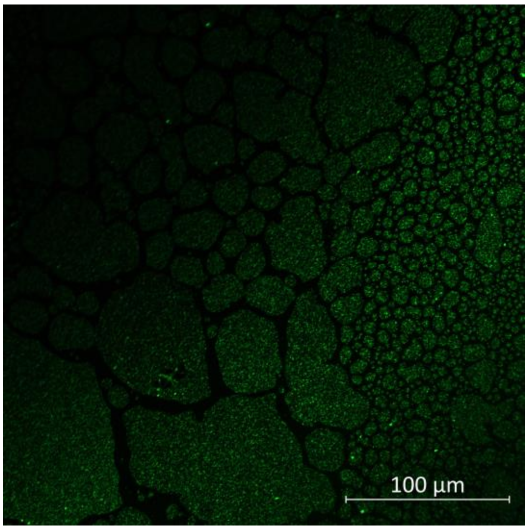

Native polypeptide sequences of selected PP2C homologs (FASTA)

AP2C1
>sp|O80871|AP2C1_ARATH Probable protein phosphatase 2C 25 OS=Arabidopsis thaliana OX=3702 GN=At2g30020 PE=1 SV=1

MSCSVAVCNSPVFSPSSSLFCNKSSILSSPQESLSLTLSHRKPQTSSPSSPSTTVSSPKSPFRLRFQKPPSGFAPGPLSFGSESVSASSP
PGGVLKRKRPTRLDIPIGVAGFVAPISSSAAVAATPREECREVEREGDGYSYCKRGRREAMEDRFSAITNLHGDRKQAIFGVYDGH
GGVKAAEFAAKNLDKNIVEEVVGKRDESEIAEAVKHGYLATDASFLKEEDVKGGSCCVTALVNEGNLVVSNAGDCRAVMSVGGV
AKALSSDHRPSRDDERKRIETTGGYVDTFHGVWRIQGSLAVSRGIGDAQLKKWVIAEPETKISRIEHDHEFLILASDGLWDKVSN
QEAVDIARPLCLGTEKPLLLAACKKLVDLSASRGSSDDISVMLIPLRQFI

AP2C2
>sp|Q8RX37|AP2C2_ARATH Probable protein phosphatase 2C 2 OS=Arabidopsis thaliana OX=3702 GN=At1g07160 PE=2 SV=1

MSSSVAVCNSPVFSPSSSLFCNKPLNTSPAHETLTLSLSHLNPPVSSTSPSAASPTSPFCLRLLKPPAKLGFGSDSGPGSILKRKRPTTL
DIPVAPVGIAAPISNADTPREESRAVEREGDGYSVYCKRGKREAMEDRFSAITNLQGDPKQAIFGVYDGHGGPTAAEFAAKNLCS
NILGEIVGGRNESKIEEAVKRGYLATDSEFLKEKNVKGGSCCVTALISDGNLVVANAGDCRAVLSVGGFAEALTSDHRPSRDDERN
RIESSGGYVDTFNSVWRIQGSLAVSRGIGDAHLKQWIISEPEINILRINPQHEFLILASDGLWDKVSNQEAVDIARPFCKGTDQKRK
PLLACKKLVDLSVSRGSLDDISVMLIQLCHLF

AP2C3
>sp|Q9XEE8|AP2C3_ARATH Probable protein phosphatase 2C 30 OS=Arabidopsis thaliana OX=3702 GN=PP2C5 PE=2 SV=1

MQLSKNPIKQTRNREKNYTDDFTMKRSVIMAPESPVFFPPPLVFSPTSVKTPLSSPRSSPPKLTMVACPPRKPKETKTTGSDSETVL
KRKRPPMLDLTAAPTVASWCSTTRETAEKGAEVVEAEEDGYYSVYCKRGRRGPMEDRYFAAVDRNDDGGYKNAFFGVFDGHG
GSKAAEFAAMNLGNNIEAAMASARSGEDGCSMESAIREGYIKTDEDFLKEGSRGGACCVTALISKGELAVSNAGDCRAVMSRG
GTAEALTSDHNPSQANELKRIEALGGYVDCCNGVWRIQGTLAVSRGIGDRYLKEWVIAEPETRTLRIKPEFEFLILASDGLWDKVT
NQEAVDVVRPYCVGVENPMTLSACKKLAELSVKRGSLDDISLIIIQLQNFLP

AP2C4
>sp|Q9FXE4|AP2C4_ARATH Probable protein phosphatase 2C 14 OS=Arabidopsis thaliana OX=3702 GN=At1g67820 PE=2 SV=2

MTNKLRSEETITSLSSFMASTLSIASPSPCSIPLSVTKVSPLKRKRPTHLNIPDLNPQQPISTDYFRFREGDKVSPLKRKRPAHLNIPDL
NPQQPIRTDYFSFTDFAHQNGTVSFGGNGFGVVSRNGKKKFMEDTHRIVPCLVGNSKKSFFGVYDGHGGAKAAEFVAENLHKY
VVEMMENCKGKEEKVEAFKAAFLRTDRDFLEKGVVSGACCVTAVIQDQEMIVSNLGDCRAVLCRAGVAEALTDDHKPGRDDEK
ERIESQGGYVDNHQGAWRVQGILAVSRSIGDAHLKKWVVAEPETRVLELEQDMEFLVLASDGLWDVVSNQEAVYTVLHVLAQ
RKTPKESEEENLVQGFVNMSPSSKLRRASLVKSPRCAKSQSYYYNSENESPSLNREIGSSPSKSPITPWKSLWAKAACKELANLAAK
RGSMDDITVVIIDLNHYKG

PP2C74
>sp|Q9FG61|PP2C74_ARATH Probable protein phosphatase 2C 74 OS=Arabidopsis thaliana OX=3702 GN=At5g36250 PE=1 SV=1

MGSCLSSSGGGGSRRSLHGSPHVPGPGRRKRPPKRRPGSCSSSFDNTEEPLLHRIPGRMFLNGSTDTVSLFSQQGKKGPNQDA
MIVWENFGSMEDTVFCGVFDGHGPYGHIVAKRVRDLLPLKLGSHLESYVSPEEVLKEISLNTDDRKISEDLVHISANGESRVYNKD
YVKDQDMIQMLIGSIVKAYRFMDKELKMQVDVDCFCSGTTAVTMVKQGQHLVIGNIGDSRAVLGVRNKDNKLVPFQLTEDLKP
DVPAEAERIKRCRGRIFALRDEPGVARLWLPNHNSPGLAMARAFGDFCLKDFGLISVPDVSYRRLTEKDEFVVLATDGIWDALTN
EEVVKIVAKAPTRSSAGRALVEAAVRNWRWKFPTSKVDDCAVVCLFLDSEPNRLSTASFSKEKHINNGVTEPEPDTASSSTPDSGT
GSPELNGVNRIDTLVNLPVYVPTKE

Multiple sequence alignment of selected native homologs

Alignment 1 – PP2C74 inlcuded

```
sp|Q9FG61|PP2C74      ------------------------------------------------------------   0
sp|Q9FXE4|AP2C4       -----------------MTNKLRS--EETITSLSSFMASTLSIASPSPCSIPLSVTKVSP   41
sp|Q9XEE8|AP2C3       MQLSKNPIKQTRNREKNYTDDFTMKRSVIMAPESPVFFPPPLVFSPTSVK---------T   51
sp|O80871|AP2C1       -----------------MSCSVAVCNSPVFSPSSSLFCNKSSILSSPQESLSLTLSHRKP   43
sp|Q8RX37|AP2C2       -----------------MSSSVAVCNSPVFSPSSSLFCNKPLNTSPAHETLTLSLSHLNP   43

sp|Q9FG61|PP2C74      ----------------------MGSCLSSSGGG----GSRRSLHGSPHVPGPGRRKRPPK   34
sp|Q9FXE4|AP2C4       LK------------RKRPTHLN---IPDLNPQQPISTDYFRFREG-DAKVSPLKRKRPAH   85
sp|Q9XEE8|AP2C3       PLSSPRS---------SPPKLTMVACPP-------RKPKETKTTG-SDSETVLKRKRPPM   94
sp|O80871|AP2C1       QTSSPSSPSTTVSSPKSPFRLRFQKPPSGFAPGPLSFGSESVSAS-SPPGGVLKRKRPTR   102
sp|Q8RX37|AP2C2       PVSST---SPSAASPTSPFCLRLLKPPAKLG-----FG-----SD-SGPGSILKRKRPTT   89
                                                                  .        :****

sp|Q9FG61|PP2C74      RRPGS---------CSSSFDNTEEPLLHRIPGRMFLNGSTDTVSLFSQQGKKGPNQDAMI   85
sp|Q9FXE4|AP2C4       LNIPDLNPQQ--PIRTDYF-SF-TDFA---HQNGTVSFGGNGFGVVSRNGKKKFMEDTHR   138
sp|Q9XEE8|AP2C3       LDLTAAPTVASW--CS--T-TRETAEK---GAEVVEAEEDGYYSVYCKRGRRGPMEDRYF   146
sp|O80871|AP2C1       LDIPIGVAGFVAPISSSAA-VAATPRE---ECREVEREG-DGYSVYCKRGRREAMEDRFS   157
sp|Q8RX37|AP2C2       LDIPVAPVGIAAPISN-----ADTPRE---ESRAVEREG-DGYSVYCKRGKREAMEDRFS   140
                                     .                .       .  .: .:.*::   :*

sp|Q9FG61|PP2C74      VWEN--FGSMEDTVFCGVFDGHGPYGHIVAKRVRDLLPLKLGSHLESYVSPEEVLKEISL   143
sp|Q9FXE4|AP2C4       IVPC--LVGNSKKSFFGVYDGHGGAKAA------EFVAENLHKYVVEMMEN------CKG   184
sp|Q9XEE8|AP2C3       AAVDRNDDGGYKNAFFGVFDGHGGSKAA------EFAAMNLGNNIEAAMAS------ARS   194
sp|O80871|AP2C1       AITN--LHGDRKQAIFGVYDGHGGVKAA------EFAAKNLDKNIVEEVVG---------   200
sp|Q8RX37|AP2C2       AITN--LQGDPKQAIFGVYDGHGGPTAA------EFAAKNLCSNILGEIVG---------   183
                              .  .  : **:****           ::   :* . :   :

sp|Q9FG61|PP2C74      NTDDRKISEDLVHISANGESRVYNKDYVKDQDMIQMLIGSIVKAYRFMDKELKMQVDVDC   203
sp|Q9FXE4|AP2C4       K---EEKV------------------------------EAFKAAFLRTDRDFLE---KG-   207
sp|Q9XEE8|AP2C3       GEDGCSME------------------------------SAIREGYIKTDEDFLK---EG-   220
sp|O80871|AP2C1       KRDESEIA------------------------------EAVKHGYLATDASFLK---EED   227
sp|Q8RX37|AP2C2       GRNESKIE------------------------------EAVKRGYLATDSEFLK---EKN   210
                           .                                 :.  .:   * .:

sp|Q9FG61|PP2C74      FCSGTTAVTMVKQGQHLVIGNIGDSRAVLGVRNKDNKLVPFQLTEDLKPDVPAEAERIKR   263
sp|Q9FXE4|AP2C4       VVSGACCVTAVIQDQEMIVSNLGDCRAVLCRAGVA-----EALTDDHKPGRDDEKERIES   262
sp|Q9XEE8|AP2C3       SRGGACCVTALISKGELAVSNAGDCRAVMSRGGTA-----EALTSDHNPSQANELKRIEA   275
sp|O80871|AP2C1       VKGGSCCVTALVNEGNLVVSNAGDCRAVMSVGGVA-----KALSSDHRPSRDDERKRIET   282
sp|Q8RX37|AP2C2       VKGGSCCVTALISDGNLVVANAGDCRAVLSVGGFA-----EALTSDHRPSRDDERNRIES   265
                        .*: .** : .  .: :.* **.***:   .         *:.* .*.   * :**:

sp|Q9FG61|PP2C74      CRGRIFALRDEPGVARLWLPNHNSPGLAMARAFGDFCLKDFGLISVPDVSYRRLTEKDEF   323
sp|Q9FXE4|AP2C4       QGGYVDNHQ------GAWR---VQGILAVSRSIGDAHLKKW-VVAEPETRVLELEQDMEF   312
sp|Q9XEE8|AP2C3       LGGYVDCCN------GVWR---IQGTLAVSRGIGDRYLKEW-VIAEPETRTLRIKPEFEF   325
sp|O80871|AP2C1       TGGYVDTFH------GVWR---IQGSLAVSRGIGDAQLKKW-VIAEPETKISRIEHDHEF   332
sp|Q8RX37|AP2C2       SGGYVDTFN------SVWR---IQGSLAVSRGIGDAHLKQW-IISEPEINILRINPQHEF   315
                        * :   .        *     .  **::*.:**  **.: ::: *:    .:  . **

sp|Q9FG61|PP2C74      VVLATDGIWDALTNEEVVKIVAKAPTRSSAGRA-LVEAAVRNWRWKFPTSKVDD------   376
sp|Q9FXE4|AP2C4       LVLASDGLWDVVSNQEAVYTVLHVLAQRKTPKESEEENLVQGFVNMSPSSKLRRASLVKS   372
sp|Q9XEE8|AP2C3       LILASDGLWDKVTNQEAVDVVRP-------------------------------------   348
sp|O80871|AP2C1       LILASDGLWDKVSNQEAVDIARP-------------------------------------   355
sp|Q8RX37|AP2C2       LILASDGLWDKVSNQEAVDIARP-------------------------------------   338
                      ::**:**:** ::*:*.*  .

sp|Q9FG61|PP2C74      --CAVVCL-FLDSEPNRLSTASFSKEKHINNGV--------TEPEPDTASSSTPD--SGT   423
sp|Q9FXE4|AP2C4       PRCAKSQSYYYNSENESP---SL--NREIGSSPSKSPITPWKSLWAKAACKELANLAAKR   427
sp|Q9XEE8|AP2C3       -YCVGV-------E---------------------------N-PMTLSACKKLAELSVKR   372
sp|O80871|AP2C1       -LCLGT-------E---------------------------K-PLLLAACKKLVDLSASR   379
sp|Q8RX37|AP2C2       -FCKGT-------D---------------------------QKRKPLLACKKLVDLSVSR   363
                        *          :                                  *...  :

sp|Q9FG61|PP2C74      GSPELNGVNRIDTLVNLPVYVPTKE 448
sp|Q9FXE4|AP2C4       GSMD--DI--TVVIIDLNHYKG--- 445
sp|Q9XEE8|AP2C3       GSLD--DI--SLIIIQLQNFLP--- 390
sp|O80871|AP2C1       GSSD--DI--SVMLIPLRQFI---- 396
sp|Q8RX37|AP2C2       GSLD--DI--SVMLIQLCHLF---- 380
                      ** :  .:     :: *
```

Alignment 2 – PP2C excluded

```
sp|Q9FXE4|AP2C4      -----------------MTNKLRS--EETITSLSSFMASTLSIASPSPCSIPLSVTKVSP     41
sp|Q9XEE8|AP2C3      MQLSKNPIKQTRNREKNYTDDFTMKRSVIMAPESPVFFPPPLVFSPTSVK---------T     51
sp|O80871|AP2C1      -----------------MSCSVAVCNSPVFSPSSSLFCNKSSILSSPQESLSLTLSHRKP     43
sp|Q8RX37|AP2C2      -----------------MSSSVAVCNSPVFSPSSSLFCNKPLNTSPAHETLTLSLSHLNP     43
                                       : ..    .  ::  * .:       *    .

sp|Q9FXE4|AP2C4      LK------------RKRPTHLN---IPDLNPQQPISTDYFRFREGDAKVSPLKRKRPAHL     86
sp|Q9XEE8|AP2C3      PLSSPRS---------SPPKLTMVACPP-------RKPKETKTTGSDSETVLKRKRPPML     95
sp|O80871|AP2C1      QTSSPSSPSTTVSSPKSPFRLRFQKPPSGFAPGPLSFGSESVSASSPPGGVLKRKRPTRL     103
sp|Q8RX37|AP2C2      PVSST---SPSAASPTSPFCLRLLKPPAKLG-----FG-----SDSGPGSILKRKRPTTL     90
                                      *  *     *                 ..     ******  *

sp|Q9FXE4|AP2C4      NIPDLNPQQ--PIRTDYFSF-TDFAHQNGTVSFGGNGFGVVSRNGKKKFMEDTHRIVPC-     142
sp|Q9XEE8|AP2C3      DLTAAPTVASW--CS--TTRETAEKGAEVVEAEEDGYYSVYCKRGRRGPMEDRYFAAVDR     151
sp|O80871|AP2C1      DIPIGVAGFVAPISSSAAVAATPREECREVEREG-DGYSVYCKRGRREAMEDRFSAITN-     161
sp|Q8RX37|AP2C2      DIPVAPVGIAAPISN----ADTPREESRAVEREG-DGYSVYCKRGKREAMEDRFSAITN-     144
                     ::            .      *     . .     . :.* .:.*::  *** .

sp|Q9FXE4|AP2C4      -LVGNSKKSFFGVYDGHGGAKAAEFVAENLHKYVVEMMENCKGK---EEKVEAFKAAFLR     198
sp|Q9XEE8|AP2C3      NDDGGYKNAFFGVFDGHGGSKAAEFAAMNLGNNIEAAMASARSGEDGCSMESAIREGYIK     211
sp|O80871|AP2C1      -LHGDRKQAIFGVYDGHGGVKAAEFAAKNLDKNIVEEVVG---KRDESEIAEAVKHGYLA     217
sp|Q8RX37|AP2C2      -LQGDPKQAIFGVYDGHGGPTAAEFAAKNLCSNILGEIVG---GRNESKIEEAVKRGYLA     200
                        *. *:::***:***** .****.* ** . :   : .        .  .*.: .::

sp|Q9FXE4|AP2C4      TDRDFLEKG-VVSGACCVTAVIQDQEMIVSNLGDCRAVLCRAGVAEALTDDHKPGRDDEK     257
sp|Q9XEE8|AP2C3      TDEDFLKEG-SRGGACCVTALISKGELAVSNAGDCRAVMSRGGTAEALTSDHNPSQANEL     270
sp|O80871|AP2C1      TDASFLKEEDVKGGSCCVTALVNEGNLVVSNAGDCRAVMSVGGVAKALSSDHRPSRDDER     277
sp|Q8RX37|AP2C2      TDSEFLKEKNVKGGSCCVTALISDGNLVVANAGDCRAVLSVGGFAEALTSDHRPSRDDER     260
                           ** .**::    .*:*****::.. :: *:* ******:. .* *:**:.**.*.: :*

sp|Q9FXE4|AP2C4      ERIESQGGYVDNHQGAWRVQGILAVSRSIGDAHLKKWVVAEPETRVLELEQDMEFLVLAS     317
sp|Q9XEE8|AP2C3      KRIEALGGYVDCCNGVWRIQGTLAVSRGIGDRYLKEWVIAEPETRTLRIKPEFEFLILAS     330
sp|O80871|AP2C1      KRIETTGGYVDTFHGVWRIQGSLAVSRGIGDAQLKKWVIAEPETKISRIEHDHEFLILAS     337
sp|Q8RX37|AP2C2      NRIESSGGYVDTFNSVWRIQGSLAVSRGIGDAHLKQWIISEPEINILRINPQHEFLILAS     320
                     :***: *****  :..**:** *****.***  **:*:::*** .  .:: : ***:***

sp|Q9FXE4|AP2C4      DGLWDVVSNQEAVYTVLHVLAQRKTPKESEEENLVQGFVNMSPSSKLRRASLVKSPRCAK     377
sp|Q9XEE8|AP2C3      DGLWDKVTNQEAVDVVRP--------------------------------------YCVG     352
sp|O80871|AP2C1      DGLWDKVSNQEAVDIARP--------------------------------------LCLG     359
sp|Q8RX37|AP2C2      DGLWDKVSNQEAVDIARP--------------------------------------FCKG     342
                     ***** *:*****  .                                         *

sp|Q9FXE4|AP2C4      SQSYYYNSENESPSLNREIGSSPSKSPITPWKSLWAKAACKELANLAAKRGSMDDITVVI     437
sp|Q9XEE8|AP2C3      V-------E----------------------N-PMTLSACKKLAELSVKRGSLDDISLII     382
sp|O80871|AP2C1      T-------E----------------------K-PLLLAACKKLVDLSASRGSSDDISVML     389
sp|Q8RX37|AP2C2      T-------D----------------------QKRKPLLACKKLVDLSVSRGSLDDISVML     373
                             :                      :      ***:*.:*:..*** ***::::

sp|Q9FXE4|AP2C4      IDLNHYKG         445
sp|Q9XEE8|AP2C3      IQLQNFLP         390
sp|O80871|AP2C1      IPLRQFI-         396
sp|Q8RX37|AP2C2      IQLCHLF-         380
                     * * :
```

Legend:

blue: phosphatase domain, yellow: disordered domain, green: both (reported by UniProt/AlphaFold)

magenta: serine residue, turquoise: threonine residue

Orange: conserved putative MAPK interaction motif (KIM) - [(K/R)$_{3–4}$,X$_{1-6}$(L/I)X(L/I)]

Grey: insertion predicted to be IDR

*(asterix): positions with a single, fully conserved residue

: (colon): positions with conservation between amino acid groups of similar properties

. (period): positions with conservation between amino acids of weakly similar properties

Macro code for BiFC quantification

```
macro "Nuclei2 [e]" {
ids=newArray(nImages); //checks how many images are currently open
n=nImages;
for (i=0;i<nImages;i++) {
        selectImage(i+1);
        title = getTitle();
                if (endsWith(title, "C=0")){
                        originalImageID = getImageID();
                        originaltitle = getTitle();
                }
}
selectImage(originalImageID);
run("Duplicate...", " ");
run("Gaussian Blur...", "sigma=2");
setAutoThreshold("Default dark");
run("Manual Threshold...");
setBatchMode("hide");
run("Create Mask");
setBatchMode("show");
setBatchMode(true);
run("Analyze Particles...", "size=120-Infinity pixel exclude add");
selectImage(originalImageID);
roiManager("Show All with label");
roiManager("Deselect");
roiManager("multi-measure measure_all one append");

for (i=0;i<nImages;i++) {
        selectImage(i+1);
        title = getTitle;
                if (endsWith(title, "C=1")){
                        roiManager("Show All with label");
                        roiManager("Deselect");
                        roiManager("multi-measure measure_all one append");
                }
                else if (endsWith(title, "C=2")) {
                        close();
                }
}
}

macro "Clear [w]" {
        run("Select All");
        close("*");
}
```

BiFC graphs- single experiments, comparable pairs tested for statistical significance

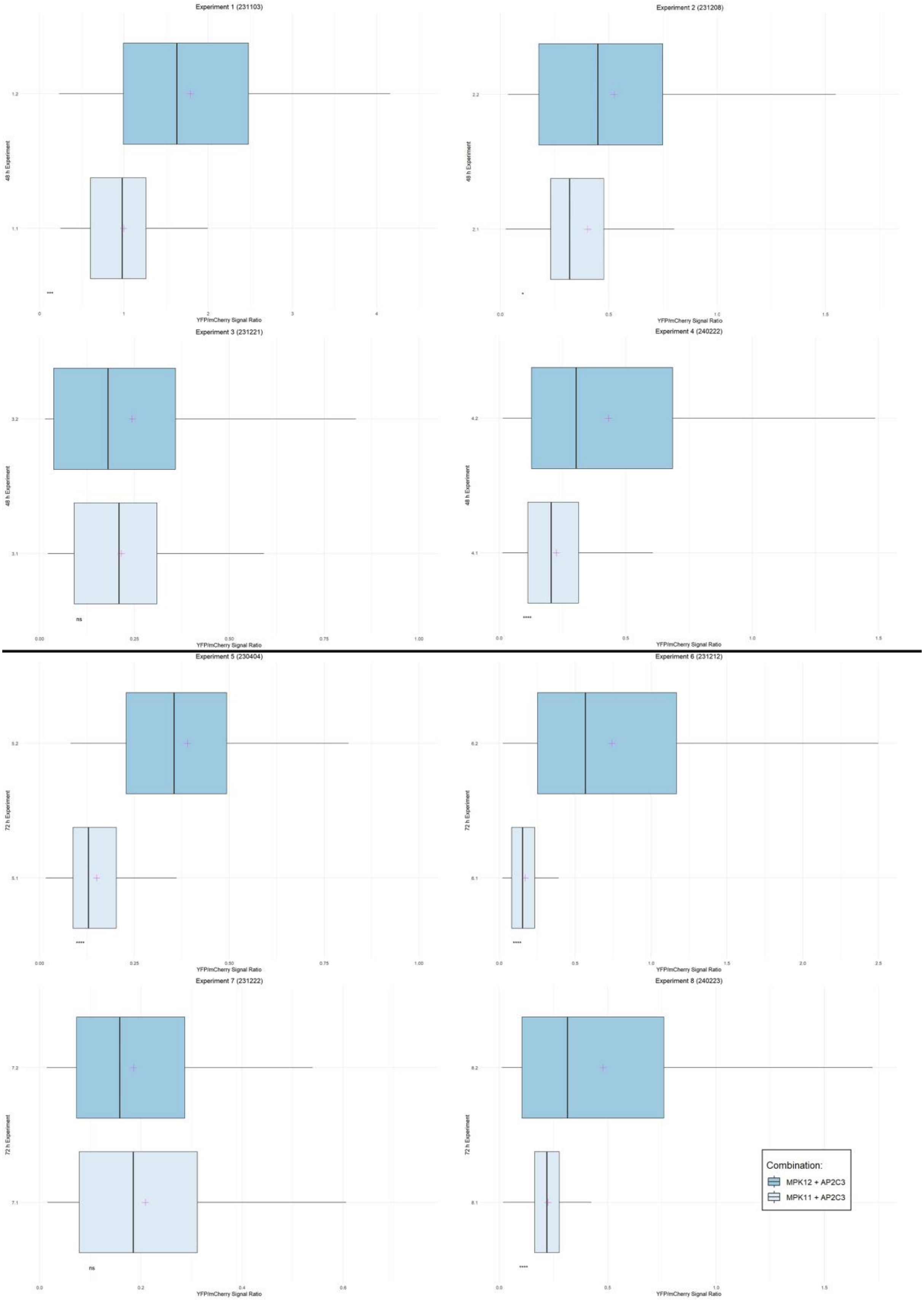

Upper: Experiment 1.1 – 4.2 (measured 48 h dpi), Lower: Experiment 5.1 – 8.2 (measured 72 h dpi)

Magenta cross: average, ns: not significant, *: significant difference of means with $p < 0.05$ (t-test)

Yield of purification

Recombinant protein	Approximate concentration [µg/µL]	Approximate molarity [µM]	Total yield [mg]
AP2C1-YFP	2.38	34.06	11.32
AP2C3-YFP	0.86	12.30	3.44
AP2C4-YFP	1.52	21.78	6.08
Tstrep-mVen-TEV-AP2C1	2.39	47.98	11.47
Tstrep-mVen-TEV-AP2C3	1.01	12.34	4.85
Tstrep-mVen-TEV-AP2C4	0.92	16.83	4.42
Tstrep-mVen-TEV-PP2C74	0.95	17.09	4.56

Sequential list of materials

- Clustal Omega (1.2.4)
- AlphaFold2 Protein Structure Data Base
- Benchling® 2024
- 35S:(PP2C gene)-YFP/pCAMBIA1390 template plasmids (provided by Yuh Shuh-Wang
- Primers synthesised by Integrated DNA Technologies, Inc. & Microsynth AG
- Phusion DNA Polymerase (Thermo Scientific™)
- dNTPs (Thermo Scientific™)
- 5× HF Phusion Buffer (Thermo Scientific™)
- thermos cycler (Aeris™ TAS™ Thermo Cycler, Peltier Technology)
- FavorPrep™ PCR Purification Mini Kit (FAVORGEN® Biotech Corporation)
- 10X FastDigest buffer (Thermo Scientific™)
- FD *Bam*HI, FD *Eco*RI, FD *Sal*I, FD *Not*I restriction enzymes (Thermo Scientific™)
- pET28a vector (provided by Yuh-Shuh Wang)
- 10X ligase buffer (Thermo Scientific™)
- T4 DNA ligase (Thermo Scientific™)
- FavorPrep™ Plasmid Extraction Mini Kit procedure (FAVORGEN® Biotech Corporation)
- NanoDrop 2000 spectrophotometer (Thermo Scientific™)
- BL21 (DE3) pLysS competent *E. coli* cells (provided by Ivar Ilves)
- Kanamycin (50 µg/mL)
- Difco™ LB Broth (LB) (Lennox)
- Multitron shaker (Infors HT)
- Centrifuge bottles (Nalegene®, 500 mL)
- Lysis buffer 1 (25 mM HEPES pH 7.6, 500 mM NaCl, one tablet Roche Protease Inhibitor Cocktail 2 (SIGMA®))
- Sorvall Lynx 6000 centrifuge (Thermo Scientific™)
- F12-6x500 LEX rotor (Thermo Scientific™)
- N500 wash buffer (25 mM Hepes pH 7.6, 500 mM NaCl, 0.2 mM PMSF, 20 mM imidazole)
- N300 wash buffer (25 mM Hepes pH 7.6, 300 mM NaCl, 20 mM imidazole)
- N300 elution buffer (25 mM Hepes, pH 7.6, 300 mM NaCl, 300 mM imidazole)
- UV light
- 50 mL falcons (Thermo Scientific™)
- 5810R table-top centrifuge (Eppendorf®, A-41-8 rotor)
- lysozyme (SIGMA® Life Science)
- Sonoplus Sonicator (Bandelin Electronics)
- SS34 centrifuge tubes (Nalgene®)
- A27-8x50 rotor (Thermo Scientific™)
- PureCube 100 Ni-NTA-Agarose (Cube Biotech)
- Poly-Prep® chromatography columns (Bio-Rad)
- IQ 7000, LC-Pak (Millipore)
- Imidazole (Fisher Scientific)
- *Spodoptera frugiperda* (Sf9) insect cells (provided by Ivar Ilves)
- FD *Bcu*I, FD *Sal*I (Thermo Scientific™)
- DH10Bac™ competent *E. coli* cells (provided by Ivar Ilves)
- Ticarcillin (80 µg/mL)
- Gentamicin (7 µg/mL)

- Tetracycline (10 µg/mL)
- IPTG
- X-gal (*Phyto*Technology Laboratories®)
- Invitrogen™ Purelink™ purification kit (life technologies™)
- EX-CELL® 420 (Merck®)
- 10 cm cell culture petri dish (Greiner Bio-One GmbH)
- Transfection 007 Reagent (Icosagen®)
- 6-well tissue cell culture dish (Corning)
- a 15 cm cell culture petri dish (Sarsted)
- Lysis buffer 2 (25 mM Hepes NaOH pH 7.6, 500 mM NaCl, 0.1% Tween 20 (Fisher BioReagents™)
- N5001 wash buffer (25 mM Hepes NaOH pH 7.6, 500 mM NaCl, 0.1% Tween 20 (Fisher BioReagents™)
- N5001 elution buffer (25 mM Hepes NaOH pH 7.6, 500 mM NaCl, 0.1% Tween 20 (Fisher BioReagents™), 50 mM biotin (VWR Life Science))
- DTT (Serva)
- Strep-Tactin® XT 4Flow® high-capacity resin (IBA Lifesciences Gmbh)
- PMSF (Thermo Scientific™)
- 1.5 mL Protein LoBind Eppendorf Tubes®
- 10 % SDS polyacrylamide gels (self assembled)
- 2x SDS-PAGE sample buffer (provided by Ivar Ilves)
- 10-180 kDa prestained protein ladder (Thermo Scientific™)
- SDS-PAGE equipment (Bio-Rad®)
- Page Blue Protein Staining Solution (Thermo Scientific™)
- Perfection V800 Photo scanner (Epson)
- Fiji (ImageJ, 2024)
- Excel | Microsoft 356®
- 0.5 mL Protein LoBind Eppendorf Tubes®
- Slide-A-Lyzer® Dialysis Casettes with molecular weight cut-off of 10 kDa and capacity of 0.5 - 3 mL (Thermo Scientific™)
- Zeiss Fluorescent Microscope System: CoolLED pE-4000 fluorescent light source, polychroic mirror (69002bs, Chroma), Zeiss EC Plan-NEOFLUAR 40x/0.75 objective, LUDL MAC6000 Filter Wheel System, VisiView software (Visitron Systems)
- Custom build CO_2 pump (construted by Andres Punn)
- Li-850 CO_2/H_2O Gas Analyzer (LI-COR®)
- LSM 900 laser scanning confocal microscope (Zeiss)
- ZEN blue version 3.7 (Zeiss)
- EC Plan-Neofluar 10x/0.30 M27 objective (Zeiss)
- Plan-Apochromat 20x/0.8 M27 objective (Zeiss)
- Plan-Apochromat 63x/1.40 Oil DIC M27 objective (Zeiss)
- , Immersol™ 518 F immersion oil (Zeiss)
- GaAsP-PMT1 photomultiplier
- Pecon® Integrated XLmulti S2 Incubator system
- Lab-Tek™ S compact heating insert (Pecon®)
- PM 2000 RBT© incubator lid (Pecon®)
- LSM 900's ASI PZ-2000 XYZ Series Automated Stage with a Piezo Z-Axis Top Plate
- Gas permeable foil (Sigma-Aldrich, Diversified Biotech)

- *Nicotiana benthamiana* (tobacco) seeds
- LED Tube lamps (Phillips)
- *Agrobacterium tumefaciens* strain GV31010 (provided by Yuh-Shuh Wang)
- p35S:PP2C-YFP/pCAMBIA1390 (prepared by Oleksii Yadlos)
- Glycerol stock of *A. tumefaciens* carrying a P19/pCAMBIA1390 gene silencing suppressor plasmid (provided by Yuh-Shuh Wang)
- Gentamicin (50 µg/mL)
- Plastic zipp bags
- Infiltration buffer (10 mM $MgCl_2$, 10 mM MES pH 5.6 and 200 µM acetosyringone)
- 1 mL syringes (NORM-JECT®-F Luer Solo, B. Braun)
- Zeiss SteREO fluorescent stereomicroscope equipped with a HXP 120 lighting unit and PlanApoS 1.5x FWD 30mm objective
- T4 DNA Polymerase (Thermo Scientific™)
- dCTP (Fermentas)
- dGTP (Fermentas)
- 35S:PP2C-YFPc/pCAMBIA1390 (prepared by Yuh-Shuh Wang and Oleksii Yadlos)
- P19_35S:Nuc-mCherry-HA/pCAMBIA1390 (provided by Yuh-Shuh Wang)
- R Studio (Version 4.4)
- Plant leaf protein extraction buffer (24 mM EDTA pH 8.0, 100 mM Tris–HCl pH 6.8, 4% w/v SDS, 864 mM β-mercaptoethanol, 20% v/v glycerol, and 0.005% w/v bromophenol blue)
- PVDF membrane (Immobilon-P)
- Anti-HA.11 Epitope Clone:16B12 antibody (BioLegend)
- Fat free skimmed milk (Valio)
- Goat-anti mouse IgG (H+L) horseradish peroxidase conjugated secondary antibody (Invitrogen™)
- BSA high grade (Fisher Scientific)
- Chemiluminescent detection kit (Amersham ECL Western Blotting Analysis System)
- AGFA CP-BU NEW Medical X-Ray film (blue)
- Cell culture imaging vessels (Lab-Tek®)
- 35 mm petri dishes with a 20 mm wide and 0.16 – 0.19 mm thin No. 1.5 cover glass bottom (MATTEK®)
- Pluronic® F127 (Merck)
- 384 well PS µCLEAR® black non-binding microplate (Greiner)
- Gas permeable observation gel (CAROLINA®)
- PEG-coated, 4x4 custom made microscopy slides with coverslip bottom (kindly provided by Sergei Kopantšuk)

NON-EXCLUSIVE LICENCE TO REPRODUCE THESIS AND MAKE THESIS PUBLIC

I, Stefan Heincz,

1. grant the University of Tartu a free permit (non-exclusive licence) to

   reproduce, for the purpose of preservation, including for adding to the DSpace digital archives until the expiry of the term of copyright, my thesis

   "*carbon dioxide sensing in Arabidopsis thaliana mediated by liquid-to-liquid phase separation of Protein Phosphatase Type 2C homologs*",

   supervised by Assoc. Prof. Yuh-Shuh Wang, Assoc. Prof. Ivar Ilves and Prof. Hannes Kollist.

2. grant the University of Tartu a permit to make the thesis specified in point 1 available to the public via the web environment of the University of Tartu, including via the DSpace digital archives, under the Creative Commons licence CC BY NC ND 4.0, which allows, by giving appropriate credit to the author, to reproduce, distribute the work and communicate it to the public, and prohibits the creation of derivative works and any commercial use of the work until the expiry of the term of copyright.

3. am aware of the fact that the author retains the rights specified in points 1 and 2.

4. confirm that granting the non-exclusive licence does not infringe other persons' intellectual property rights or rights arising from the personal data protection legislation.

Stefan Heincz

22/05/2024